

Development of microstructured and protein patterned hydrogels to investigate the influence of the microenvironment on cancer cells

Christine Franke

A thesis presented for the degree of Doctor of Philosophy

in

Electrical and Computer Engineering

at the

University of Canterbury

Christchurch, New Zealand

October, 2021

Don't be afraid to think big, take risks and challenge yourself.

The small blue poster in the ECE wing

Abstract

Ovarian cancer is one of the most lethal gynaecological diseases. One of the reasons for its poor survival rates is its typically late diagnosis at an advanced stage of tumour progression. A better understanding of why and how cancer initiates and develops is crucial for early diagnosis and the development of improved treatment methods. To this point, investigations of mutations on genes of cells to reduce mortality of ovarian cancer have not lead to the desired outcome. Recently, increased attention has been paid to the influencing factors in cancer cell progression such as the cellular microenvironment. It is known that the natural microenvironment of tumours differs greatly from that of healthy tissues and that modification of the cell's environment causes cellular responses such as changes in morphology, protein expressions, cell division and migration behaviour.

In this work, an experimental set-up was developed to trap cells in defined 3D wells to investigate how physical properties of the microenvironment influence ovarian cancer cells. Polyacrylamide gels were simultaneously structured and protein patterned to create a platform for cell experiments, which allows the tuning of individual physical properties of the microenvironment of cells (such as stiffness, available volume and protein compositions for cell attachment) independently of each other. The designed and optimised fabrication process begins with optical lithography to transfer a pattern onto a Silicon (Si) substrate and a dry etching step to obtain an array of pillars while transforming the Si-substrate into a Si-mould. The Si-mould serves as a stamp during a μ -contact printing approach to transfer defined patterns of protein, and simultaneously as a mould during polyacrylamide polymerisation. The resulting microstructured and protein patterned polyacrylamide gels can then be used as cell culture substrates for cell experiments.

Si-moulds and polyacrylamide gels were characterised with scanning electron microscopy, atomic force microscopy and confocal laser scanning microscopy. By investigating four differently sized circular patterns (with diameters of 20 μm , 30 μm , 40 μm and 60 μm) and four different stiffnesses of the polyacrylamide gels (1 kPa, 8 kPa, 30 kPa and 100 kPa), it was shown that the fabrication process is robust and easy to adjust.

Computational analysis protocols were developed and established for traction force microscopy and brightness fluctuation analysis of cells, including the corresponding brightness autocorrelation functions. It was shown that microstructured and protein patterned polyacrylamide gels can be used for investigations of protein expressions, cellular traction forces and brightness fluctuations of cells. While the analyses of protein expressions and autocorrelation functions of the brightness fluctuations need further improvement, the results of the traction force experiments allow a first hypothesis to be formulated:

cellular traction forces increase with decreasing volume available to the cell, as indicated by analysis of cell experiments on ovarian cancer cells of the cell line SKOV3. The developed microstructured and protein patterned polyacrylamide gels are an important step to gain a better understanding on how mechanical properties of the microenvironment influence cellular responses. This experimental set-up can be easily adapted and optimised for further investigations of cancer cells and can thus help in the development of new treatment approaches.

Contents

1	Introduction	1
2	Biological background	5
2.1	Cells	5
2.1.1	Cellular cytoskeleton	6
2.1.2	Extracellular matrix	8
2.2	Cellular forces	9
2.2.1	Mechanotransduction	11
2.2.2	Influence of the microenvironment on cellular forces	13
2.2.3	Available methods for cellular force measurements	13
2.3	Cancer	16
2.3.1	Ovarian cancer	16
2.3.2	Cancer microenvironment	16
2.3.3	Differences between cancer and healthy cells	17
3	Methodology background	19
3.1	Fabrication of protein patterned and microstructured polyacrylamide gels	19
3.1.1	Optical lithography	20
3.1.2	Inductively coupled plasma etching for structuring silicon	23
3.1.3	Polyacrylamide fabrication	25
3.1.4	μ -Contact printing for protein patterning	27
3.2	Cell experiments	28
3.3	Analysis	29
3.3.1	Optical profilometer and scanning electron microscopy for analysing silicon moulds	29
3.3.2	Atomic force microscopy for analysing mechanical properties of hydrogels	30
3.3.3	Confocal laser scanning microscopy for analysing fluorescence labelled structures	32
3.3.4	Traction force microscopy	34
4	Materials and Methods	37
4.1	Fabrication	37
4.1.1	Preparation of silicon moulds using photolithography and inductively coupled plasma etching	39

4.1.2	Preparing microstructured polyacrylamide gels	40
4.1.3	Preparing protein patterned and microstructured polyacrylamide gels for cell culturing	41
4.2	Cell experiments	43
4.3	Analysis	44
4.3.1	Characterisation of silicon moulds and polyacrylamide gels	44
4.3.2	Traction force microscopy	47
4.3.3	Cell fluctuation analysis	49
4.4	Conclusion	53
5	Results and discussion	55
5.1	Silicon moulds and microstructured and protein patterned polyacrylamide gels	55
5.1.1	Characterisation of silicon moulds	55
5.1.2	Characterisation of polyacrylamide gels	59
5.1.3	Protein transfer for cell experiments	61
5.2	Cell experiments	62
5.2.1	Cells cultured on microstructured and protein patterned polyacrylamide gels	62
5.2.2	Cellular traction forces	65
5.2.3	Cell fluctuation analysis	69
5.3	Conclusion	74
6	Summary and future outlook	76
7	Appendix	80
7.1	Protocols	80
7.1.1	Optical lithography	80
7.1.2	Polyacrylamide gels	81
7.1.3	Polyacrylamide gel preparation with APS and TEMED	82
7.2	Scanning Electron microscopy results	83
	Bibliography	84

Abbreviations

Abbreviation	Explanation
AA	Acrylamide
AA-NHS	Acrylic acid N-hydroxysuccinimide
AFM	Atomic Force Microscope
APTES	(3-Aminopropyl)triethoxysilane
APS	Ammoniumperoxidsulfat
bis-AA	bis-Acrylamide
BSA	Bovine Serum Albumin
BSE	Back-Scattered Electrons
CAM	Cell Adhesion Molecules
CCP	Capacity Coupled Plasma Modes
CLSM	Confocal Laser Scanning Microscope
DMEM	Dulbecco's Modified Eagle Medium
DNA	Deoxyribonucleic Acid
ECM	Extracellular Matrix
E-Module	Elasticity Module
ELISA	Enzyme-Linked Immunoabsorbent Assay
FAK	Focal Adhesion Kinase
FBS	Fetal Bovin Serum
FEM	Finite Element Method
FTTC	Fourier Transform Traction Cytometry
FUCCI	Fluorescent Ubiquitin-Based Cell Cycle Indicator
GAG	Glycosaminoglycan
GDA	Glutaraldehyde
HA	Hyaluronic Acid
HEPES	4-(2-hydroxyethyl)-1-piperazineethanesulfonic acid
HF	High frequency
HMDS	Hexamethyldisilazane
ICP	Inductively Coupled Plasma
KOH	Potassium Hydroxide
NHS	N-hydroxysuccinimide
NMP	N-Methyl-2-pyrrolidon
mRNA	Messenger Ribonucleic Acid
MSD	Mean Square Displacement
PAA	Polyacrylamide
PAGE	Polyacrylamide Gel Electrophoresis

Abbreviation	Explanation
PBS	Phosphate-Buffered Saline
PDMS	Polydimethylsiloxane
PIV	Particle Image Velocitometry
polyHEMA	Poly-2-Hydroxyethyl Methacrylate
PTV	Particle Tracking Velocitometry
ROI	Region of Interest
RT	Room Temperature
SE	Secondary Electrons
SEM	Scanning Electron Microscope
Si	Silicon
Sulfo-SANPAH	Sulfosuccinimidyl 6-(4'-azido-2'-nitrophenylamino)hexanoate
TAV	Time Averaged Video
TEMED	Tetramethylethylenediamine
UV light	Ultraviolet light

1 Introduction

Cancer is the second leading cause of death worldwide after ischaemic heart diseases and stroke [1], but despite all research efforts, questions about why and how cancer develops remain open. Answering those questions is not just complicated by the complexity of cancer itself, but also the fact that the term “cancer” refers to a whole group of diseases. Over 100 types of cancer in humans are known and they all have different gene mutations and appearances. Nevertheless, there are some characteristics all cancer cells have in common, as they all proliferate and grow in an uncontrolled way and are able to invade healthy tissues and metastasise [2]. However, early detection and location of the cancer’s origin in the body often strongly determine therapy success. Ovarian cancer, for example, is often diagnosed in an advanced state of the disease and has survival rates of 45% for the most common epithelial ovarian cancer [3]. Obviously, there is an urgent need for a better understanding of initiation and progression of ovarian cancer to enable early detection and for the development of new effective treatment methods.

Even though there are several generally accepted influencing factors that favour cancer formation such as smoking, radiation and nutrition [4], the mechanisms which turn a healthy cell into a cancer cell are still unknown. The focus of cancer research has long been on analysing DNA changes of cells and the need for gene mutations during cancer progression. However, factors such as the microenvironment and cell-cell contacts have been neglected, even though cells can communicate with both. The cellular process of sensing external mechanical signals and translating them into an internal biochemical signal is called mechanotransduction. In the first step of mechanotransduction, complex structures made out of several proteins on the cell surface, called focal adhesions, allow cells to perceive their surrounding [5]. Here, focal adhesions connect the external structures with the internal scaffold of the cell, the cytoskeleton, and are the starting point of a signalling cascade which finally influences the expression of genes. This means physical properties of the microenvironment can lead to cellular responses such as changes in morphology, or even influence the drug resistance of cancer cells [6].

It is known that the tumour microenvironment differs greatly from a healthy microenvironment but it is not entirely clear whether the tumour first induces changes in the microenvironment or if maybe an altered microenvironment favours the development of a tumour [7]. These changes of the microenvironment of the cells can be physical ones, such as the stiffness or the shape of the surrounding, or they can be biochemical ones, such as the composition and concentration of proteins. How far reaching each of these changes is for the cell, and how cellular reactions to different simultaneous changes interfere with each other, needs to be investigated. Therefore, a variety of cell properties

can be analysed, such as the morphology, the cytoskeleton and the protein expression. However, cells can not only sense their microenvironment through focal adhesions, but also react to and actively influence it by applying mechanical forces [8]. These cellular forces are necessary for cell migration, e.g. during wound healing, but also for metastasis of cancer. Investigations of these forces and how they are influenced will not only help to gain a better understanding of cancer development, but can also lead to a treatment of cancer, especially in connection with metastasis.

In order to decipher the complex mechanism of cancer initiation and progression, the ability of cells to receive, process and return signals must be investigated, as well as the influence of the external factors on the cellular signalling cascades and responses.

The purpose of this PhD Thesis was to develop an experimental set-up for investigations of how physical properties of the microenvironment influence cellular forces, morphology, protein expression and cell division in the context of cancer. The aim was to design a platform which allows the identification of triggers and dependencies between the microenvironment and cellular responses in form of protein expressions within the cells, as well as forces exerted by the cells. Examinations should be made possible of how the effect of different external factors on cellular responses amplify or overwrite each other. In order to be able to investigate these correlations, an experimental set-up was required that allows to tune individual physical properties independently of each other. Furthermore, the numbers of cells needed to be controlled and the whole set-up had to be biocompatible and robust.

Therefore, in this work, a microstructured and protein patterned hydrogel was designed, developed and successfully established for cell experiments. Polyacrylamide, a polymer widely used to determine cellular forces, was used as a substrate material, as its stiffness can be easily tuned and its non-adhesive properties allow to coat defined areas of its surface with a protein for the cells to attach to. Silicon (Si) moulds were patterned and etched, using soft lithography and a dry etching process. They were then used for a μ -contact printing method to transfer a protein pattern and as a mould for 3D structures during the polyacrylamide polymerisation process. The resulting microstructured and protein patterned polyacrylamide gels were characterised and optimised for cell culture experiments. These cell experiments are possible as cells can only attach to the lower areas of the 3D structures and are therefore trapped in confined and well defined wells. In this Thesis it was shown that the experimental set-up designed is working reliably, independent of the stiffness of the polyacrylamide and the size of the pattern.

It was shown that several experiments on ovarian cancer cells cultured on microstructured and protein patterned polyacrylamide gels are possible. These experiments included fluorescent protein investigations, cellular traction forces and brightness fluctuation of cells over 48 h. Furthermore, computational analysis protocols were developed and established for traction force microscopy, the brightness fluctuations and the cor-

responding auto correlation functions of cells monitored with a brightfield microscope. Even though more experiments are needed in order to be able to make a reliable statement, the results of traction force analysis of ovarian cancer cells in three differently sized patterns indicate that with an increase of volume available for the cell, traction forces decrease.

The structure of this thesis includes the biological background in Chapter 2, where information will be given about cells, cellular forces and cancer. In the first part the focus will lie on the actin cytoskeleton of cells, as it is not only important for the stability and mechanical properties of the cell, but is also involved in the cellular process of sensing and applying forces. The extracellular matrix (ECM) and its components, as the natural microenvironment of cells, will be introduced before the mechanism of cellular force applications will be explained, including a brief overview of the molecular clutch model. It will be discussed that the microenvironment can influence cell behaviour and cellular forces and which methods are available to measure these forces. In the complex field of cancer, the focus will be on ovarian cancer, the tumour microenvironment and the characteristics of cancer cells.

Chapter 3 will introduce the basic principles behind the methods used in the fabrication and analysis processes for this thesis. This chapter will give some background information, so that the reader understands the method including its parameters and how those can be adjusted. The methods presented include optical lithography, for transferring a pattern design onto a silicon wafer, and the following dry-etching process of this silicon wafer to obtain an array of pillars. Also, the basics of polyacrylamide fabrication and μ -contact printing techniques, to pattern a surface with a protein, will be explained. Analysis methods will be covered, such as scanning electron microscopy, optical profilometry, atomic force microscopy, confocal laser scanning microscopy and traction force microscopy to determine the structures of silicon moulds and polyacrylamide gels, the stiffness of a material, the appearance of fluorescently labelled samples and cellular forces.

In Chapter 4, it will be described how the methods for fabrication and analysis, explained in Chapter 3, are used to establish a protocol for simultaneously microstructuring and protein patterning polyacrylamide gels. This chapter includes limitations of the methods used, as well as alternative processes which could not be established successfully, such as using a passive pumping approach to fabricate a cell sorting grid made out of polyHEMA. In addition, image analysis to obtain brightness cell fluctuation and the corresponding autocorrelation functions will be introduced.

In Chapter 5, it will be shown that the developed fabrication process of microstructured and protein patterned polyacrylamide gels was successfully established. By investigating four differently sized circular patterns and four different stiffnesses of the gel, it will be shown that the fabrication process is robust and flexible. Cell experiments, using ovarian cancer cells of the cell line SKOV3, will show that the process is optimised for cell culture and can be used for analysing cellular responses to changes of physical properties of

the microenvironment. Here, the results of traction force microscopy experiments with varying sizes of pattern diameters indicate that cellular traction forces increase with a decrease of volume available to the cell.

The last Chapter 6 summarises the work presented and will give an overview on which experiments the microstructured and protein patterned polyacrylamide gels can be used for. The chapter will highlight the flexibility of the experimental set-up developed here and will give an insight into the wide field of cell analysis the developed polyacrylamide gels are opening up. It will be discussed how microstructured and protein patterned polyacrylamide gels can help to understand how cancer cells react to changes in their microenvironment. This will be an important step towards an improved understanding of initiation and development of ovarian cancer.

2 Biological background

The aim of this chapter is to give a brief introduction to the biological background that is important in the context of this work. It will introduce the cell and the extracellular matrix and how cells can sense mechanical properties of the microenvironment. It will give an overview of how cells can react to external mechanical signal, as well as how cells can apply forces themselves and how these cellular forces can be detected. It will become clear how important the interaction between cells and their environment is, especially in the context of cancer. Therefore, the differences between healthy and cancerous tissues and cells will be outlined.

2.1 Cells

Cells are the smallest unit of life. They form the building blocks which tissues, organs and eventually whole animals such as humans are composed of. However, cells do not only build up complicated constructions, they are a complex and dynamic system themselves. They are only a few micrometers in size, but consist of many different cellular organelles (Figure 2.1), all having their own important duty [9]. In eukaryotic cells such

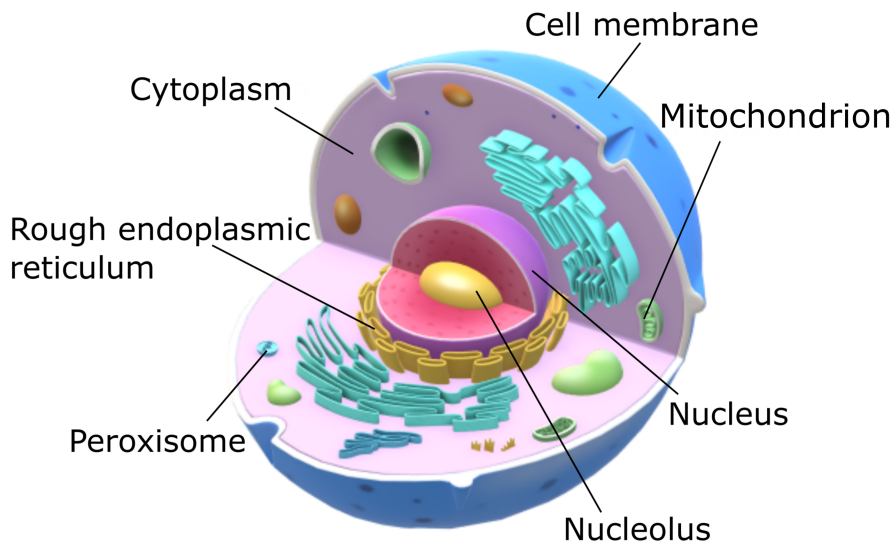


Figure 2.1: Structure of an animal cell.

as animal, plant or fungi cells, one of these organelles is the nucleus, which is made up of its own building blocks with the nucleolus being the biggest one [10]. The nucleus protects and regulates the deoxyribonucleic acid (DNA). The DNA carries genetic information with nucleotides forming a double helix, which can be transferred into messenger ribonucleic acid (mRNA), in a process called transcription. mRNA is transported into the cytoplasm and then decoded and translated into proteins by ribosomes in the rough endoplasmic reticulum. The whole process from DNA to protein is referred to as biosynthesis [11]. Other examples for cell organelles are peroxisomes which are responsible for the degradation of toxic molecules and mitochondria, the “powerhouse of the cell”, in which most of adenosine triphosphate (ATP), a storage molecule for chemical energy, is generated [12]. However, mitochondria are also known for regulating metabolism, cell cycle and cell death [13]. The whole cell is encapsulated by a lipid bilayer, the cell membrane. The cell membrane contains a variety of proteins which are especially important for transport and signalling, as well as cell adhesion [14].

Cells are able to divide into two daughter cells by going through a process called cell cycle. The cycle of an eukaryotic cell, is divided into four different phases, namely G₁ phase, S phase, G₂ phase and M phase [15]. During G₁ phase, the cell grows in size and increases the number of organelles. DNA replication takes place during S phase (synthesis phase), while during the following G₂ phase, cell growth continues and mechanism check if the cell is ready for the M phase in which cell division is carried out. During the M phase, mitosis (division of the DNA) and cytokinesis (division of the cytoplasm including its organelles such as the nuclei and the cell membrane) take place. The newly formed two daughter cells contain the same genetic information.

2.1.1 Cellular cytoskeleton

Another important organelle of the cell is the cytoskeleton, which is responsible for the mechanical stabilisation of the cell and its external shape. It is composed of three main components: actin filaments, microtubules and intermediate filaments. All three proteins are dynamically polymerised and depolymerised from individual monomers [16]. The possibility of rapid growth or disassembly of these polymeric structures allows the cell to react flexibly and quickly to changes in its environment [17]. These changes can affect the shape of the cell, migration behaviour or protein expressions [18, 19]. This is possible as the cytoskeleton also serves as a transport scaffold for the transmission and control of many intracellular signals and therefore can influence the transcription of specific genes [20, 21].

In terms of mechanical stability of the cell and cellular reactions to mechanical stimuli, Actin in particular seems to be important [22]. Actin is crucial for cell contractility and matrix reorganisation, as experiments of cells cultured in 2D and 3D cell culture platforms show. Here an treatment of cells with agents that perturbed actin, disrupted force generation [23].

Actin filaments consist of two helical strands of polymerized actin (F-actin), which

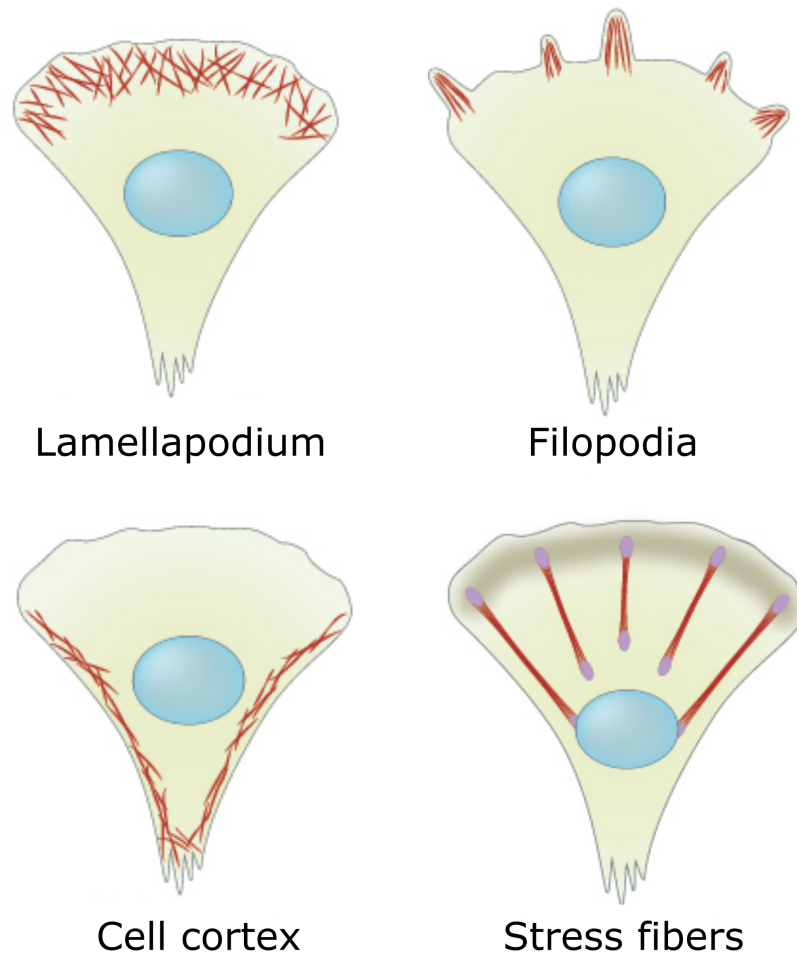


Figure 2.2: Actin formed structures within the cell (modified from [24], licensed under CC BY-NC 4.0.)

are composed of globular monomers (G-actin) [25]. In the presence of ATP, actin is constantly polymerised at one end, which is called barbed end, and depolymerised at the other end, referred to as pointed end [26]. If the rates of assembling and disassembling are the same, the term treadmilling is used. The flexible actin structures can be organised in linear bundles, 2D networks and 3D gels, as shown in Figure 2.2 [27]. An example for branched and crosslinked 2D networks in cells is the lamellopodium, which polymerises against the cell membrane at the leading edge of cell movements and therefore is the main motor for cell migration [28]. Filopodia, on the other hand, are parallel aligned bundles of actin and play an important role in cell adhesion and migration in the absence of lamellopodium on soft substrates [29]. Actin structures are also known to maintain and change the cell shape, by underlying the cell membrane with a thin layer of a 3D

network, called the cell cortex. The cell cortex is involved in cellular processes such as morphogenesis, mitotic cell rounding, cytokinesis and cell migration [30]. Additionally, densely bundled and ordered F-actin structures form, together with the motor protein myosin II and cross-linking proteins, so-called stress fibres. Stress fibres connect the cell cytoskeleton to the extracellular matrix through focal adhesions and are able to sense mechanical forces as well as they are involved in applying cellular forces [31]. It becomes evident how many diverse intracellular tasks the actin cytoskeleton is involved with and how important it is for communication between the cell and its environment.

2.1.2 Extracellular matrix

The natural microenvironment of cells is the extracellular matrix (ECM), as shown in Figure 2.3. Cells are surrounded by a three dimensional organised structure which is not rigid and static, but highly dynamic and varies with tissues and age. The ECM influences many important cell behaviours such as proliferation, adhesion, migration, polarity, differentiation, and apoptosis [32].

The matrix composition of the ECM is made out of two major components: ground substances and fibres. The main ground substances are proteoglycans, which have a protein core and glycosaminoglycans (GAGs), such as hyaluronic acid (HA), as side chains. Proteoglycans play an important role in many functions of the ECM, such as trapping and storing growth factors, but are also involved in cell adhesion [33]. The other major component of the ECM, fibres, are divided into structural fibres (collagen

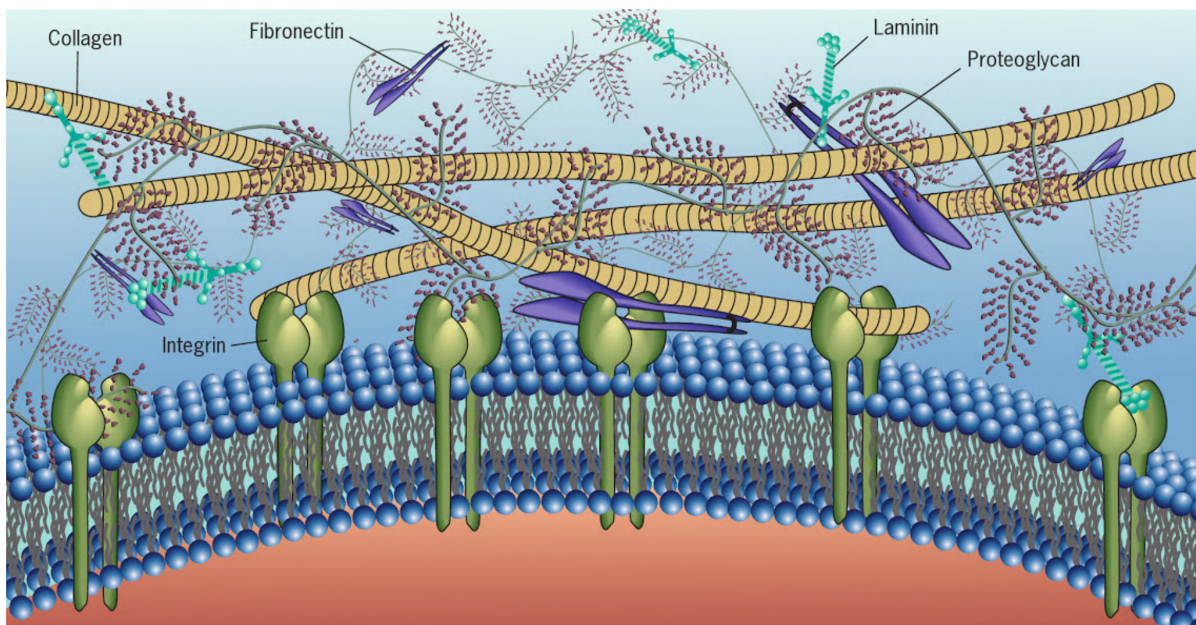


Figure 2.3: Composition of the natural extracellular matrix ([34], license ID 1152790-1).

and elastin) and adhesive fibres (fibronectin and laminin). The structural fibre collagen is the most common protein in the human body with making up to $\sim 30\%$ of all proteins. It is a trimer of helically wound glycoproteins and an important structural support for cells in tissues [35]. Long fibrils of collagen are not only crucial for the tensile strength and the shape of a tissue but also for its microstructural and mechanical properties [36, 37].

The adhesive fibre fibronectin organises the interstitial ECM and plays an important role in cell attachment [38]. Fibronectin can mechanically unfold through the action of external forces and is involved in the cellular binding process to the extracellular matrix. It is thus highly involved in the mechanosensing process of the cell [39, 40]. When cells interact with the ECM they can bind to collagen as well as to fibronectin. Therefore both ECM proteins have cellular binding domains which can bind to cellular adhesion molecules (CAMs), such as integrins, in the cell membrane [36, 38]. These connections are important for many processes of cells, such as applying mechanical forces.

2.2 Cellular forces

The ability of cells to apply mechanical forces on their microenvironment, such as the extracellular matrix and other surrounding cells, is essential for many cellular functions such as differentiation, migration, wound healing and cancer [41–45]. For a physical transfer of cellular forces, a connection between the microenvironment and the cell must be established. For this, CAMs in the cell membrane serve as anchor points. CAMs are proteins which generally have three domains. An intracellular domain which interacts with the cytoskeleton, a transmembrane domain, and an extracellular domain which can bind to other CAMs or ECM ligands. A classification of CAMs distinguishes into two superfamilies, the calcium dependent CAMs, such as cadherins and selectins which are associated with cell-cell adhesion and integrins, and the calcium independent CAMs, such as immunoglobulin CAMs [47]. Integrins mediate interaction between cells and ECM ligands, including collagen and fibronectin, and they are also involved in converting mechanical stimuli into molecular signals in a process called mechanotransduction which will be further explained in the next Section 2.2.1 [22].

Integrins have two conformational states. When integrins are inactive, the non covalently bound glycoproteins of the α and β subunits lie together and adhere to one another in a bent shape. In this state, there is only a low-affinity integrin-ECM binding as shown in Figure 2.4. When integrins are activated, the extracellular domain unfolds, the contact between the subunits breaks and the chains move apart, which leads to a high binding affinity [48]. The activation of integrins can happen in either direction across the cell membrane. In the case of an “inside-out activation”, regulated binding of proteins to the cytosolic end of the integrins take place. If ECM proteins such as fibronectin bind to the the extracellular side of integrin, the activation is referred to as “outside-in” activation. In either case, if integrin is activated, the talin binding site of the β subunit is exposed.

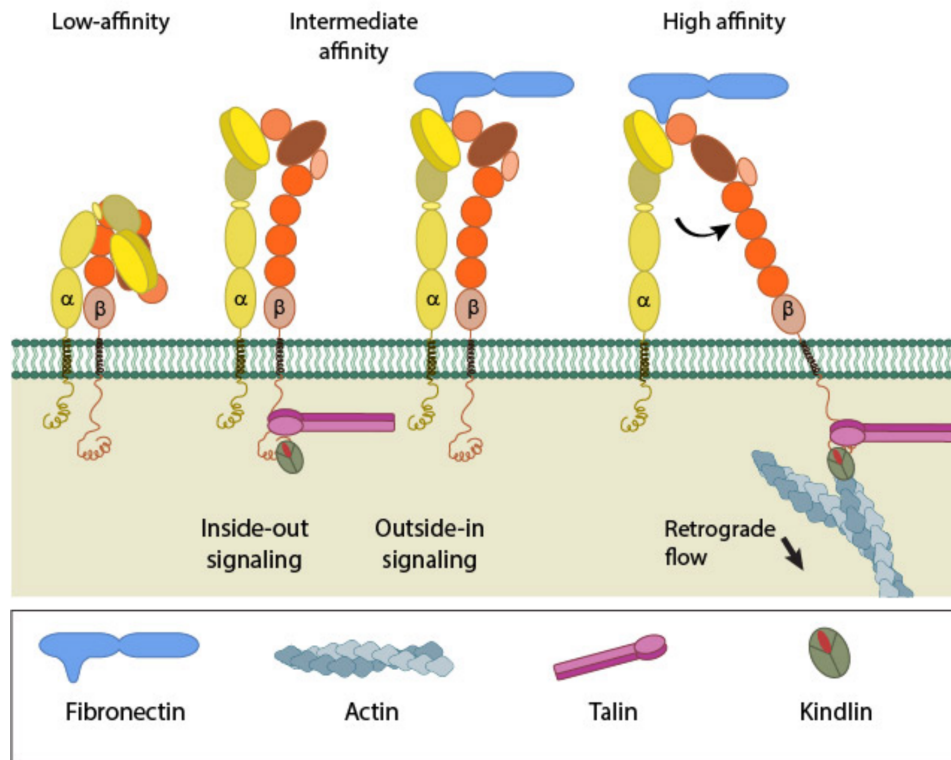


Figure 2.4: Activation of integrin by either an “inside-out” or “outside-in” activation (modified from [46], licensed under CC BY-NC 4.0.).

Binding of talin and kindlin inside the cell leads to an assembly of actin filaments, and allows a force application to the point of attachment to the ECM [48, 49]. As integrins lack an direct actin binding site, they are normally part of a complex protein formation called focal adhesions, which consists of many different proteins such as talin, vinculin, tensin, α -actinin, paxillin, src and focal adhesion kinase (FAK), to link the actin cytoskeleton to the ECM [50].

However, the formation of focal adhesions and their binding to the ECM alone is not sufficient for the cells to exert forces. In order to clarify and better understand the mechanism behind the transmission of forces from cells to the microenvironment, the molecular clutch model was developed. The idea behind that model and its historical development was nicely summarised by Elosegui-Artola et al. [51]. The background of the model is that during cell migration, the actin containing, leading edge protrusions are polymerised against the plasma membrane. Together with myosin induced contractility, this leads to a retrograde flow, due to the dynamic depolymerisation at the pointed end of the actin fibres. Only if the actin filaments are engaged through anchorpoints to the ECM, the retrograde flow is slowed down and can lead to traction forces and a forward movement of the cell (Figure 2.5). The forces applied by these clutches are variable and depend on the organisation of actin structures and if the clutch is only partly or fully

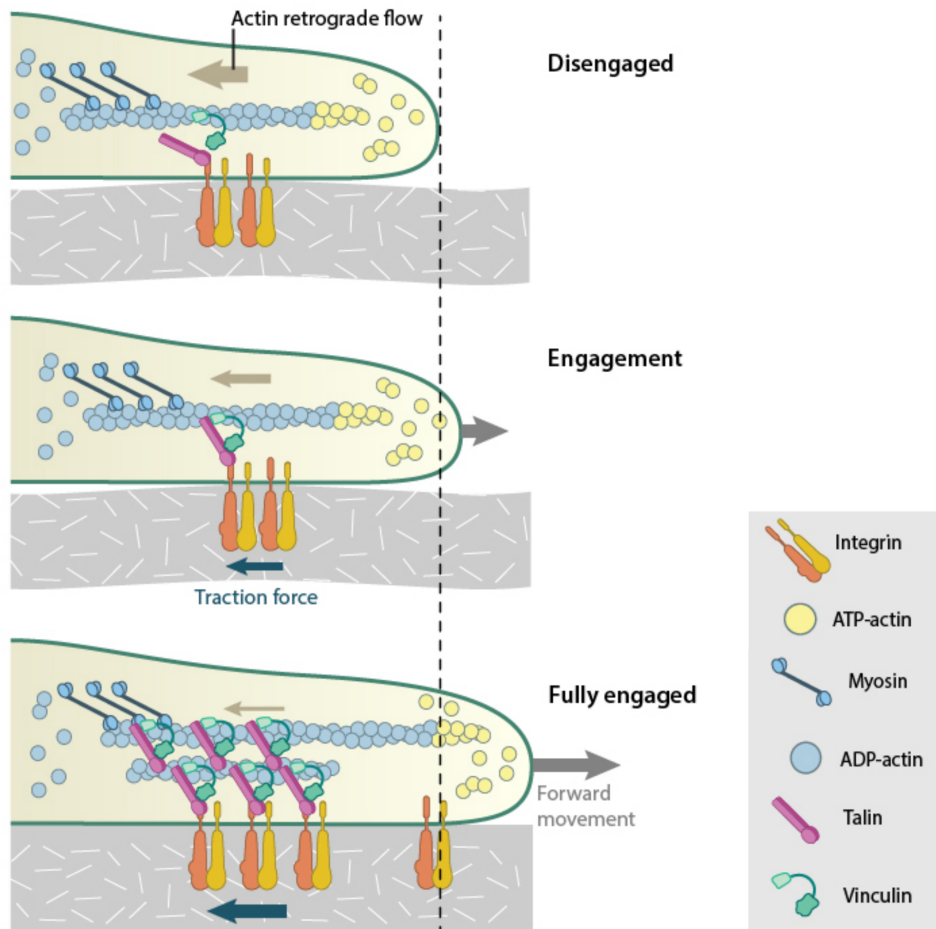


Figure 2.5: The molecular clutch model, as an explanation for cellular force application, during different states of engagement (modified from [52], licensed under CC BY-NC 4.0).

engaged [51, 53]. However, the mechanosensitivity is mainly controlled by the force loading rate, which depends on substrate rigidity and speed of retrograde flow. This mechanism described in the molecular clutch model does not only enable the cell to sense mechanical properties of its microenvironment but also to tune and change the microenvironment by applying a force itself.

2.2.1 Mechanotransduction

The process of cells sensing mechanical properties of the microenvironment and then translating them into a biological response is called mechanotransduction. The mechanotransduction process starts at the cell membrane with proteins such as integrins. The

activation of integrins and the resulting binding between the cell and the ECM does not only allow the cell to apply forces as explained in the last section, but is the first step in a signalling process which results in physical responses of the cell. These response can be a change in the overall morphology, the (re)organisation of the cytoskeleton, or the migration of the cell. However, these responses do not occur separately, but often simultaneously, and are connected to and influenced by each other.

The cell's ability to respond to external stimuli requires that mechanical signals are converted into intracellular ones, which in many cases leads to a regulation of gene transcription of the DNA and consequently protein synthesis. Two main mechanisms exist behind these cellular conversions: biochemical signalling and direct force transduction [54]. For biochemical signalling, complicated pathways, which are often not fully understood yet, are initiated at the cellular adhesion molecules embedded in the cell membrane. In the case of focal adhesions, it is believed that the proteins of the complex can be divided into two modules. A structural module (including talin, vinculin and tensin) which senses mechanical stimuli and a signalling module (including FAK and paxillin) which are directly involved in mechanosignalling cascades [55]. Commonly, in signalling cascades in the cell, proteins activate or deactivate each other by transferring phosphoryl, also referred to as phosphorylation. Many biomolecules are involved in these signalling cascades, which allows overlaps of the pathways of cellular responses to different triggers. An example is the central Hippo pathway which, beside many other functions, links signalling cascades activated by the ECM with the ones activated by cell-cell contacts [56, 57]. These complex interrelationships allow the cell to react in a differentiated way to external influences.

Even though biochemical signalling is highly flexible, it is a slow process as it relies on diffusion of molecules and therefore leads to a cellular response on a time scale of minutes to hours. Direct force transmission, on the other hand, can lead to reactions of the cell within seconds [54]. For example, Mitrossilis et al. found that cells react to changes in the substrate stiffness by applying traction forces in less than a second [58]. Forwarding these mechanical signals inside the cell is possible due to the cytoskeleton and its physical properties. Furthermore, direct force transmission is involved in regulation of genes, as nucleus and cytoskeleton are directly linked to each other and mechanical stress can lead to a physical deformation of the nucleus [59]. The role of the nucleus during mechanotransduction is complex and it is often not easy to discern whether the nuclear reactions are at the beginning or the end of a force induced cellular response. However, three mechanisms were proposed for nuclear mechanotransduction [60]. First, induced force can lead to conformational changes or phosphorylation of nuclear proteins [61]. Second, mechanical stretching of the nucleus can induce opening of the nuclear pore complexes and therefore facilitate transport of proteins into the nucleus [62]. Third, deformations of the nucleus can initiate DNA reorganisation, including modifications of the histone proteins they are wrapped around [63].

In most cases of mechanotransduction, an external applied force activates both mechanisms, biochemical signalling and direct force transmission, so that the cell can respond

to the stimuli on different time scales [54].

2.2.2 Influence of the microenvironment on cellular forces

Mechanotransduction allows the cell to react to changes in the microenvironment. As already mentioned, the actin cytoskeleton plays an important role in the process of mechanosensing and mechanosignalling within a cell. On the other hand, organisation and distribution of actin in a cell can be altered by the microenvironment, too, such as on stiff substrates or in defined volumes [64]. In cells on stiff substrates, actin fibers get more numerous, are more organised and align parallel to each other [65]. The consequence is a polarisation of the cell and an adjustment of a cell's shapes with a change in substrate stiffness. A more rounded shape of cells was observed on soft materials, while a stiff substrate led to a more spread out cell and thus to a larger spreading area [66]. How far reaching the effects of substrate stiffness on the differentiation of mesenchymal stem cells can be was shown by Engler et al. [41]. They found that soft (mimicking brain tissue), stiff (mimicking muscles) and rigid (mimicking bones) cell culture substrates led to a differentiation of the cells into neurogenic, myogenic and osteogenic lineages.

Additionally, stiffness of the cell culture substrate influences cell migration, as cell migrate towards stiffer substrates in a process called durotaxis [42]. However, besides mechanical properties of the microenvironment, migration speed also depends on geometrical (such as topology) and chemical factors (such as ligand density) [67, 68].

Since cells have to exert forces to migrate, it is only logical that traction forces are also influenced by the microenvironment. While most investigations were able to see a correlation in between increasing substrate stiffness and an increase in cellular traction forces [66, 69, 70], Oakes et al. on the other hand, suggested that traction forces solely depend on spreading area. They proposed that substrate stiffness and focal adhesion density have little effect on the work done by the cell on the substrate [71]. The independence of traction force from focal adhesion density would fit the observations of Califano and Reinhart-King, that higher ligand density on the substrate leads to higher spreading area and higher traction forces but the applied force per area stays the same independently of the ligand density [66]. However, to clarify which physical properties of the microenvironment influence cellular traction forces the most, and to test if several effects can overwrite each other, an experimental set-up in which all these parameters can be controlled independently of each other is necessary for a systematic investigation.

2.2.3 Available methods for cellular force measurements

To measure cellular forces, a variety of methods has been developed. They can be divided into two main categories: active stimulation methods (such as the atomic force microscopy (AFM) or tweezers) and passive force methods (such as micro-engineered platforms or traction force microscopy) [72]. While active stimulation methods can

apply an active force to the cell and measure its reaction, passive force methods are not invasive and therefore measure passively the forces cells apply. An overview of the methods developed, the main advantages and disadvantages, as well as the traction force measurable with each method, are shown in Figure 2.6. The principles behind an AFM will be explained in detail in Section 3.3.2 in the context of cellular force measurements, it should be mentioned that the AFM can measure mechanical properties of the cell by “pushing” a cantilever onto the cell membrane and measuring force-distance curves. Additionally, the cantilever can be modified with a particle (e.g. a protein or another cell) at the end and then be used for “pulling” experiments to test the adhesion between the cell and the particle [73].

Tweezing methods for cellular force measurements include optical and magnetic tweezers. Optical tweezers use a highly focused laser beam to trap a small particle due to the interaction between the light intensity gradient and the particle. This particle can be a coated polystyrene bead which binds to a cell membrane. By controlling the position of the bead, a force can be applied to the cell in one direction while a known force is applied to the opposite direction [74]. However, the biggest advantage of optical tweezers is the ability to measure forces inside the cell [75], such as the force applied by the cargo carrying, motor protein kinesin [76]. The concept of magnetic tweezers is similar to the one of optical ones, but uses an magnetic field instead of light to control the bead trapped. Magnetic beads can be twisted and therefore apply a force on the cell. This method can determine mechanical properties of the cell and help to investigate mechanotransduction [77, 78].

To passively measure forces cells apply to their environment, a variety of platforms had been engineered. One of the most common platforms includes pillars made out of a silicon elastomer (polydimethylsiloxane, PDMS) which are covered with a protein and on which cells can be cultured. Cells can bend these pillars by applying a force and by using Hooke’s law and knowing the material properties, the force can easily be calculated [8, 79, 80].

Traction force microscopy is the other widely used group of cellular force measurement methods. The origin of traction force microscopy are the experiments of Harris et al. who visualised cellular forces on a thin elastic rubber substrate by wrinkles caused by the cell. Wrinkles, however, are hard to analyse and therefore traction force microscopy in 2D was developed. Here, fluorescent beads embedded in a gel are tracked and their displacements indicate the strength of the applied cellular forces. The principles of fluorescence microscopy will be explained in detail in Section 3.3.4. Traction force microscopy exists in 2D and 3D. While in most cases, the hydrogel polyacrylamide is used for 2D measurements, for 3D measurements cells are embedded in a collagen matrix [45, 81]. By using collagen gels 3D measurements have the advantage of measuring cellular forces of cells who are embedded in non-linear elastic material, which is closer to the native environment than linear elastic polyacrylamide gels. However, this means calculation of the forces is more complicated and stiffness of the cell environment can not be changed without simultaneously changing ligand density and density of the gel the cell

is embedded in [82].


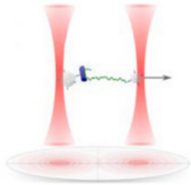
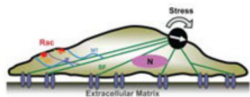
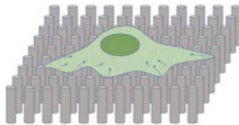
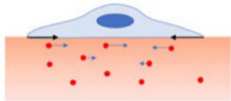
Mode	Technique	Sketch	Typ. force range	Strengths/limitations
ACTIVE	AFM		5 pN ÷ 10 nN	<ul style="list-style-type: none"> ✓ Wide force range –well established technique × Direct contact with the specimen otherwise tip must be labeled
	TWEEZING OPTICAL		0.1 ÷ 100 pN	<ul style="list-style-type: none"> ✓ High sensitivity ✓ Wide force range × Heating issues
	MAGNETIC		0.01 ÷ 100 pN	<ul style="list-style-type: none"> ✓ High sensitivity ✓ Wide force range × Custom equipment – little standardization
PASSIVE	MICRO-ENGINEERED PLATFORMS		10 ⁻¹² ÷ 10 ⁻³ N	<ul style="list-style-type: none"> ✓ Different designs translate into extremely wide force range ✓ Stability, scalability of manufacturing process ✓ Sophisticated microfabrication procedures/facilities
	TRACTION FORCE MICROSCOPY		2 ÷ 120 nN	<ul style="list-style-type: none"> ✓ Widespread (needs standard lab equipment) ✓ Easily coupled with microscopy equipment (i.e., fluorescence/confocal) ✓ 2D/3D measurements × Computationally demanding × Non-linear behavior of ECM-mimicking hydrogels

Figure 2.6: Overview of different methods for measuring cellular forces (modified from [72], licensed under CC BY 4.0). (AFM sketch adapted from [83], optical tweezing sketch adapted from [84], magnetic tweezing sketch adapted from [77].)

2.3 Cancer

2.3.1 Ovarian cancer

Ovarian cancer is one of the most lethal gynaecological diseases with over 300,000 new cases in 2020 worldwide [85]. It has a 5 year survival rate of 45% [3]. However, the survival depends greatly on the stage of the cancer at the time of detection. While a diagnosis of ovarian cancer at an early stage has a 5 year survival rate of 92%, the survival rate decreases to 5% at an advanced stage [86]. The lack of early detection markers and the unspecific symptoms such as fatigue and bloating are the main reasons for these poor survival rates, as 70% of patients are diagnosed at an advanced stage of the disease [86]. However, even after a successful therapy, the post-treatment recurrence rate of ovarian cancer is 70% within 18 month [86]. This makes ovarian cancer the fifth leading cause of cancer-related deaths in women [87].

The term ovarian cancer does not stand for a single disease but includes heterogeneous subtypes which have in common that they appear in the ovary but can differ in many other characteristics. Ovarian cancers are divided into three main types, depending on the tumour's origin within the ovary. These types are sex-cord-stromal, germ cell and surface epithelial tumours, with epithelial tumours being the most common one representing 85-90% of the cancers detected. Epithelial tumours are further classified into histological subtypes, such as high grade serous, low grade serous, endometrioid, clear cell and mucinous histotypes [88]. Cells of these subtypes differ with regard to migration speed and metastasis potential [89].

2.3.2 Cancer microenvironment

Tissues including their components such as cells and the ECM can change during various events. The process of ageing, for example, becomes particularly visible through a changed structure of the skin surface of a person. The soft, firm skin of a child contrasts with the wrinkles and lines of aged skin. However, not only the part of tissue visible from the outside changes with time, the components and composition of tissues vary as well. For example, the concentration and cross linking of collagen fibres is enhanced in aged tissue ECMs. This leads to less elastic and weaker properties of aged tissue in comparison to young tissue [38]. As the probability to get afflicted with them increases with age for many cancers, it seems reasonable to assume that the changes in the ECM may favour or even trigger cancer development [90].

The tumour microenvironment is a complex structure which contains cancer cells, non-cancer cells, growth factor and ECM proteins, among many other components [91]. However, not only chemical and biological parameters are altered in cancer microenvironment, but physical parameters differ from a healthy microenvironment, too. A tumour is a lot stiffer and has a higher cell density than normal tissue [92]. Normal

ovarian tissue for example has a stiffness of 4.33 kPa (including discrete localized areas of 35.88 kPa) [70], while stiff high-grade serous ovarian cancers tumours with up to 120-140 kPa and even soft tumours of stiffnesses not higher than 60 kPa, are much stiffer [93]. These differences of tumour stiffnesses are affiliated to mesenchymal and non-mesenchymal tumours, respectively, whereby especially mesenchymal tumours are associated with poor survival rates.

In healthy ovarian tissue collagen is organised in long fibrils which are arranged parallel to the epithelial boundary. In the cancer microenvironment, however, collagen fibrils are much shorter and thicker and tend to point perpendicular to the epithelial boundary, resulting in an increase in stiffness, similar to changes of the ECM during ageing [94]. In addition, the presence of collagen enhances cell migration of ovarian cancer cells [95]. Another critical promoter for cell migration and invasion of ovarian cancer cells is fibronectin. Overexpression of fibronectin is an indicator of poor patient prognosis, and blockage of it decreases adhesion, invasion, proliferation and metastasis of ovarian cancer cells [96, 97].

While most fibrous proteins of the ECM, such as collagen, fibronectin and laminin, are upregulated in a tumour microenvironment, many proteoglycans are downregulated [94]. However, hyaluronan is one of the exemptions, as changes of its concentration are associated with tissue reorganisation and correlated with tumour grade and metastasis [98]. This is plausible, as hyaluronan binds and regulates the distribution of fibronectin fibrils [99].

Apart from the altered ECM components, a wide variety of enzymes exists which influence the cancer microenvironment. Especially matrix metalloproteinases play a major role by remodelling the ECM, promoting tumour growth and metastasis and therefore promote cancer progression [94]. While both the enzyme and the ECM side of cancer microenvironment play a huge (and interrelated) role in determining tumour cell fate, the ECM with its mechanical properties is more important in the scope of this work.

2.3.3 Differences between cancer and healthy cells

The cancer microenvironment is not the only component of a tissue that changes during cancer development. Cancer cells themselves differ in significant characteristics and behaviour in comparison to healthy cells. In this context Hanahan and Weinberg proposed six biological hallmarks of cancer [2]. They include that cancer cells can replicate indefinitely and escape cell death (apoptosis). They are bigger than healthy cells and can evade growth suppression, leading to enhanced cell proliferation. Cancer cells are able to induce angiogenesis, the process of forming new blood vessels, to supply a tumour with oxygen and nutrition. And cancer cells are able to actively invade other tissues and metastasis through the body. In addition to these hallmarks it is also known that cancer cells are softer, have a different migration velocity and are less polarised than healthy cells [67, 100–102]. The latter was recognised by Kushiro et al. by showing that cancer cells are able to climb 90 degrees walls while non-cancerous epithelial cells can not [102].

They proposed that the loss of geometrical recognition of cancer cells is correlated to their increasing cancer malignancy. An enhancement of metastatic potential of cancer cells was also found with an increase in substrate stiffness of cell culture platforms and higher traction forces [70, 103]. For ovarian cancer cells a higher translocation of YAP1 (an oncogenic transcription factor associated with aggressive metastatic ovarian cancer) into the nucleus and disaggregation of multicellular spheroids (a behaviour associated with metastasis) had been detected [70].

3 Methodology background

To investigate cancer cells and how they are influenced by the microenvironment, the establishment of an experimental set-up for single cell analysis is an advantage. This design has to meet some fundamental requirements such as being biocompatible and stable in liquid and at 37°C over several days. To measure cellular forces, the materials used for the substrates needs to be soft enough that forces applied by a cell can be detected and analysed. To investigate how characteristics of the microenvironment such as stiffness, available volume and shape, protein concentration and cell-cell contacts influence cellular behaviour, an experimental set-up is needed in which these parameters can be controlled independently of each other. For this work, a fabrication process for protein patterned and microstructured polyacrylamide gels for cell analysis was developed and established, meeting all the above criteria. To fabricate these cell culture substrates, various methods and steps are needed. Before each of these individual steps is described in detail in Section 4, background information of the respective methods is given in this chapter to provide the reader with a better understanding. The fabrication process of protein patterned and microstructured polyacrylamide gels for cell culture is highly interdisciplinary and covers state of the art methods and principles of different fields such as microengineering, chemistry, biology and physics. The same applies to the analysis process, where in addition a basic understanding of image analysis is required to understand the methods used in the presented work. To get an overview of how the methods work, what the basic ideas are and what parameters can be adapted, the principle of each method will be explained.

3.1 Fabrication of protein patterned and microstructured polyacrylamide gels

To fabricate a protein patterned and microstructured hydrogel for cellular force measurements, a method has been established which combines the principles of **μ -contact-printing** with microstructuring and nanoimprinting. Figure 3.1 diagrammatically shows the steps followed in this fabrication process. **Optical lithography** is used to achieve a photoresist pattern on a silicon wafer. The photoresist serves as a mask for a silicon etching process performed with an **inductively coupled plasma reactive ion etching** set-up. The process yields silicon moulds with an array of pillars with diameters of 10-60 μm and a depth of 8 μm . After removal of the photoresist, the moulds are used for a **μ -contactprinting** technique where a PDMS substrate covered with a

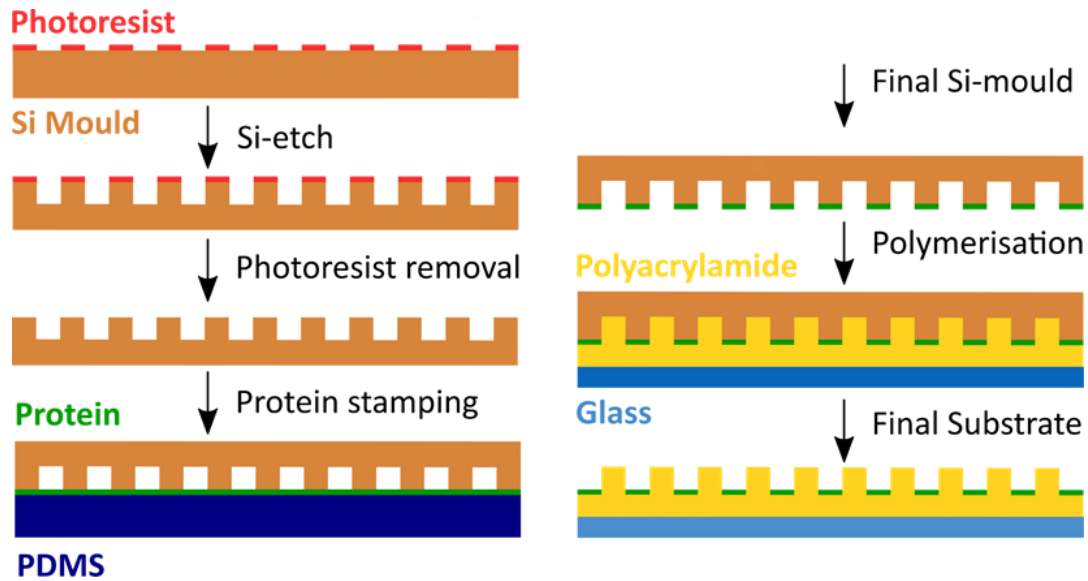


Figure 3.1: μ -contact printing method for structuring and patterning of polyacrylamide gels.

protein serves as a stamping pad. The structured silicon mould retains protein when it is pressed onto the protein coated substrate. The etched and protein patterned silicon mould can be used to **microstructure** a **polyacrylamide gel** on a glass substrate during polymerisation. The final protein patterned and microstructured hydrogel can then be used as a substrate for **cell culturing** and for the investigations of cellular responses due to changes of the microenvironment. The following sections provide details of the principals relating to each step of the fabrication process.

3.1.1 Optical lithography

Optical lithography is a technique to replicate, define and fabricate patterned structures on a substrate, called wafer. It is accurate down to the micron scale dimensions [104]. Optical lithography is widely used in the semiconductor industry for fabricating microelectronics devices such as transistors [105]. The most common wafer material is silicon (Si) which is cheap and easy to process. The first step in the fabrication process is to apply a thin photoresist layer on a silicon wafer. Two main types of photoresist exist, dry film photoresists and liquid photoresists. Depending on the type of photoresist, different techniques are used in the application process. Dry film photoresists are laminated onto the silicon wafer by using a controlled degree of pressure, temperature and speed [106]. Often, a laminator is used to achieve uniform and reproducible conditions. The most common application process for liquid photoresists is spin-coating. For this purpose, the Si-wafer is spun rapidly while the viscous photoresist solution is dispersed on it to

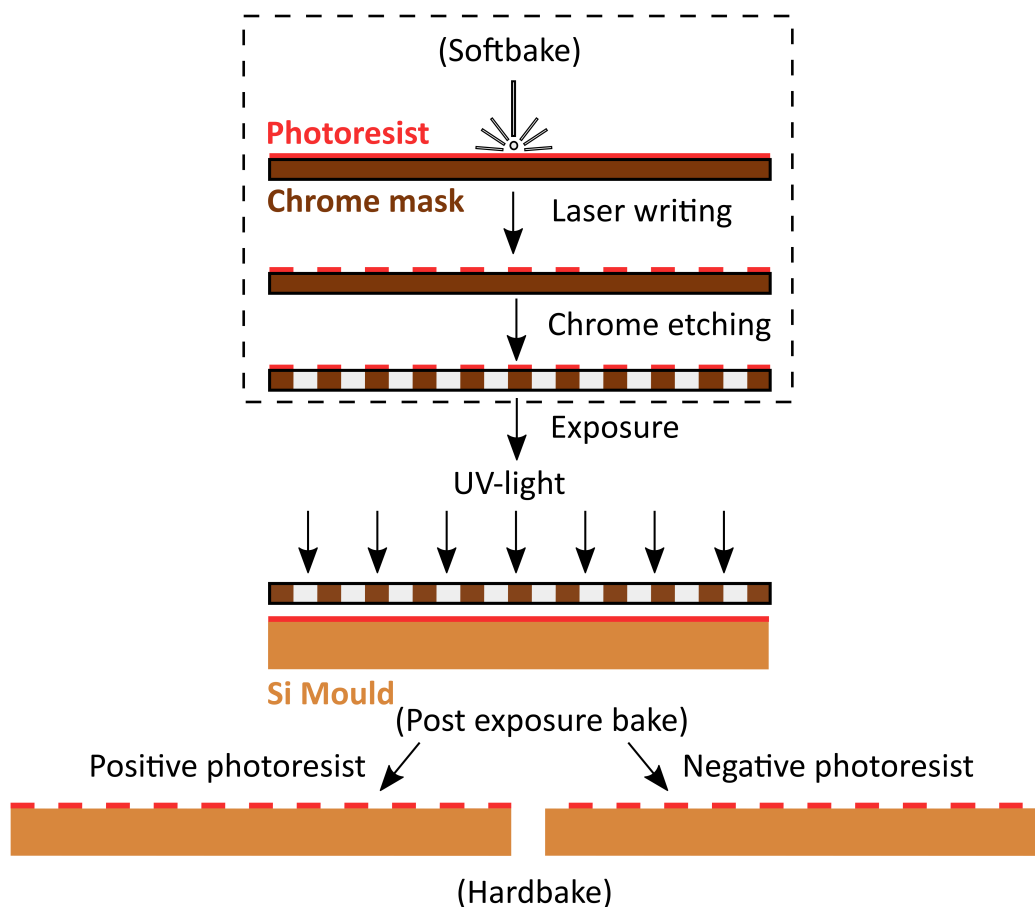


Figure 3.2: Lithography process for positive and negative photoresists including mask preparation (in dotted lines).

achieve a uniform layer with a defined thickness. The thickness of the layer of photoresist can be determined by varying the rotation speed and time during the spin-coating process. Photoresists are light sensitive and become chemically altered during exposure of UV-light. Depending on the photoresist, either exposed (positive photoresist) or unexposed (negative photoresist) areas are dissolved and removed by a developer during the developing step. The choice of developer solution and time depends on the material and thickness of the photoresist layer. To achieve a certain pattern in the photoresist two options are available for selective illumination during UV-light exposure. It is possible to either write a design directly into the photoresist by using a laser, or to use a chrome mask and a large scale UV-light for transferring a design onto a substrate as illustrated in Figure 3.2. While direct laser writing is easy to apply and a straightforward approach, it is often worth investing time into mask fabrication, especially if multiple Si-wafers with the same design are needed. Masks allow a fast pattern transfer with

exposure time of a few seconds, depending on the photoresist thickness, while the direct laser writing can take a few hours, depending on the complexity and size of the designed pattern. For chrome mask preparation, commercial chrome masks covered with a layer of photoresist are used. A laser mask writer then writes the designed pattern on the photoresist, which is developed afterwards. The resulting photoresist pattern serves as a mask during the chrome etching of the chrome mask. While chrome is simply etched away in the area where photoresist had been removed by the developer, it will remain in areas still covered with photoresist. This process is followed to fabricate the final chrome on glass mask with the required pattern for the following lithography steps. Before using the mask for further fabrication steps the rest of the photoresist is removed.

Several techniques exist to improve the micropatterning process. First of all, the whole process is highly sensitive to contaminants such as dirt. This is the reason why the process described should be performed in a cleanroom and wafers are first cleaned in a two-step washing procedure with isopropanol and acetone. It is also critical to get a good adhesion between the Si-wafer and the applied photoresist. Pure silicon is hydrophobic and binds well to hydrophobic photoresists, but due to reactions with water molecules in the air, pure silicon is normally covered with a thin silicon dioxide layer about 2 nm thick, when stored at room temperature and in air. The silicon dioxide layer is hydrophilic and therefore degrades binding properties to the photoresist. To regain stronger adhesion, various methods are available. It is possible to bind a chemical compound such as hexamethyldisilazane (HMDS), which forms hydrophobic tri-methylated silicon dioxides. Another way of promoting adhesion is to remove the silicon dioxide layer of the wafer before applying the photoresist. This is possible by breaking the OH-bonds using heat, or by etching the silicon dioxide layer away with an etching process. Additionally, a variety of other baking steps exist to obtain better results [107]. For removing the remaining solvent concentration of the photoresist, a softbake step can be added after the coating step, and is always needed in the case of spin-coating application of photoresist. This process prevents sticking of the Si-wafer to the chrome mask, improves photoresist adhesion to the Si wafer and prevents altering of the photoresist during thermal stress such as caused by dry etching. The post-exposure bake is performed after exposure but before development. The step is often required for a better crosslinking of negative photoresists and can be used for mechanical relaxation of thick photoresist layers to avoid cracks. It is also possible to apply a baking step after development, called hardbake. A hardbake can increase the thermal, chemical and physical stability of the photoresist which may be necessary for a subsequent etch process.

As already mentioned, a Si-wafer with patterned photoresist can be etched to form deeper structures or it can be used directly as a mould, for example for PDMS devices. PDMS devices are useful tools for Lab-on-a-chip or microfluidic applications [108, 109]. The whole process used to produce PDMS devices is called soft lithography.

3.1.2 Inductively coupled plasma etching for structuring silicon

Etching is the process of removing materials, for example for structuring a substrate during a pattern transfer process. This can be done by either a wet-etching or a dry-etching process [110]. For the wet-etching process a solution of chemicals is used to dissolve the surface atoms of a substrate (Figure 3.3 A). For Si a common choice is potassium hydroxide (KOH). The process of wet etching is reliable, but has the disadvantages of most chemicals used being toxic and the etching process being isotropic, leading to curved edges (called undercutting) instead of straight sidewalls. The dry-etching process on the other hand uses gases instead of liquids [111]. Two techniques can be applied to etch a material with gases, chemical etching and physical etching [112]. For chemical etching, reactive gas molecules, such as radicals, bind specifically to atoms of the substrate material and the bound atoms are then released into the gas phase. The principle behind this process is the same as the one behind the wet etching process leading to similar advantages and disadvantages. For the physical etching process, ions are bombarded

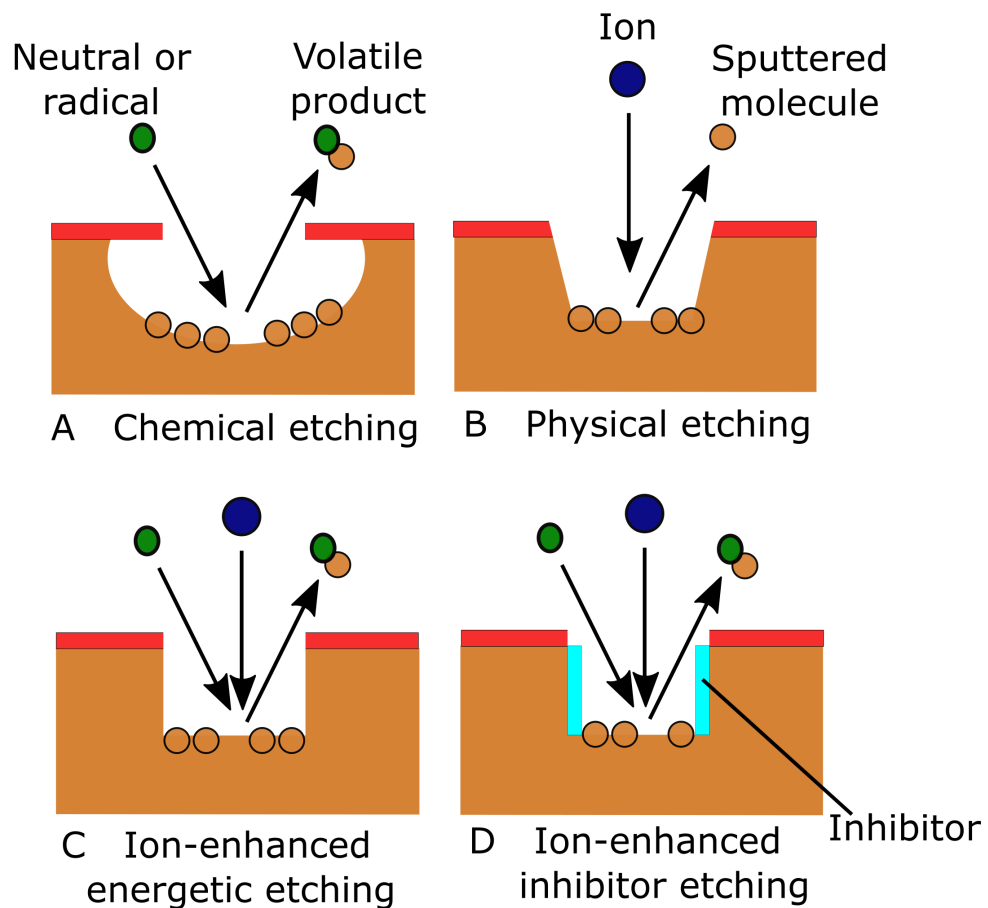


Figure 3.3: Principles of the etching processes.

onto the surface of the substrate, removing atoms by transferring kinetic energy and knocking out small pieces of the material (Figure 3.3 B). Physical etching or sputtering is highly anisotropic but not material specific. As a result, every surface exposed will be removed, the mask as well as the substrate. This can lead to a plain etched substrate without a patterned structure. Ion-enhanced energetic etching combines both, chemical and physical etching (Figure 3.3 C). Here, reactive etchants and energetic ions are used to modify the substrate surface. The release of reactive species bound to surface atoms into the gas phase can be blocked by lattice energies of the substrate. Energetic ions can help to set off these byproducts by transferring energy. To achieve higher anisotropic etching and steep sidewall profile, a passivation of the sidewalls is possible (Figure 3.3 D). The process is then called ion-enhanced inhibitor etching and allows the etching of high aspect ratio structures. Passivation can be achieved by a passivation gas in the reaction chamber which forms a protective coating along the vertical sidewalls [113]. For dry etching a plasma needs to be generated. Plasma is an ionised gas containing ions, electrons, radicals and neutral atoms. For etching processes, just partially ionised gases are used, where less than 1% of the gas molecules are ionised. A high frequency (HF) electromagnetic field induces the plasma by ionising the gas molecules at a low

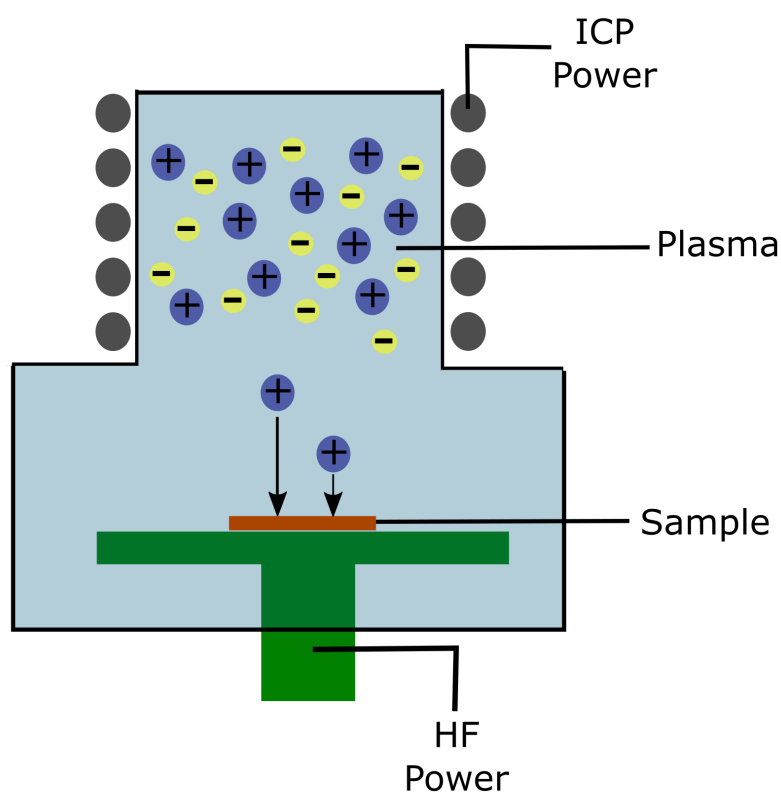
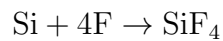


Figure 3.4: Design of an inductively coupled plasma (ICP) etching set-up.

pressure (vacuum). For capacity coupled plasma modes (CCP), the wafer is placed on an electrically insulated holder, which becomes negatively charged by the electrons moving with every oscillation of the electrical field. The positively charged but much slower ions in the gas become accelerated by the high voltage between the highly charged sample and the gas, which is slightly positive charged due to a lack of electrons. In CCP mode the voltage level for producing ions and accelerating them is the same. A further development in dry etching processes is the usage of an inductively coupled plasma (ICP) etching system (Figure 3.4). ICPs have two power sources. One feeds an anode outside the gas chamber which induces the plasma (ICP power) and the other power source is connected to the anode the sample is placed on (table bias). This means the density of ions and the ion energy are controlled independently, improving the anisotropic characteristics of the etching process and increasing etching yield.

For dry etching of the commonly used substrate material silicon, sulphur hexafluoride (SF_6) is widely used as an etchant for the chemical etching process [114]. In a plasma, SF_6 forms single fluoride atoms. Four of these fluoride atoms (F) can bind to a Si atom and form volatile tetrafluorsilane, SiF_4 which is pumped out through the pumping system, the resulting chemical reaction is:



To achieve an anisotropic etching, passivation of the sidewalls by a layer of difluorocarbene, CF_2 is possible. Therefore, CHF_3 can serve as a supply for CF_2 . For the physical etching of silicon, noble gases such as argon or helium are commonly used [113].

3.1.3 Polyacrylamide fabrication

Polyacrylamide (PAA) is a synthetic polymer of acrylic acid (AA) and a hydrogel. Hydrogels are crosslinked polymers which can take up water without dissolving. They need to remain hydrated to maintain their structure and mechanical properties [115]. In biochemistry, polyacrylamide gels are primarily used for the separation of proteins and nucleic acids by gel electrophoresis (PAGE) [116]. However, the polymer network can also be used to produce cell culture substrates of different elasticities, which makes it possible to study cell behaviour that depends on mechanical substrate properties. Elastic properties of polyacrylamide gels can be easily adjusted by changing the ratio of cross-linking bis-acrylamide (bis-AA) to acrylamide [117]. Radical polymerization of acrylamide needs to be started by a radical initiator, which can be a chemical one or a photoinitiator activated by UV light. Photoinitiators are chemical compounds that decompose in a photolysis reaction after absorption of UV light and thus create reactive species [118]. A chemical system for a reproducible gel polymerisation is a combination of ammonium peroxide sulphate (APS) as a starter and tetramethylethylenediamine (TEMED) as a catalyst. Without the bis-acrylamide crosslinker only linear polyacrylamide chains would form. Only the addition of bis-acrylamide will lead to the formation

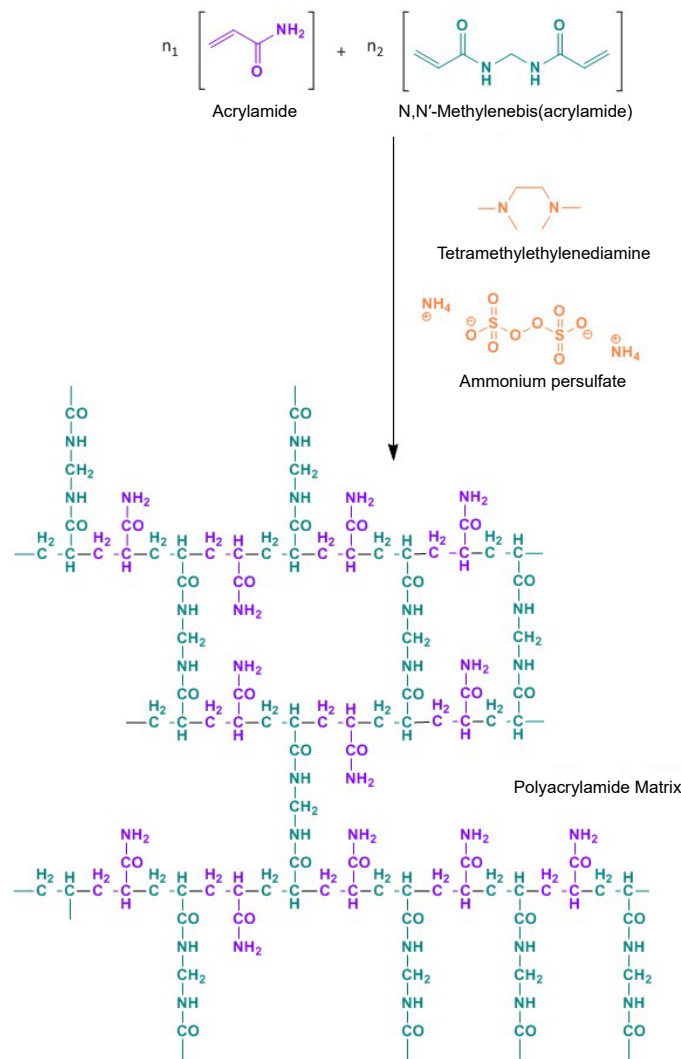


Figure 3.5: Reaction scheme of the radical polymerization of polyacrylamide gels. (Courtesy of Dr. Helen Nöding.)

of the net-like structures which cause the elasticity of the gels (the corresponding reaction scheme is shown in Figure 3.5). Radical polymerisations are highly sensitive to oxygen, as oxygen can quench essential radicals during the gel formation process [119]. Polyacrylamide gels are linear elastic and isotropic, which means stress increases linearly with strain and material properties are independent of direction [120]. They can be characterised by a single parameter: their Young's modulus, E , the ratio of stress to strain. These characteristics simplify the analysis process of gel deformation caused by external forces, such as those initiated by cells.

As polyacrylamide gels are non-adhesive to cells, they need to be coated with a protein for cell culturing. There are two main approaches to achieve protein binding to the gel:

by direct surface functionalisation of the polymerised polyacrylamide gel using sulfo-SANPAH (sulfosuccinimidyl 6-(4'-azido-2'-nitrophenylamino)hexanoate) crosslinkers or by binding acrylic acid N-hydroxysuccinimide ester into the hydrogel during polymerisation [117, 121]. Sulfo-SANPAH contains an amine-reactive N-hydroxysuccinimide (NHS) ester, which effectively binds proteins, and a photoactivatable nitrophenyl azide group, which can bind to the polyacrylamide surface. Acrylic acid N-hydroxysuccinimide ester has the same binding group for proteins, however the acrylic acid part binds directly into the polymer network during polymerisation. While sulfo-SANPAH is used to cover the whole hydrogel, Acrylic acid N-hydroxysuccinimide ester (AA-NHS-ester) can bind to the protein before polymerisation, which makes it suitable for patterning techniques such as μ -contact printing [122].

3.1.4 μ -Contact printing for protein patterning

Patterning a surface is one method to control properties of a substrate for different applications such as biosensors and tissue engineering research [123, 124]. In terms of biological applications, protein patterning of hydrogels for cell culturing is of particular interest [125–127]. By changing the available area cells can attach to, the number of cells in one place can be controlled from single cells to multiple cells [128, 129]. To achieve such a pattern, a non-adhesive substrate is needed, which most synthetically produced hydrogels are. Adhesive patterns formed by coating are often made from proteins such as collagen or fibronectin. These proteins are part of the natural cell environment (the extracellular matrix, ECM) *in vivo*, and mimic a natural cell environment better than a glass or plastic surface of a standard petridish [122]. Several methods exist for transferring proteins from a surface onto the gel. The material properties of the substrate, such as surface charges, are important for transferring the protein. It needs to be able to bind the protein well enough when it first is covered with it but needs to be able to release the protein again during polymerisation of the hydrogel. If the material is used during an oxygen-sensitive polymerisation, such as one involving polyacrylamide, it additionally needs to be impermeable to oxygen. For patterning 2D polyacrylamide, a protein patterned glass substrate is commonly used to bring the protein in contact with the gel surface. Therefore the glass substrate needs to be patterned first. Either a lift-off or a μ -contact printing technique can be used to achieve this patterning as shown in Figure 3.6 [130, 131]. For the lift-off process, photoresist patterned silicon wafers are incubated with polymer brushes (Figure 3.6 A). PLL-g-PEG for example is a copolymer with a poly(L-lysine) backbone and polyethylene glycol side-chains that can be used for passivation of a surface. After the photoresist is removed (lift-off), non-coated areas on the surface can be backfilled with a protein and the patterned glass employed for polymerisation. μ -contact printing contains only three steps (Figure 3.6 B). A patterned silicon master is used to fabricate a PDMS mould which is covered with the protein. The PDMS mould then serves as a stamp and is placed on a glass substrate. The result is a patterned glass substrate suitable for polymerisation. Besides biological

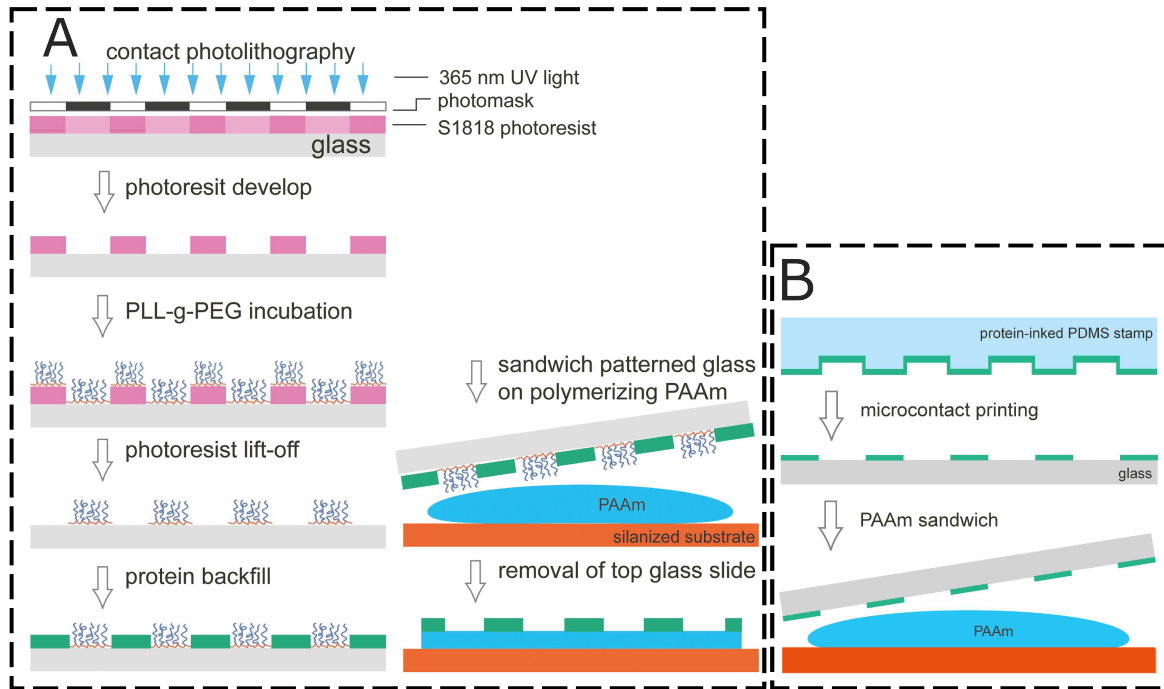


Figure 3.6: Lift-off (A) and μ -contact printing (B) techniques for patterning glass slides for polyacrylamide gel polymerisation (modified from [130], licensed under CC0 1.0).

applications, μ -contact printing has also been widely used for patterning metal surfaces with self assembled monolayers [132]. The monolayers can be used as a mask for wet etching processes and are therefore a cheap and easy alternative to lithography methods.

3.2 Cell experiments

Cell culturing is the process in which cells are cultured in a laboratory outside their native environment [133]. The environment cells are cultured in *in vitro* is controlled and normally includes a specific cell medium with essential nutrients and an incubator with a constant CO_2 concentration and a defined temperature (37°C in the case of mammalian cells). Cell culturing simplifies the highly complex system of a whole organism to considerably less but still complex system of one or several cells. It is a good model system for fundamental research in science and medical studies. As well as saving time and resources, it makes it possible to reduce the number of ethically difficult *in vivo* experiments in living animals. External influences such as substrate properties, the number of cell contacts and the presence of drugs can be controlled during cell culture studies. For example, the investigation of cancer cells *in vitro* can help to understand why and

how cancer occurs (including the triggering mechanism), how it develops and by which factors it is influenced [134, 135]. This is especially important for cancer types such as ovarian cancer, which often show no or unspecific symptoms during development.

A wide range of cell lines have been isolated for cell culture systems, including the human ovarian cancer cell line SKOV3 used in this work. SKOV3 is a cell line derived from a 64 year-old Caucasian female and is positive for many of the antigens used to identify cancers of epithelial origin in clinical practice [136, 137]. The cell line is suitable for investigating problems and peculiarities associated with ovarian cancer, such as the often late diagnosis of the disease [134].

3.3 Analysis

3.3.1 Optical profilometer and scanning electron microscopy for analysing silicon moulds

A profilometer is an instrument for measuring topographical features of a sample's surface [138]. To measure these profiles either stylus profilometers or optical profilometers can be used. Stylus profilometers use a moving probe in physical contact with the sample to analyse its surface. A force feedback mode maintains a constant force between the probe and the sample during the scanning process. Probe material, size and shape influence the measured information and can limit the resolution. The physical detection of the surface is extremely sensitive, which provides high resolution measurements of the surface roughness especially in z-direction, but makes it susceptible to alterations of the probe or sample. By contrast, optical profilometers use the wave properties of light and the ability of waves to interfere to gain the surface information of the sample and are therefore contact free [139]. Different shapes, roughness or heights of a sample will lead to different interference patterns, which in turn provides information about the structure of the object under investigation. Coherence scanning interferometry is the most common method to obtain this information, with visible light used for measurements. In this method, the location of interference fringes of the interference patterns are analysed. Depending on the profilometer, interference fringe phases may be evaluated too. Optical profilometers are easy to operate and have the advantage of allowing fast, large area measurements to be performed, without any sample preparation needed. The main disadvantage is that optical profilometers can only operate in air and not in liquid as they need a reasonably reflective surface. The consequence is that images of silicon moulds can be taken, but not of hydrogels such as polyacrylamide gels, as these need to be kept immersed in liquid.

Another method to investigate the structure of a surface is scanning electron microscopy (SEM) [140]. Scanning electron microscopes use a focused beam of electrons to scan the sample surface. The electrons interact with the atoms of the surface, producing signals such as secondary electrons (SE), reflected or back-scattered electrons (BSE), charac-

teristic X-rays and transmitted electrons. These signals include information about the surface, structure and material properties of the sample. For most SEMs, the measurements need to take place under vacuum to avoid collisions of electrons with molecules in the air. As samples absorb some of the electrons they need to be conductive to be measurable. Nonconductive samples can accumulate charge resulting in scanning faults and other imaging artefacts. To scan nonconductive samples these need to be coated with a thin layer of metal or another conductive material. While SEM is often used for analysing surfaces and structures of semiconductors such as silicon, the method is again not suitable for hydrogels, as these need to be measured in a hydrated state which cannot be maintained in vacuum.

3.3.2 Atomic force microscopy for analysing mechanical properties of hydrogels

The atomic force microscope (AFM) is a microscope which can image nano-scale structures by utilising attractive and repulsive forces between atoms [141]. These forces can be van der Waals forces, electrostatic forces or chemical forces. A laser beam is deflected at the surface of a cantilever and the reflected beam then is detected by a four quadrant detector (Figure 3.7 A). The cantilever bends if its tip gets close to or in contact with a surface. As a result, the laser beam is reflected at a different angle and a displacement of the signal of the laser beam is observed at the detector. For measurements of surface structures as well as mechanical properties of the sample, first a calibration is necessary. Therefore a calibration measurement on a well-characterised stiff substrate such as glass is carried out to set the correct relationship between the bending of the cantilever and the force expended. For force calculation, the spring constant of the cantilever has to be known, which can be determined by the thermal noise method [142]. In this, thermal fluctuations are used to oscillate the cantilever and to detect the resonant frequency. By scanning an object with the cantilever an image up to atomic resolution can be constructed depending on the cantilever tip used. The AFM is a high resolution technique, but it is limited by the maximum displacement of the built-in piezos in all three dimensions. It follows that only objects which do not exceed certain dimensions can be examined. To determine mechanical properties of a sample, force distance curves can be recorded with an AFM [143]. To measure this, the tip approaches the surface, contacts with the sample (contact point), bends until a defined criterion is fulfilled before the cantilever is retracted again and the tip is removed from the surface. The force exerted can be plotted against the amount of indentation to produce a curve such as the one shown in Figure 3.7 B. The criterion before retraction can be a maximum force, maximum laser deflection or maximum z-piezo voltage, and is called the triggerpoint. The resulting force distance curves can be evaluated using a model generated fit. Often the model of Bilodeau, which uses Hertzian contact mechanics as a basis, is used.

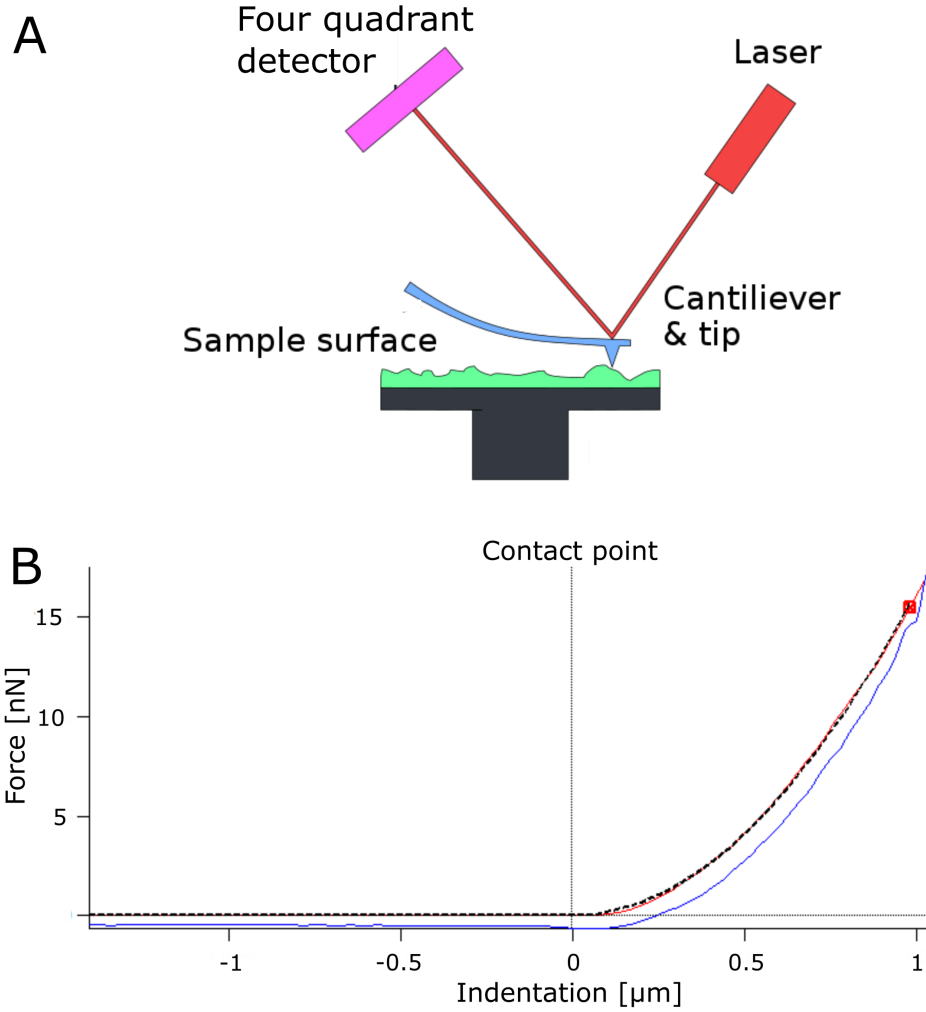


Figure 3.7: A) Principle of an AFM ([144], licensed under CC0 1.0) and B) Force distance curve (approach red, retrace blue, fit (using Hertzian contact mechanism) dotted).

The Hertzian contact mechanism describes the contact of two elastic spherical bodies, whereby it is assumed that the halves of the sphere are infinitely large, homogeneous and friction-free [145]. Bilodeau further developed this idea for the indentation of a four-sided pyramid, which describes the tip geometry for pyramidal cantilevers [146]:

$$F = \frac{3E \tan \Theta}{4(1 - \nu^2)} \delta^2$$

Where the force F depends on the Young's modulus E , poisson ratio ν , indentation depth δ and opening angle Θ of the pyramid.

3.3.3 Confocal laser scanning microscopy for analysing fluorescence labelled structures

If a fluorophore is excited with a photon, energy is absorbed which raises an electron from its energetic ground state S_0 to an energetically higher state S_1 of the same spin known as the Franck-Condon principle [147]. The dwell time of the electron in this state is known as its lifetime and is in the nanosecond range for fluorescence. The energy released during the spontaneous return of the electron to the ground state is emitted as electromagnetic radiation. However, energy is also converted into vibrational energy during the excitation and emission process and therefore the wavelength of the emission is longer than the excitation one. This is known as Stokes shift and must be considered when multiple fluorophores are used within the same measurement, as an overlap of emission and excitation wavelengths can lead to image distortion and false signals [148]. Despite the possibility of this cross-correlation of dyes, fluorescence is a powerful tool, especially for protein analysis, as it allows the labelling and tracking of small particles. The fluorescent labelling of biomolecules can be achieved by direct binding of the fluorophore (direct molecule detection) or indirect binding of the fluorophore (indirect molecular detection) [149]. A widely used biochemical method for indirect detection is immunolabelling. Here, a primary antibody binds to the specific antigen of the substance under investigation. This antibody does not fluoresce itself, but enables the binding of fluorescently labelled secondary antibodies. Since several secondary antibodies can often bind to the same primary antibody, a brighter and stronger fluorescence signal can be detected [148].

For observing fluorescence, either an epi-fluorescence or a confocal laser scanning microscope (CLSM) can be used [150]. In a CLSM a laser beam is directed via a dichromatic mirror through an objective lens which focuses the beam onto the sample, as shown in (Figure 3.8). Long-wave light emitted by excited electrons of the fluorescent dye is not reflected by the dichromatic mirror, due to the longer wave length. The light emitted by the sample passes through the dichromatic mirror and can be detected on a light-amplifying detector. A pinhole is located between the mirror and the detector, allowing only the light of one image plane of the sample to pass through. This leads to a focussed and less blurry image since light that originates above and below the focal plane cannot pass the pinhole. The reduction of stray light and the ability of the microscope to scan the sample in the z-direction allows for a high resolution and 3D reconstruction of the sample.

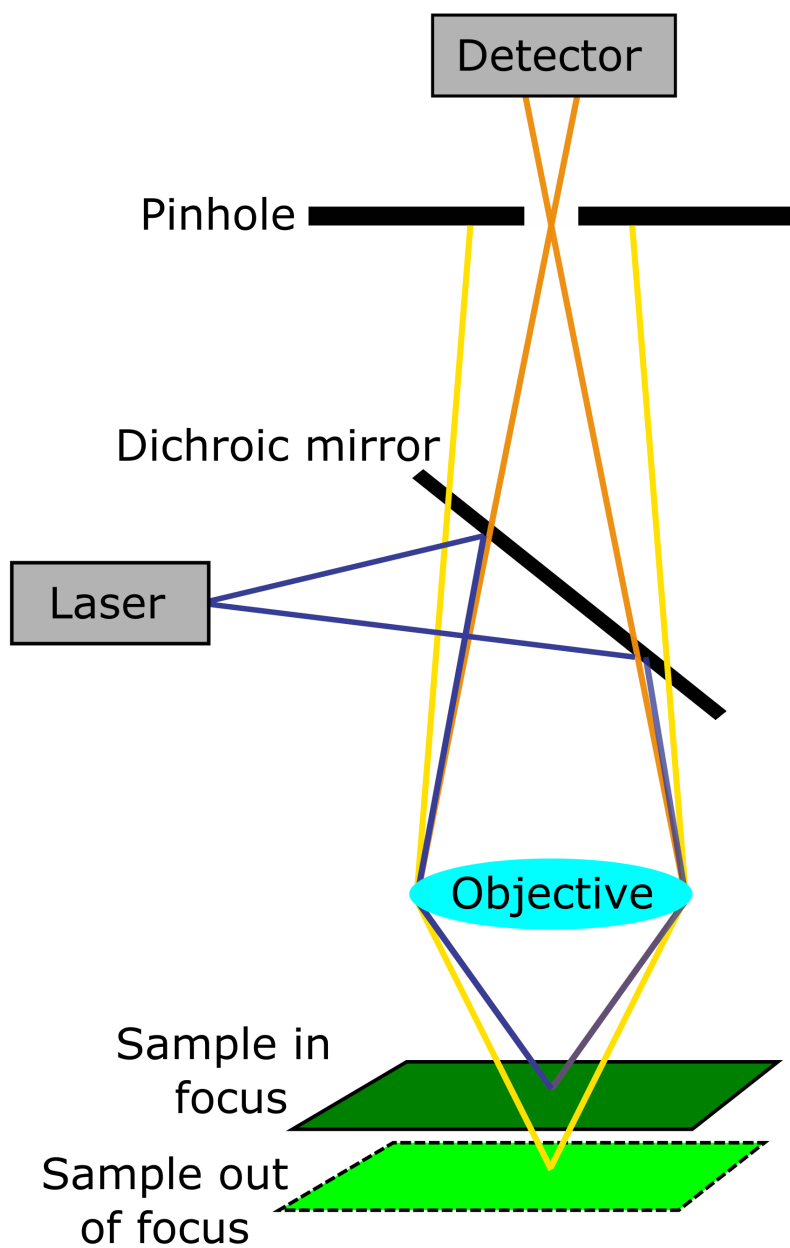


Figure 3.8: Principle of a confocal laser scanning microscope.

3.3.4 Traction force microscopy

Traction force microscopy is a method to measure cellular traction forces [151]. Fluorescent beads are embedded in a soft hydrogel such as a polyacrylamide gel. If cells cultured on these gels apply a force by pulling or pushing the substrate, the beads are displaced as schematically shown in Figure 3.9. Analysing these displacements allows conclusions to be drawn about the forces the cell applied. For capturing data in different layers of the sample, a confocal laser scanning microscope can be used. Normally, pairs of images are taken: one with the cell attached applying a force onto the surrounding environment and one without the cell as a reference. A practical approach to make sure both images capture the same area consists of taking the first image of the cell on the gel with the embedded beads and then adding a chemical for altering, detaching or killing the cell without moving the sample. In doing this, the forces applied by the cell are eliminated and the second reference image can be taken as it is a temporary deformation of the gel and it returns into its original state [152].

To track the displacement of fluorescent beads in the images with and without a cellular force, either particle tracking velocitometry (PTV) or particle image velocitometry (PIV) can be used [152–154]. While for PTV single beads are analysed, PIV divides both images of a pair into smaller regions, known as *interrogation windows*, and compares these windows [155]. Single bead analysis in PTV has the disadvantage that individual beads are difficult to distinguish, which can quickly lead to misinformation. This is particularly important in the context of beads moving in the z-direction and going out of focus, as the appearance or disappearance of beads reduces the accuracy of the method. In comparison, interrogation windows in PIV cover more than one bead and a cross-correlation algorithm analyses the shift of the whole window [156]. This leads to higher accuracy than the PTV approach, but also to a lower resolution, as the displacement of the area of an interrogation windows (and therefore the movement of several beads) is represented by a single velocity vector. A good compromise between accuracy and resolution is to choose the size of the interrogation window so that there are 4–5 beads covered [155]. For PIV, two approaches exist to find the correlation peak of two images. It is possible to either use the conventional cross-correlation method using two interrogation windows with the same size, or a template matching method for which a bigger search window is compared to a smaller interrogation window. The template matching method ensures that beads in the smaller interrogation window are tracked correctly even with large displacements [157]. Another improvement is the usage of iterative PIV. Here, a series of PIV analyses are run in a row. The first run uses a big interrogation window size, while for subsequent iterations the size of the interrogation windows (and the corresponding search windows) is reduced with each run. The results of the preceding correlation run are used to build a predictor displacement field. This displacement field is used as a guidance for the next iteration of PIV. This approach allows a progressive refinement of the window size and at the same time compensates step by step for disturbances which can occur in smaller scale iteration [158].

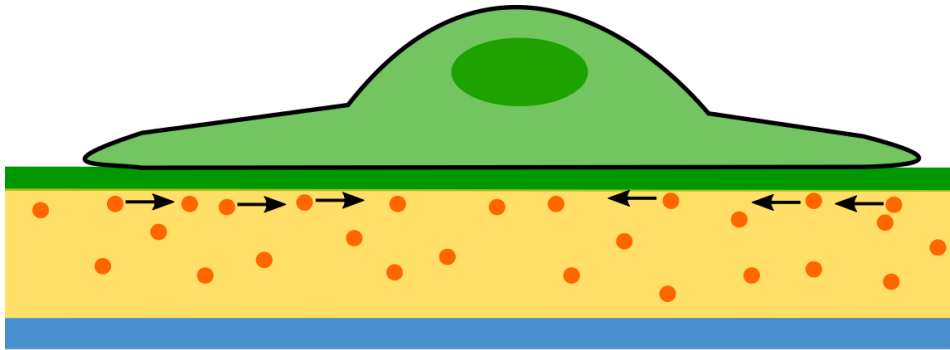


Figure 3.9: Principle of traction force microscopy. A hydrogel (yellow) on a glass substrate (blue) is covered with a protein layer (green) and has orange fluorescent beads embedded. If the cell on top (light green) applies a force, the beads are displaced (black arrow).

As polyacrylamide gels have linear and isotropic elasticity and are homogeneous, Fourier transform traction cytometry (FTTC) can be used to translate the resulting translational displacement field into a force field [152, 155]. Here, the fact is used that the displacement of the fluorescent beads can be described as the convolution of point forces and an elastic Green's function. As a solution for the Green's function, a Boussinesq function, valid for a semi-infinite half space of linearly elastic substrates, can be used [159]. To extract estimates of the forces from the displacement field, a deconvolution is necessary. While this is highly complex in real space, it is much easier in Fourier space as the deconvolution becomes a simple division [160]. As the linear system in Fourier space is now an ill-posed problem (a problem with more than one solution, or with a solution discontinuously depending on the data), it is very sensitive to small changes of the displacements. To stabilise the results of the estimated forces and to reduce the effect of noise in the displacement data, a regularisation factor can be added to the solution [161]. The ImageJ (Fiji) FTTC plugin needs only the PIV displacement field, the pixel size of the image, the elastic modulus and poisson ratio of the gel and the regularisation factor to translate the displacement field into an force field [155]. FTTC is an easy and fast alternative to measure cellular forces in comparison to computationally extensive finite element simulations [162].

Several critical parameters for traction force microscopy exist as summarised by Martiel et al. [155]. One is the size and density of the fiducial markers. If the density is too low, information is lost because gel deformations are not observed. On the other hand, if densities are too high it is hard to track individual beads and their displacements without having overlaps with the information of surrounding beads. The same applies to intercellular distances: short distances between cells make an individual assignment of the forces difficult. Accurate knowledge of the thickness and stiffness of the gel and

the expected range of force is important, as assumptions are made during the analysis process. For FTTC one assumption is that the substrate is half infinite, which is valid if the substrate thickness falls within a suitable range. Another assumption is that gel deformations are small and therefore the stiffness of the gel needs to be chosen depending on the expected force. Image size and quality, as well as the size of the interrogation window and correlation threshold during PIV analysis, and the regularization factor for FTTC are important to obtain reliable data. More information about different approaches towards image analysis including theoretical background [163] and guidelines for finding the right parameters for the analysis process [155] can be found in literature.

4 Materials and Methods

In the previous chapter, background information about the methods used for fabrication and analysis of microstructured and protein patterned hydrogels for cell experiments was presented. This chapter explains in detail how experiments were performed and which chemicals and equipment were used. It describes the individual steps of the fabrication and analysis processes, why a certain method was chosen and how parameters were set. The chapter mentions the challenges which were faced and how these were solved. In addition to the working protocol, it also provides information about processes and methods which could not be established successfully. These are provided to help future replication or adaptation of the experiments. A detailed protocol of the individual steps performed and followed in this work can be found in the appendix without further discussions. This should be of interest to those who want to establish the described experiments and methods themselves.

4.1 Fabrication

Passive pumping of polyHEMA as a first approach of forming a cell culture grid

The first approach for fabricating a structured gel for cell sorting and measuring cellular forces started with the idea of using non-adhesive, biocompatible poly-2-hydroxyethyl methacrylate (polyHEMA). PolyHEMA is commonly used for manufacturing contact lenses and has been established for cell culture experiments [164, 165]. Ye et al. have used polyHEMA for forming cell sorting grids using a passive pumping approach [166, 167]. An attempt was made to adapt this approach for grid formation and then extend it to the measurement of forces applied by cells on the walls of the grid. As it is known, that polyHEMA is non adhesive to cells, it was tried to form an array of holes in a polyHEMA layer on a glass substrate. This would lead to a limited space of uncovered glass for the cell to attach to. To form this grid, a PDMS mould with the designed arrays of holes served as a mask, and capillary forces were meant to fill the grid in between the PDMS structure with polyHEMA as shown in Figure 4.1 A. For the first experiments, polyHEMA solutions made out of three different molecular weights (20,000 g/mol, 30,000 g/mol and 100,000 g/mol) depending on the length of the polymer chain were prepared. Varying concentrations of polyHEMA (10 mg/mol, 30 mg/mol, 50 mg/mol and 70 mg/mol) dissolved in ethanol were used, however only around 20 % of the grids were found to be filled in all cases (Figure 4.1 B). This could be due to the designed channel width or aspect ratio of the designed grid or the fast evaporation rate of

ethanol. It was also noticed that, after a few days in cell culture medium, all fabricated grids dissolved into the medium Figure 4.1 C. It is possible that further crosslinking of the linear polyHEMA chains could have prevented the problem of dissolution. Furthermore, a stamping method where the PDMS stamp is pushed onto the substrate to displace some polymer solution could have replaced the passive pumping approach. However, instead of attempting to optimise the cross-linking process and grid fabrication, it was decided to instead switch to widely used and well characterised polyacrylamide gels. Polyacrylamide has the same properties as polyHEMA of being non-adhesive, biocompatible and stable in media (when crosslinked). Additionally, it is known as linear elastic and isotropic, and protocols of tuning the elasticity for a certain stiffness can be found in literature [117]. The properties of polyacrylamide were found to be more suitable for the intended purpose of cell sorting and cellular force measurements as they simplify the analysis process compared to polyHEMA.

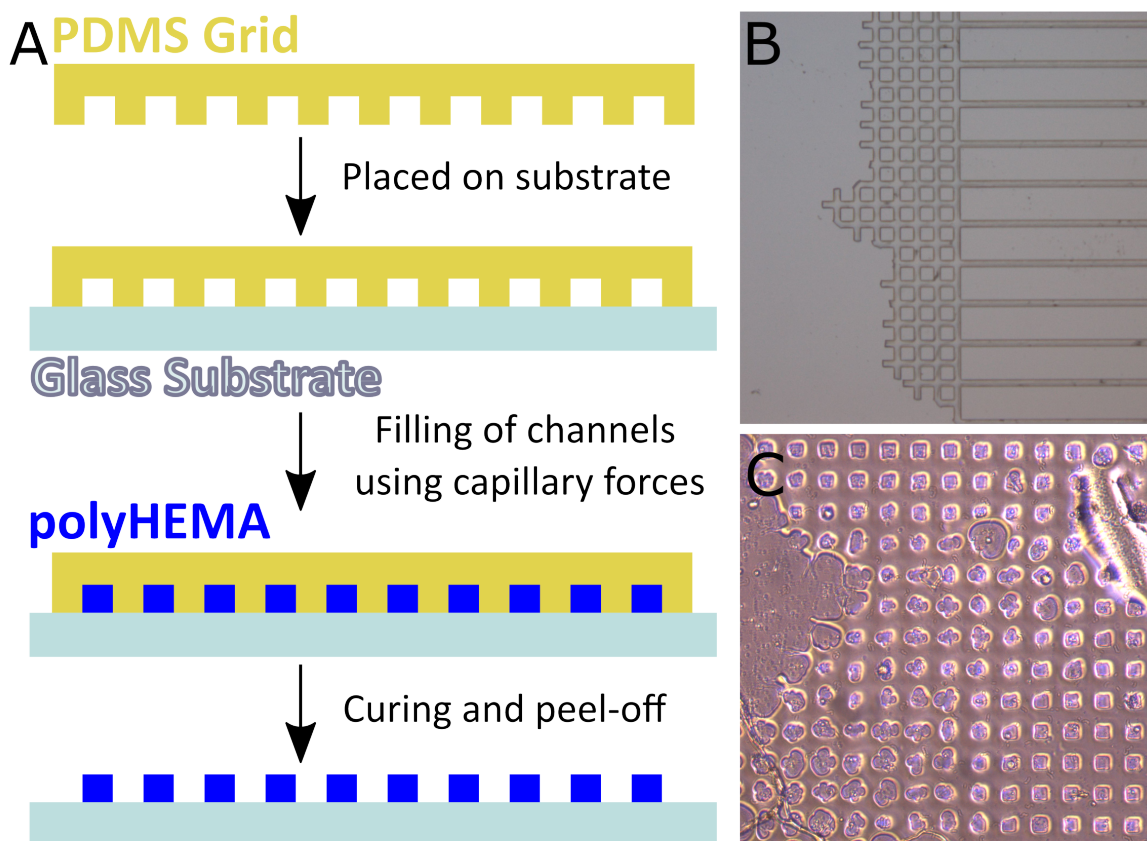


Figure 4.1: A) Passive pumping approach to form a cell sorting polyHEMA structure. B) Partially formed polyHEMA grid using passive pumping. C) PolyHEMA grid (concentration 30 mg/ml, molecular weight 30,000 g/mol) in media after 24 h.

Microstructuring polyacrylamide gels - PDMS is not suitable as a mould material

As polyacrylamide is non adhesive for cells it needs to be covered with a protein before it can be used for cell experiments as already discussed in Section 3.1.3. To form a cell sorting grid in a 3D environment a simultaneously structuring of polyacrylamide gels and patterning of defined areas with a protein is necessary. A few modifications needed to be made to the classical μ -contact printing method explained in Section 3.1.4. μ -contact printing uses soft lithography to form a structured PDMS device, which is then used as a stamp. While PDMS has many advantages, such as being flexible, non-toxic, cheap and easy to handle, it has the disadvantage of being oxygen permeable [168]. As a consequence, it cannot be directly used for combined structuring and patterning of polyacrylamide gels, as the oxygen concentration in the air is high enough to quench radical polymerisation of acrylamide [169]. For the work here, different physical modifications and chemical treatments were investigated to reduce the presence of oxygen molecules to achieve a polymerisation of acrylamide under PDMS (Sylgard 184 Silicone Elastomer Kit mould, Dow Corning). These modifications included treatment of PDMS with an oxygen plasma or curing it for 30 h at 80 °C prior to the experiment. Other approaches involved making PDMS oxygen impermeable by sputtering chrome onto the mould (around 5 nm layer thickness) or excluding oxygen from the polymerisation by using a vacuum. To achieve the latter, PDMS was treated with vacuum for 2 h, before the whole polymerisation experiment was done under vacuum in a desiccator. Chemical treatments were tried as well in form of vapor-coating of PDMS with Trichloro(1 H, 1 H, 2 H, 2 H perfluorooctyl)silane (Sigma-Aldrich, 97 %) or solution-coated with hydroxypropyl methylcellulose (HPMC, Sigma-Aldrich). Acceleration of the polymerisation was also attempted, either by using higher concentrations of catalyst ammonium persulfate (APS, 1:50 and 1:25, Carl Roth) and polymerisation starter Tetramethylethylenediamine (TEMED, 1:500 and 1:50, Sigma-Aldrich) or a photoinitiator (Irgacure 2959; 0.1 % w/v). However, none of these modifications were successful. As it was not possible to polymerise polyacrylamide gels under PDMS substrates, silicon was used instead as the mould material for further experiments. Silicon itself is also cheap, easy to structure and work with and, most importantly, oxygen impermeable.

4.1.1 Preparation of silicon moulds using photolithography and inductively coupled plasma etching

To fabricate microstructured and protein patterned hydrogels, first the dimensions of the wells to trap cells were chosen based on a typical ovarian cancer cell size under study. As spreading diameters of SKOV3 cells in 2D are around 46 μm [170] and cell heights 2.5-3.5 μm [171, 172], circular patterns of the diameters 20 μm , 30 μm , 40 μm and 60 μm were designed. To minimise the probability of cells climbing out of their wells and the uncertainty, how much the height of the cells would change in a more rounded

cell shape, a constant depth of 8 μm was set for all wells.

In the first step of the fabrication process, optical lithography was used to form a Si mould for imprinting a hydrogel. For this, a chrome mask was fabricated, using a mask writer (uPG101, Heidelberg instruments) to write a pattern created in software (L-Edit V16, Tanner) into a photoresist covered chrome mask (Chrome Photoplates with AZ1518, Nanofilm). The mask was then developed in AZ326 MIF developer for 1 min and the chrome was etched with a chrome etching solution (10.9 % ceric ammonium nitrate, 4.25 % perchloric acid and 84.85 % water). Remaining photoresist was removed with acetone and the mask was cleaned with methanol and isopropanol before usage.

A 4 inch Si wafer (4 inch prime grade silicon, Silicon Quest International) and a positive photoresist (AZ1518, Microchemicals) were used for the mould fabrication. The Si-wafer was cleaned with acetone and then isopropanol in an ultrasonic bath for 5 min each. To remove the silicon dioxide layer, an inductively coupled plasma reactive ion etching setup (ICP, PlasmaPro 100 Cobra, Oxford Instruments) was used with the settings 25 sccm SF_6 and 25 sccm Ar high frequency power 10 W, ICP power 1000 W, chamber pressure 5 mTorr for 1 min. The liquid and positive photoresist AZ1518 was spincoated (PWM32, Headway Research, 3000 rpm, 1 min), achieving a photoresist film thickness of approximately 2 μm . A softbake was performed for 90 sec at 90°C on a hotplate, before a mask aligner (MA6, Suess) was used to transfer the designed pattern from the mask into the photoresist covering the Si-wafer. The photoresist was then developed in AZ326 MIF developer for 1 min followed by a hardbake for 6 min at 120°C on a hotplate. The photoresist served as a mask for subsequent Si-etching process performed with ICP. Again, the silicon dioxide layer was removed first (25 sccm SF_6 , 25 sccm Ar, ICP power 1000 W, 30 sec), before the silicon wafer itself was etched (40 sccm SF_6 , 80 sccm CHF_3 , Helium backing 10 torr, high frequency power 50 W, ICP power 1000 W, chamber pressure 15 mTorr, 5:30 min) to achieve 7-8 μm high circular pillars. The photoresist was removed by immersion in N-Methyl-2-pyrrolidone (NMP) for 10 min in an ultrasonic bath, followed by cleaning with deionised water (10 min, ultrasonic bath).

4.1.2 Preparing microstructured polyacrylamide gels

During the fabrication of polyacrylamide gels, the elasticity of the polymerised gel is determined by the concentrations of acrylamide and the crosslinking agent bis-acrylamide [173]. Four different compositions of acrylamide (Sigma-Aldrich) and bis-acrylamide (Sigma-Aldrich) were used to prepare polyacrylamide gels with stiffnesses of 1 kPa, 8 kPa, 30 kPa and 100 kPa as shown in Table 7.1. These stiffness ranges are close to the values of natural ovarian tissue, soft and stiff ovarian tumours which are 4.33 kPa, 60 kPa and 120 kPa, respectively [70, 93]. For casting of the gels, glass cover slips or 35 mm glass bottom dishes for cell culturing (untreated glass bottoms, ibidi) were used as a base. These were hydrophilically functionalised before polymerisation, to achieve an increased adhesion of polyacrylamide gels to the substrate [174]. For this, the glass

surfaces were first treated with an oxygen plasma (Zepto, Diener electronic, 15 min, 0.4 mbar, 20 sccm) before being placed in an ultrasonic bath (5 min) in pure ethanol. The surfaces were dried again and NaOH (250 μ l, 0.1 M, 5 min) was added to increase the general roughness of the glass surface, as NaOH reacts with glass and forms soluble silicates [175]. When removing NaOH, care was taken to keep the NaOH film as thin as possible before adding (3-aminopropyl)triethoxysilane (APTES, Abcr, 100 μ l, 3 min). APTES causes silanisation, by which alkoxy silane molecules bind to the surface [176]. After washing with water (3 times, 10 min), a glutaraldehyde solution (200 μ l, 0.5 %, 30 min, GDA, Sigma-Aldrich) was added to enable cross-linking of the surface molecules. After repeated washing with deionised water (3 times, 10 min) the functionalised substrates were stored dry.

For polyacrylamide polymerisation, APS (1:100) and TEMED (1:1000) were added to the respective acrylamide/bis-acrylamide presolution for the desired gel stiffness. A total of 100 μ l of the solution was poured in the middle of the substrate and the Si mould was carefully placed on top, forming a “sandwich” of glass, presolution and mould. The polyacrylamide gels were then allowed to polymerise for one hour and immersed in PBS overnight at 4°C before the Si mould was peeled off. For characterisation of the depth of structured polyacrylamide gels, orange fluorescence beads (0.2 μ m, orange fluorescent, FluoSpheres, Fisher Scientific) were added to the presolution and sonicated in the ultrasonic bath for 10 min.

Table 4.1: Composition of the polyacrylamide solutions used to prepare gels with defined Young’s modulus.

Young’s modulus, E [kPa]	Acrylamide [%]	Bis-acrylamide [%]
1	3	0.14
8	4	0.25
30	10	0.10
100	10	0.50

4.1.3 Preparing protein patterned and microstructured polyacrylamide gels for cell culturing

As described above, to achieve a structured and protein patterned polyacrylamide gel a modified μ -contact printing method was established. Etched silicon substrates were used for this purpose both as a mould and as a stamp, while flat PDMS substrates served as a stamping pad. For stamping pad preparation, PDMS (Sylgard 184 Silicone Elastomer Kit) and curing agent were mixed 1:10 w:w and degassed to avoid bubbles in the polymer. It is poured into a petri dish and cured at 80°C for one hour in an oven. Before the PDMS surface could be covered with a protein solution, a number of prepara-

tion steps were necessary. For cell culture, proteins were bound into the non adhesive polyacrylamide gels by using AA-NHS-ester. For cell experiments, 5 mg/ml AA-NHS-ester (ACROS Organics, Fisher Scientific) and either 0.5 mg/ml collagen (Collagen I, Bovine, 5 mg/ml, Fisher Scientific) or 0.3 mg/ml fibronectin (Bovine, 1 mg/ml, Sigma Aldrich) were incubated in phosphate-buffered saline (PBS) with a pH of 6.0 for one hour at room temperature. To visualise the protein transfer from PDMS substrates to the polyacrylamide gels, fluorescently labelled gelatine (100 $\mu\text{g/ml}$, fluorescein conjugate, Invitrogen, Thermo Fischer Scientific) was used instead of collagen because of its similar structure and commercial availability. A pH of 6.0 was found to be a critical parameter for the protein transfer, as at a higher pH the NHS-ester can be hydrolysed [177]. Another critical parameter was the additional treatment of the PDMS stamping pads with an oxygen plasma (1 min, 0.4 mbar, 20 sccm) before these were covered with the protein/AA-NHS-ester solution and incubated (1 h, RT). These could be due to the temporary hydrophilisation of the otherwise hydrophobic PDMS surface, after the oxygen plasma treatment [178]. These hydrophilic properties of the surface could improve the binding affinity to the proteins. Afterwards, the PDMS stamping pad was carefully dried with nitrogen. Plain and etched silicon moulds were treated with oxygen plasma (10 min, 0.4 mbar, 20 sccm) before being pressed on the dry protein covered PDMS (10 min, RT). Protruding areas of the silicon mould took up protein during this process and were used for the polyacrylamide polymerisation, as described in Section 4.1.2 and shown in Figure 3.1. It was observed that, if the oxygen plasma treatment of the silicon mould before the stamping step was omitted, silicon moulds were difficult to peel off after the polymerisation and the polyacrylamide could easily be destroyed. Again, this could be due to the change of the surface charge of the Si mould and the altered binding properties to polyacrylamide during or after polymerisation.

Challenging issues establishing a lift-off process

Before the μ -contact printing method had been optimised, an attempt was made to establish a lift-off process for structuring and patterning polyacrylamide gels for cell culturing [130]. Here, the photoresist was not removed instantly from the silicon wafer after dry etching. Instead, the whole surface was covered with a solution of poly(L-lysine)-graft-poly(ethylene glycol) co-polymers (SuSoS). These polymer brushes build a non-fouling, non-adhesive and biocompatible mono-layer [179]. Next, the photoresist, and by extension the polymer brushes on top of it, was removed with NMP. This lift-off process was thought to lead to areas of plain silicon, where photoresist previously had been, and areas still covered with polymer brushes. During the following protein backfill, protein could then simply bind to the plain silicon, while being blocked in the other areas by the polymer brushes. The protein structured silicon moulds were then be used for polyacrylamide polymerisation as described for the modified μ - contact printing method. Unfortunately, the protein transfer step did not work well and cells were observed to either grow everywhere on the gel or nowhere. The first assumption was, that all polymer

brushes were removed during the lift-off process. However, by carrying out experiments with fluorescent labelled gelatine, it was noted that a selective protein transfer was not possible, when HMDS was used for a better photoresist adhesion. When instead a dry etching process of the ICP was applied, for removing the silicon dioxide layer, before applying the photoresist, the protein pattern was visible on the Si mould. This suggests that the HMDS chemically alters the Si surface in a way, that the polymer brushes cannot effectively bind any more. As the exact fault in the procedure of the protein transfer could not be determined and consequently the lift-off technique not be used reliably, μ -contact printing was used for further experiments.

4.2 Cell experiments

Ovarian cancer cells of the cell line SKOV3 were cultured in EMEM with Earle's salts with L-glutamine (Thermo Fisher Scientific) medium and Fetal Bovin Serum (FBS, 10 %, Sigma-Aldrich). Cells were trypsinised with a PBS solution containing 0.25 % trypsin (Bio-west) after 2-4 days and a confluency of 90 %. A stop solution containing equal amount of media and FBS was added and the cell suspension centrifuged for 3 min at 1200 U (270 x g, Hereaus Megafuge 16 R Centrifuge, Thermo Scientific). The supernatant was discarded and the formed cell pellet resuspended in 1 ml media. Cells were then reseeded in a cell culture flask or used for cell experiments. For experiments on polyacrylamide gels, penicillin-streptomycin (1 %, Biochrom) and Amphotericin B (1 %, Biochrom) were added to the normal cell culture medium to eliminate contamination during the experiments. Polyacrylamide gels were sterilised with UV light (30 min, RT) before cells were seeded on them with a density of 186 cells/cm².

Live cell experiments were done with a Keyence Live Cell Imaging Microscope BZ. Usually, experiments were started directly after cell seeding. Images were taken in one spot and as a stack covering 10-15 μ m in the z-direction. This procedure enabled the use of the built-in auto focus function of the Keyence microscope software. It ensured that the right focus level was covered even over a long period of time during measurements, where the level of focus might shift slightly with time. It was ensured that cells could attach without disruption for at least 20 h before other regions of the substrate were investigated. Here 2-4 areas of the polyacrylamide gel were randomly chosen and monitored for further 24 h. All live cell experiments were performed at 37°C and a CO₂ concentration of 5 %. Brightfield images were taken every 5 min.

For cell fixation and staining, cells were fixed after 24 h using a 4 % Paraformaldehyde solution (Thermo Fisher Scientific). Afterwards, the cell membrane was permeabilised with Triton X (Sigma-Aldrich) and washed with HEPES. A blocking buffer (0.3 % Triton X, 5 % BSA in PBS) was used to block all unspecific binding sites. The cellular DNA (Hoechst 33342, Thermo Fisher Scientific), actin cytoskeleton (Phalloidin-iFluor 488 Reagent, Abcam) and vinculin (Vinculin Monoclonal Antibody (7F9), eFluor 570, eBioscience, Thermo Fisher Scientific) were stained in three steps (1 h each). Between

steps cells were washed three times with a washing buffer (0.3 % Triton X, 1 % BSA in PBS).

4.3 Analysis

To demonstrate that the fabrication process for microstructured and protein patterned polyacrylamide gels was suitable, the silicon moulds and polyacrylamide gels were characterised by determining their height, diameter and stiffness. The analysis conducted in the context of traction force microscopy included image alignment, cropping, particle image velocitometry and Fourier transform traction cytometry. Furthermore brightfield images of cells were analysed for brightness fluctuations and the corresponding autocorrelation functions.

4.3.1 Characterisation of silicon moulds and polyacrylamide gels

Silicon mould characterisation

For silicon mould characterisation, a scanning electron microscope (SEM, Raith 150) and an optical profilometer (Profilm 3D, Filmetrics) were used to determine the diameter, height and the steepness of the sidewall profile as well as to image the silicon mould. Five images were taken on each of three samples and were analysed for each diameter using an optical profilometer, in combination with the Profilm software (Filmetrics).

Polyacrylamide characterisation

Analysing polyacrylamide gels can be challenging, due to its high water content and the fact that most measuring techniques are optimised for solids and in air [180]. For this work, polyacrylamide gels were characterised with an optical microscope (Eclipse Ti Fluorescence Microscope, Nikon), a confocal laser scanning microscope (Fluoview 1200, Olympus) and an atomic force microscope (AFM, MFP-3D Origin, Asylum Research). To determine the diameter of the wells, five images each of three samples were analysed for each diameter, using the optical microscope and ImageJ (Fiji) [181]. With the AFM, force maps with 67×67 or 32×32 force curves were taken for every stiffness prepared in this work. A triangular Cantilever tip (MLCT, Bruker, 163.63 pN/nm) for scanning and a commercial Asylum Research software were used to fit the Hertzian model, described in Section 3.3.2, to the force curves to estimate the Young's modulus. An example of such a force map is shown in Figure 4.2. For each sample, four force maps were collected on random location on the gel. For each stiffness at least 1600 force curves were analysed. Measurements were taken the day after fabrication, at the same time the cells would be cultured on the gels. With a depth of the structures of 8 μm , the dimensions of the gels were just on the limit of the range the AFM z-piezo can measure. Due to this some force curves could not be recorded in the lower areas of the gel. An example of such

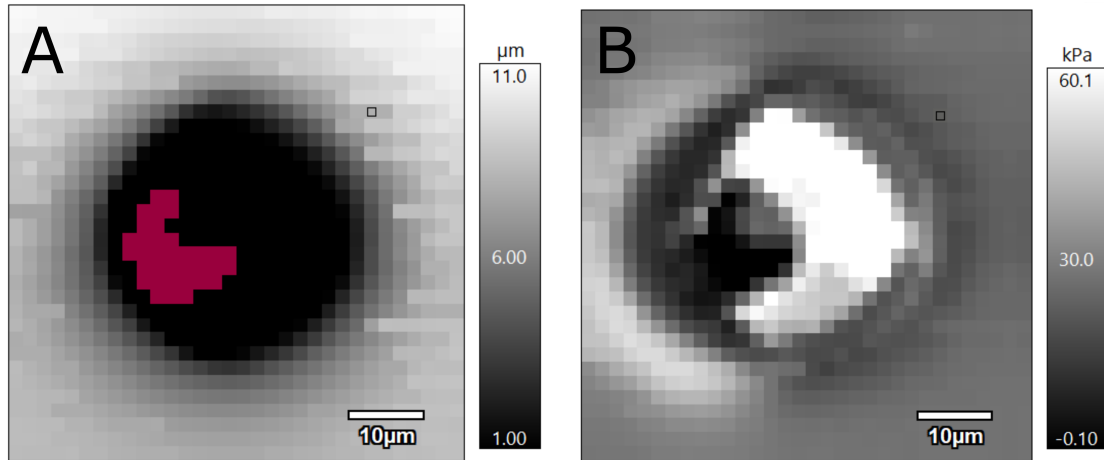


Figure 4.2: Force map measurements of a structured polyacrylamide gel with the measured depth (A) and map of the estimated Young's modulus (B). In pink areas trigger-point could not be reached.

data points, where the triggerpoint could not be reached, is shown marked in pink in the force map in Figure 4.2 A. Analysis of the depth measurements and the calculated stiffness of the force map showed that lower areas of the 8 μm structures recorded are much stiffer. An example is shown in Figure 4.2 B where the fit of the force curves on the bottoms of the well lead to a stiffness around 60 kPa instead of the measured 30 kPa in the areas outside the well. Given that the rest of the gel had a homogeneous stiffness, it is unlikely that the gel was actually stiffer in the lower areas. It is much more likely that, while measuring the deep structures, not only the tip of the cantilever was in contact with the sample, but that some other cantilever parts were also resting on the gel. This was supported by the observation that the effect of faults measurements was less distinct in structures with a big diameter than in structures with a small diameter. It is presumed that the cantilever is less hindered in the big structures. These cantilever substrate contacts can change the bending properties of the cantilever and thus alter the measurements. Therefore, to determine the stiffness of the gels, only the higher areas of the gels that provided reliable contact with the AFM tip were considered. This was done with the help of a custom MATLAB script, which generated a histogram of the measured Young's modulus. By manually defining a threshold, only bars with a certain incidence were considered. This selection process did not only exclude the force curves of the lower areas of the gel, but also eliminates any measurement artefacts and incorrectly fitted data.

As mentioned, such an analysis of force maps highlights some difficulties of measuring the depth of polyacrylamide gels. Optical profilometers and SEMs could not be used for characterising the morphology of hydrogels because neither technique can measure in liquid, and polyacrylamide gels need to remain hydrated to maintain their structure.

AFMs can measure in liquid, but as discussed above, the z-piezo range of commercially available instruments is not large enough to obtain useful results. An alternative to the methods mentioned uses the ability of confocal laser scanning microscopes to scan in the z-direction and thus produce a three dimensional image. Microstructured polyacrylamide gels with 0.05 % embedded orange fluorescence beads were fabricated and measured with a confocal laser scanning microscope. Images obtained were analysed with ImageJ (Fiji) by loading the whole stack and cropping images in xy-direction to analyse the individual wells in the image independently. This was done to minimise the effect of the tilt of the sample on the results. The z-axis profile was used to determine the height of the surface of the gel relative to the bottom of the well. If the focus level was above the gel surface, the fluorescence signal intensity was low. The signal increased when the fluorescence beads were coming more into focus (Figure 4.3 left blue area). Once the surface was reached during the scanning process, the increase in fluorescence intensity was reduced. The slope of the z-profile plot became less steep, as the number of fluorescence beads did not change much during the scanning of the well (Figure 4.3 yellow area). Only when the bottom was reached, did the number of fluorescence beads in focus change

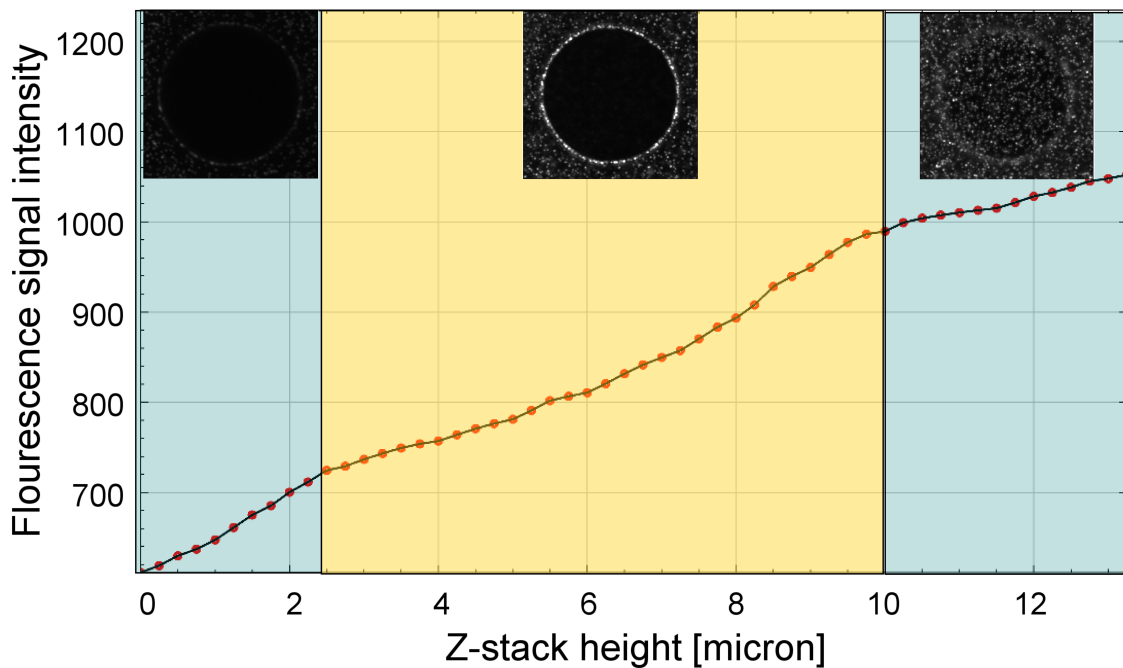


Figure 4.3: Z-stack profile obtained with a confocal laser scanning microscope of a structured polyacrylamide gel with embedded fluorescence beads. The plot is divided into three regions based on the focal depth. The blue area on the left is where the microscope is focused above the gel surface, the yellow area where it is focused within the well, and the blue area on the right where it is focused below the bottom of the well. Typical images from these different areas are shown.

again and a steeper slope in the z-stack plot was the consequence (Figure 4.3 right blue area). The location of these gradient changes were used to determine the height of the microstructured polyacrylamide gels.

4.3.2 Traction force microscopy

For the analysis of traction forces, gels were fabricated with 0.05 % 0.2 μm fluorescent beads. The beads were mixed into the polyacrylamide presolution and the microstructured and protein patterned polyacrylamide gels prepared as explained in Section 4.1.3. Images were taken with a confocal laser scanning microscope and a 100x oil immersion objective. The first image was taken before adding trypsin (2.5 %). After 30 min incubation time, a second image was taken of the same area. The addition of trypsin led to the detachment and rounding of the cells. This could be observed in the images taken and allowed one to check whether the trypsinization was working (Figure 4.4 A). As the original images were stacks covering the whole well in z-direction, for the analysis process with Fiji, first a focus level was chosen and the respective images of the first and second stack extracted. A bead-based registration step was used to align the two images [182]. For this step, the non-cropped images before and after the addition of trypsin were used to increase the number of registered points and thus improve the accuracy of the registration (Figure 4.4 C). In the overlay of the images, the movement of beads after cell detachment was already visible. Next, images were cropped so that the well was in the centre of the image (Figure 4.4 B). To analyse the displacement of the beads, a particle image velocimetry (PIV) plugin was used [154, 155]. Three interrogation window sizes were chosen based on the cropped image size. The size of the first interrogation window was set to 1/4, the second to 1/8 and the third to 1/12 of the cropped image size. The size of the interrogation windows was chosen so that even in the smallest window an average of 4-6 beads were presented. As it can be seen in Figure 4.4 B, the distribution of fluorescent beads was not uniform over the whole image. The bead density was higher in the lower areas of the polyacrylamide structure. While this would theoretically enable smaller interrogation window sizes in these areas, the relatively low bead density in the rest of the gel did not allow that, as the low number of particles in the areas outside the well would not result in a detectable signal. The search window size was set to double the interrogation window size in all three passes of PIV. Each pass yielded a displacement map of the beads, as shown in Figure 4.4 D for the 1/12 window. Here, each vector represents one interrogation window and the colour and length of the vector indicates how big the displacement had been. The map of the pass with the smallest interrogation window size was used for the FFTC plug-in in Fiji to translate the displacements into a force field (Figure 4.4 E) [154, 155]. Each displacement vector of the PIV analysis was converted into a force vector, where again colour and length visualise the strength of the force.

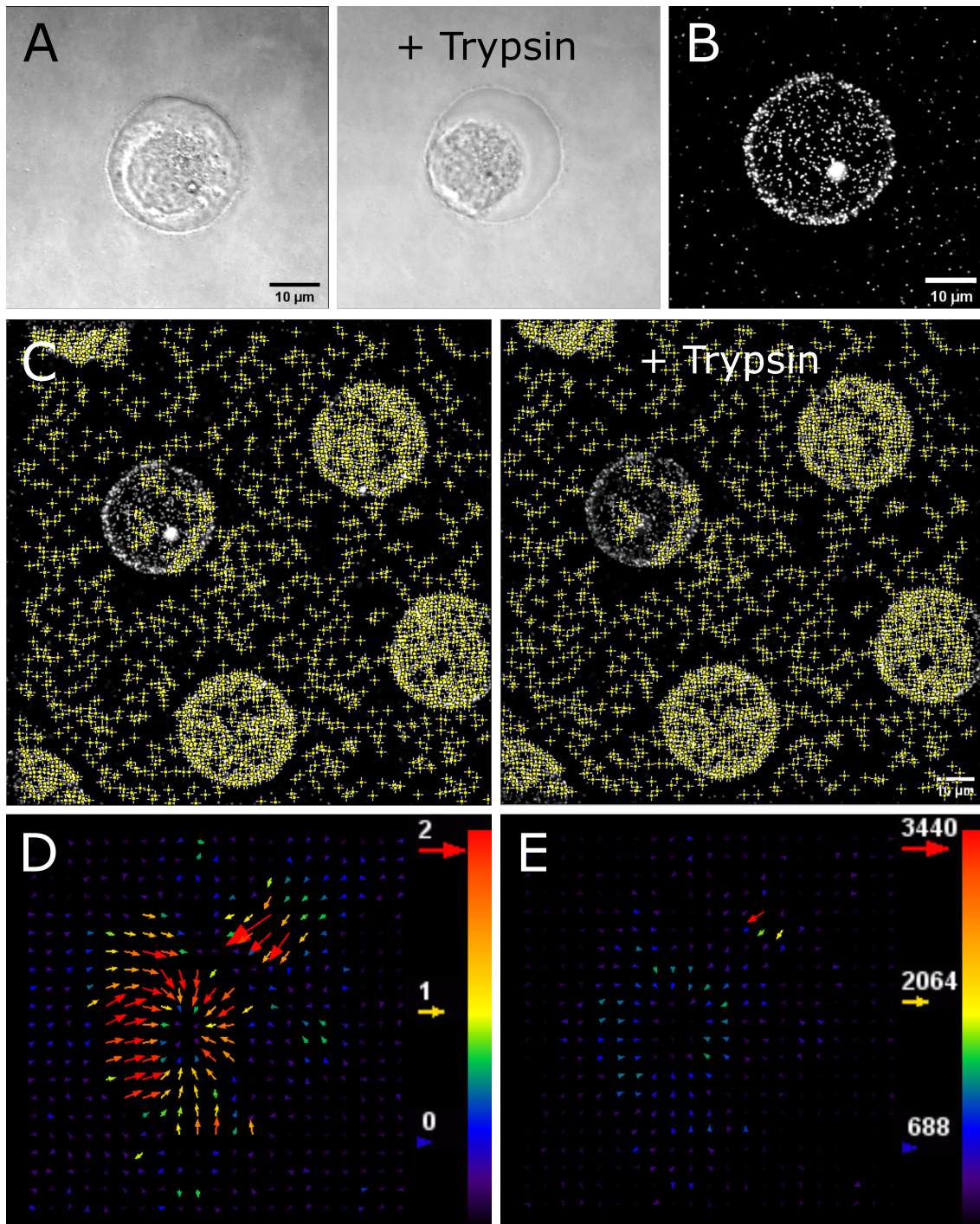


Figure 4.4: Analysis steps of traction force microscopy: A) Brightfield images of the cell before and after adding trypsin. B) Fluorescence beads on the bottom of the well with the cell attached. C) Points detected for registration of images before and after adding trypsin. D) Displacement map of beads (in pixels). E) Force map (in Pa) estimated from the displacement map in D.

4.3.3 Cell fluctuation analysis

Originally, live cell images were taken at regular intervals of 5 min over 48 h (as explained in Section 4.2), in the hope of capturing deformations of the side walls of the wells in the microstructured and protein patterned polyacrylamide gels when the cells push against them. Unfortunately, these deformations were very difficult – and in many cases, impossible – to observe, and any analysis of the images would have been unreliable due to optical effects. However, it proved possible to analyse the fluctuations of the cell shapes within the wells in videos produced from the images. The procedure of fluctuation analysis, as well as the corresponding Python script, presented in the following paragraphs were developed and written by Prof. Burkhard Geil.

Images taken every 5 min in the live cell measurements were combined to form a video. In the first step, an image was generated which contains the information of the time averaged brightness of all images in a certain video as shown in Figure 4.5 A. To obtain a higher contrast, an inverse Gaussian gradient filter was applied to the time averaged image (Figure 4.5 B). This increase in contrast had an effect on the appearance of the edges of the wells in the images in particular and is important for the next step of active contour segmentation. Active contours, also referred to as snakes, are a concept in which the shape of an object is described by a deformable spline. A spline is a function describing a curve which is piecewise polynomial, continuously differentiable to some order to ensure smoothness. The shape of these curves is influenced by external energies, such as a gradient vector flow, and internal energies, calculated by the shape of the contour. An algorithm is used to find the minimum of the sum of these energies [183]. Therefore, the shape of these snakes are optimised until the minimum of the sum of the energies is found. Described in other words, applying active contours can be imagined as a process of spanning an elastic band around the image and finding the well edges by contracting this elastic band. Well shapes determined by this time intensive procedure, as shown in Figure 4.5 C, are defined as regions of interests (ROI). The detected edges were then transferred back to the time averaged image of the video (Figure 4.5 D) and the individual images. The ROIs/wells were labelled with a number for better assignment of data to the well/cell in the video (Figure 4.5 E).

In the next step, the brightness of each ROI in each image of the video was analysed. Here, a distance ΔI between the brightness of two images F and G was defined as

$$\Delta I = \left[\frac{1}{A} \sum_{i \in ROI} (F_i - G_i)^2 \right]^{\frac{1}{2}}$$

where A is the area of the ROI (number of pixels). Summation takes place over all pixels within a ROI, which means the index i is two dimensional. This means F_i and G_i are a value of brightness of pixel i in images F and G . This definition was then used to analyse fluctuations within the wells/ROIs over time, where the values of brightness of pixels in each image t are compared to the brightness value of the time averaged

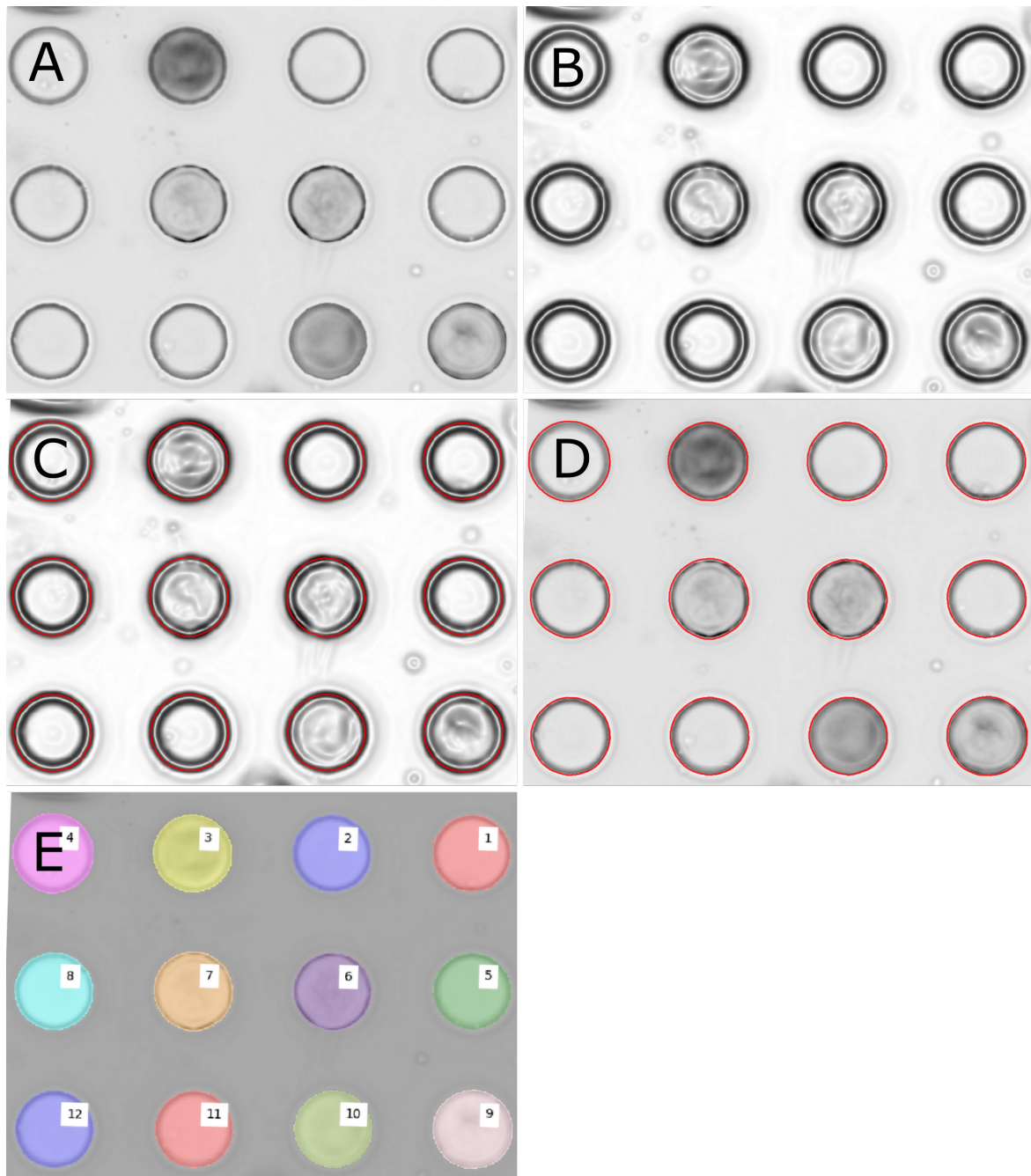


Figure 4.5: Brightness fluctuations analysis of live cell videos: A) Image of the time averaged video (TAV) of wells. B) TAV image after applying an inverse Gaussian gradient filter for a higher contrast. C) Using an active contour concept to obtain well shapes. D) Back transfer of the detected well shapes to the original TAV image in A). E) Labelling of wells for better assignment of data to wells in video.

video (TAV) image generated in the first step. The brightness difference $\Delta I_{ROI}(t)$ within an ROI at time t is calculated as

$$\Delta I_{ROI}(t) = \left[\frac{1}{A} \sum_{i \in ROI} (F_{ROI,i}(t) - TAV_{ROI,i})^2 \right]^{\frac{1}{2}}$$

Plotting $\Delta I_{ROI}(t)$ shows the fluctuations in one well and therefore fluctuations of the cell cultured in this well over time. An example of a fluctuation trace within an ROI is shown in Figure 4.6 A.

These fluctuation time traces can be used to generate autocorrelation functions. Autocorrelation describes how much a signal/information has changed over time by comparing the original information to the information at another time point. The value returned by the autocorrelation function is 1 in case the information stayed exactly the same. With increasing changes in the images, this value decreases. The autocorrelation for the previous example fluctuation trace is shown in Figure 4.6 B. Each point in this autocorrelation shows the average similarity between images separated by a certain time lag. This means for the values in the autocorrelation, not only one image was compared to another one per data point. The second data point, for example, includes the correlation between the first image of one well/ROI and the third one, the second image and the fourth one, the third image and the fifth one and so on. In other words, the second

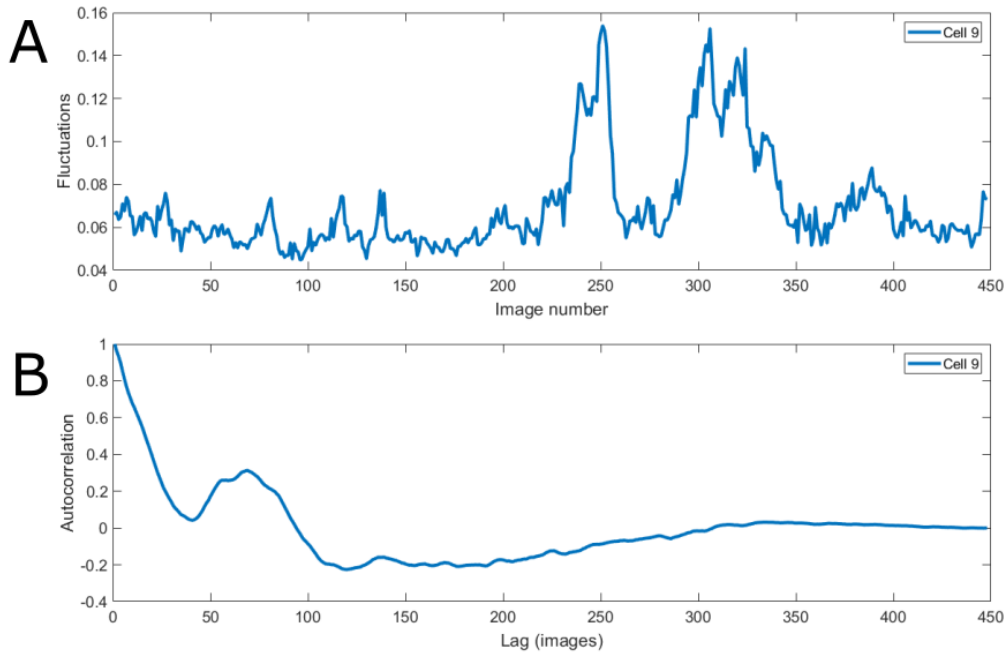


Figure 4.6: Exemplary analysis of cell 9 of Figure 4.5: A) Fluctuation time trace. B) Autocorrelation function.

data point provides averaged correlation between all pairs of images that are two time steps apart. This means the data points give information about how much the image has changed after a certain numbers of time steps/lag. It should be noted that fewer values are averaged for larger lags. For N images, there are $N - 1$ neighbouring pairs, $N - 2$ separated by a single gap and so forth. This means there is only a single value for the largest lag. If the plotted curve decreases fast, the changes within in the ROI are big and fast. If the plotted curve decreases slowly, not many changes occur. It is also possible to see an oscillation of the curve. This happens if the information within the video is repeatedly inverted, fluctuating between two opposite states. In the case of cells in wells, this is possible if the cell is going around in circles. For a better comparison of this data, a time constant can be estimated as the exponent of an exponential function fitted to the autocorrelation function of the respective well. This time constant can be understood as being similar to a decay time. However, as the autocorrelation function is not an exponential function this should only be understood as an approximation.

4.4 Conclusion

This chapter described how the fabrication process of microstructured and protein patterned hydrogels for cell sorting was developed and established, and how it can be used for cellular force measurements. The initial passive pumping approach for polyHEMA might be feasible for creating a non-adhesive cell sorting grid in the future if it can be optimised to solve the problems of partial filling of the structures and the dissolving of the material in media. As a result of these issues, polyacrylamide was selected as a more suitable material for measuring cellular forces. Silicon was chosen as the mould material for the microstructuring and protein patterning process as it is impermeable to oxygen unlike PDMS. These moulds were etched using an ICP setup with the prior removal of the silicon dioxide layer to ensure uniform results. The resulting moulds had pillars with a depth of 8 μm .

For cell experiments, these pillars were coated with a protein using a μ -contact printing approach wherein a PDMS substrate covered with a layer of protein served as a stamping pad onto which the silicon mould was pressed. After coating, the moulds were used during polyacrylamide polymerisation. Four different compositions of acrylamide and cross-linking bis-acrylamide were used to prepare polyacrylamide gels with Young's moduli of 1 kPa, 8 kPa, 30 kPa and 100 kPa. This μ -contact printing approach for fabricating microstructured and protein patterned polyacrylamide gels was successfully established, while an alternative lift-off process was not. The polyacrylamide gels were then used as substrates for culturing ovarian cancer cells of the cell line SKOV3.

To analyse the structure of the silicon moulds, optical profilometry was used. Various methods of analysing the polyacrylamide gels were considered. An AFM could be employed for measuring the stiffness of the gel, but was not suitable for measuring inside the wells. Instead, a CLSM and fluorescent beads embedded in the gel was used. A similar arrangement was used to track the movement of embedded fluorescent beads in the gel when cellular traction forces were applied. The displacement of the beads was determined and converted into estimates of the applied forces using the PIV and FTTC plugins in ImageJ (Fiji).

Brightness fluctuations of cells during live cell measurements over 48 h were analysed. In the images taken, edges of the microstructured wells the cells were cultured in were found by using an active contours concept. Fluctuation of brightness in the wells were investigated by analysing fluctuation time traces combined with cell videos of the images taken during measurements. Autocorrelation functions were generated to obtain information about how much the brightness of a cell had changed. Additionally, a time constant, similar to a decay time, were defined for further investigations.

Overall this analysis showed that microstructured and protein patterned hydrogels for

cell sorting were fabricated, characterised and successfully used for cell experiments, including the measurement of cellular traction force and brightness fluctuation analyses.

5 Results and discussion

To verify whether the developed fabrication process of microstructured and protein patterned polyacrylamide gels as described in Chapter 4 was successful, each fabrication step has been investigated. These quality controls did not only show that the methods and techniques used were working reliably, but can also serve as a base for characterisations of the the structures developed. A well defined experimental set-up is especially important when the influence of physical properties of the microenvironment on cellular responses is investigated. To study the effect of changing a certain parameter on the cell's behaviour, it is important to keep all other factors in the experimental set-up constant. For example, if the diameter of structures in microstructured and protein patterned polyacrylamide gel is changed, the depth should still be the same. The results of the characterisations of Si-moulds and polyacrylamide gels will be presented in this chapter.

Additionally, cells cultured on these gels need to be observed, to check if they spread and behave as expected. Only if the cell appearance is normal, analysing the impact of changes in the physical properties of the microenvironment on cellular protein expressions, morphological changes and traction forces is sensible. In this chapter, the results of cell experiments of ovarian cancer cells cultured on microstructured and protein patterned polyacrylamide gels will be shown. This will include traction force microscopy experiments of differently sized patterns and analysis of morphological fluctuations of the cells.

5.1 Silicon moulds and microstructured and protein patterned polyacrylamide gels

5.1.1 Characterisation of silicon moulds

For the full characterisation of the experimental set-up, the structuring of Si-moulds has been checked first. For this it was important to determine if the diameter and depth had been etched correctly, as well as the examination of critical parameters such as steepness of the sidewalls profile. Images of the Si-moulds after the dry etching procedure and removal of residual photoresist were taken with two independent methods, an SEM (Figure 5.1 A) and an optical profilometer (Figure 5.1 B). Figure 5.1 A and B show a straight profile of the sidewall, a diameter of the pillars of around 32.5 μm and a height of the structures of around 8 μm (see 7.2). Both images shown in Figure 5.1 give the

same information, but the SEM measurements take significantly longer, due to the sample loading procedure and the requirement to pump the chamber down to a vacuum. The following analysis of Si-mould morphology with different target pillar diameters used optical profilometry because of this speed difference. Note that in the analysis the indicated diameters (20 μm , 30 μm , 40 μm and 60 μm) refer to the diameters of the pillars in the pattern design in L-edit and in the chrome mask used. The diameters for the designs were chosen based on the average spreading area of ovarian cancer cells on 2D substrates of 1.700 μm^2 [170]. The largest diameters leaves the cell some space to move as it is larger than the average size, while the smallest sizes restrict the volume available to the cell. Thus, it is important to verify the sizes of Si-moulds and wells in the polyacrylamide gels, for knowing how much the cells are restricted by the wells. The diameters of the etched Si-moulds determined with the optical profilometer are shown in Figure 5.2 C (orange bars). The average measured pillar diameters were $14.5 \pm 0.79 \mu\text{m}$, $25.2 \pm 0.97 \mu\text{m}$, $33.7 \pm 1.28 \mu\text{m}$ and $56.2 \pm 0.62 \mu\text{m}$ corresponding to the mask diameters 20 μm , 30 μm , 40 μm and 60 μm , respectively. It was noticed that the relative variance of the size between the mask and the Si-mould decreases with increasing pattern diameters. While the smallest Si-mould diameter of 14.5 μm represents 72.5 % of the designed mask of 20 μm , the 56.2 μm of the largest Si-diameter measured is equivalent to 93.6 % of the mask with a diameter of 60 μm . However, analysing the absolute errors for the different diameters shows that the values of 5.5 μm , 4.8 μm , 6.6 μm and 3.8 μm are very close to each other. This suggests that a systematic error is causing these deviations in size between the designed mask and resulting Si-moulds. A similar trend is observed for the analysis of Si-mould heights measurements, as visualised in Figure 5.2 D. In the process used, the aim was to etch pillars with a 8 μm height, to ensure deep enough wells, in the next step of moulding polyacrylamide gels, to confine ovarian cancer cells in defined volumes. The average heights measured of Si-mould pillars with the mask diameters of 20 μm , 30 μm , 40 μm and 60 μm were $7.7 \pm 0.15 \mu\text{m}$, $8.4 \pm 0.12 \mu\text{m}$, $8.6 \pm 0.03 \mu\text{m}$ and $8.9 \pm 0.06 \mu\text{m}$, respectively. While the differences in height between the differently sized patterns are not as big as for the diameters, they are still noticeable.

This discrepancy in dimensions has several potential explanations. It is possible that some diameter reduction occurred during the transfer into the photoresist in the lithography process. This could be due to a non-optimised exposure time, leading to an overexposure of the photoresist during pattern transfer. Here, the diffraction of the UV light at the pattern design of the chrome mask could result in smaller pattern in the photoresist and rounded corners. Similar artefacts can be seen during an overdevelopment, where the photoresist is removed in unwanted areas because it was immersed in the developer for too long [184]. The difference in depth, which seems to depend on the pattern diameter of the Si structures, could be explained by a reverse microloading effect during the etching process. This effect describes a faster etching rate of large open areas in comparison to smaller areas and may be due to a high density of neutral reactive gas molecules and low density of ions on the surface [185]. This stands in contrast to the effect of classical microloading, where the etching rate depends on pattern size as well,

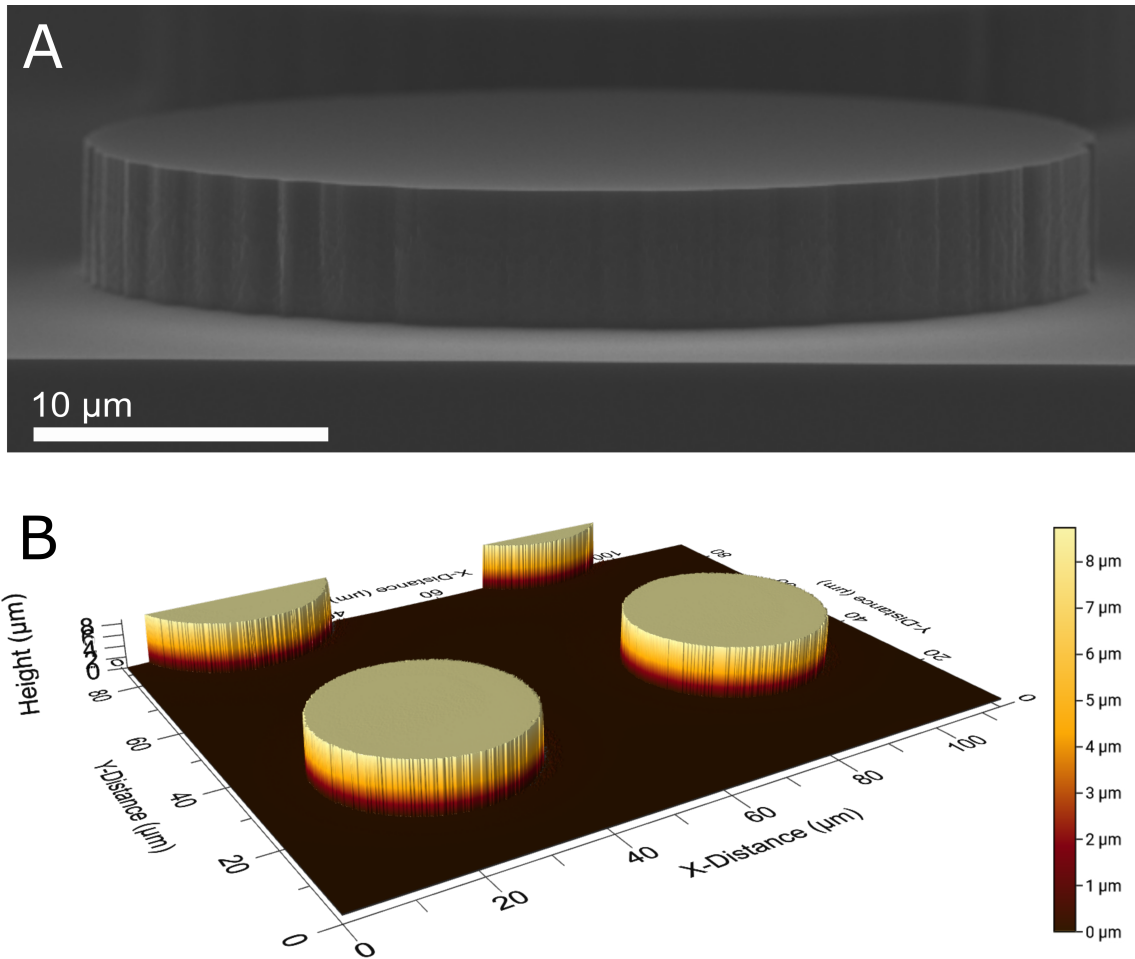


Figure 5.1: Images of silicon moulds taken with A) an SEM and B) an optical profilometer.

but smaller features tend to be etched less [186, 187]. This is explained by unavailability of etchant gases in high concentration inside small holes.

A further optimisation of the lithography and etching steps may lead to an even better transfer with less loss in pattern size. However, it should be noted that the aim of the work presented here was to design a cell culture platform for cell sorting and force measurements with the ability of changing single parameters independently. A perfect transfer of dimensions from a design into the photoresist is not critical in this work as long as the whole process is reliable, reproducible and the system well characterised.

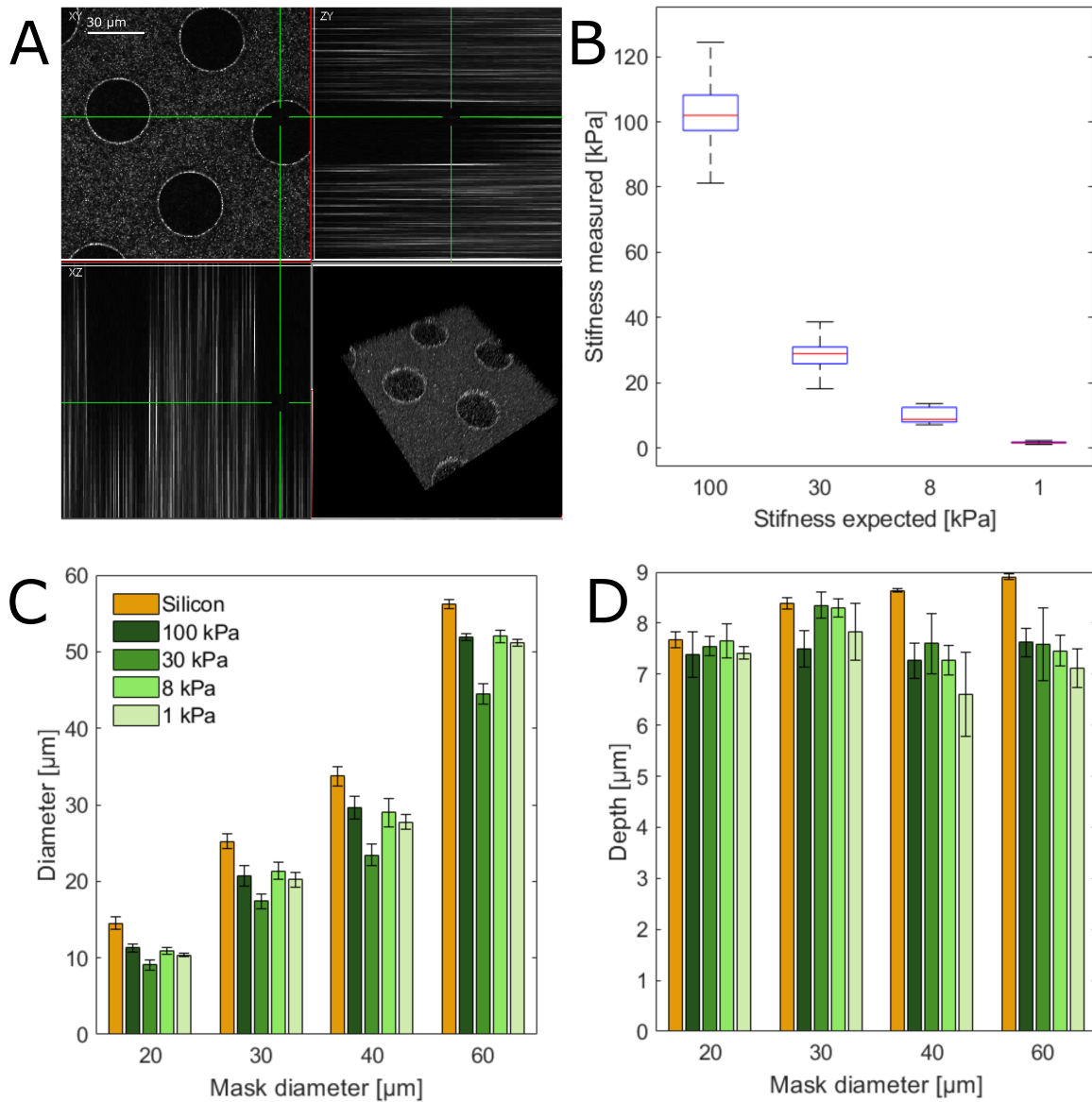


Figure 5.2: A) 3D image of a PAA gel with fluorescent beads taken with a CLSM (bottom right). Crosshair indicates in the XY image (top left) where the ZY profile (top right) and the XZ profile (bottom left) were taken. B) Stiffness of PAA gels with different AA and bis-AA compositions as a boxplot (Central line in box indicates the median, bottom and top edges indicate the 25th and 75th percentiles, respectively, whiskers extend to the most extreme data points, and outliers are marked with '+'). Comparison of diameter C) and depth D) of Si moulds and PAA gels with different stiffnesses.

5.1.2 Characterisation of polyacrylamide gels

Characterisation of structured polyacrylamide gels was challenging in parts, as mentioned in Section 4.3.1. To measure the four different gel stiffnesses of 1 kPa, 8 kPa, 30 kPa and 100 kPa, which were targeted by using four different compositions of acrylamide and bis-acrylamide, an AFM was used as explained in Section 4.3.1. The average Young's moduli determined by the analyses of the force maps were 102.3 ± 9.5 kPa, 28.7 ± 4.1 kPa, 9.6 ± 2.2 kPa and 1.7 ± 0.4 kPa for the expected stiffnesses of 100 kPa, 30 kPa, 8 kPa and 1 kPa, respectively, as presented in Figure 5.2 B as a boxplot. Finding the right composition of acrylamide and bis-acrylamide for a desired stiffness is not easy, as there is a complex relationship between total polymer content, cross-linker concentration and Young's modulus [188]. Denisin and Pruitt found that the stiffness of a polyacrylamide gel is dependent on the composition of the polymerisation solution (including acrylamide, bis-acrylamide, polymerisation initiator and catalyst concentration), temperature and time of polymerisation, and storage time of the gel before it is used for cell culture experiments [173]. These parameters were kept constant for all polyacrylamide gel fabrication done in the presented work, independent of whether the gels were used for cell experiments or analysed to characterise stiffness and dimensions of the structures. Despite these precautions, some outliers were detected during the AFM measurements. These irregularities could have had their origin based in irregular polymerisation, for example caused by a slight heterogeneity of bis-acrylamide concentrations, or in measurement artefacts during characterisation, or incorrectly fitted data points. However, the results illustrated in Figure 5.2 B show that the fabrication of polyacrylamide gels with four different stiffness, ranging from a few kPa to 100 kPa, was successful.

For visualisation and characterisation of depth of the pattern of wells in the polyacrylamide gel, fluorescent beads with a diameter of $0.2 \mu\text{m}$ have been embedded in the gel and a CLSM have been used for investigation. Here, a high density of fluorescent beads is necessary in order to achieve a uniformly high fluorescent colouring of the gel. This is especially important for detecting the edges of the structures within the polyacrylamide gel. The images taken not only allow the determination of the dimensions of the structures in the gel, but also the ability to construct a 3D image of the sample, with an example seen in Figure 5.2 A. Here, the wells in the gel are clearly visible due to the absence of beads. This also confirms that it is essential to wash the gels thoroughly after polymerisation. If this washing step is omitted, fluorescent beads (along with non polymerised polyacrylamide) can be present in the solution the gel is immersed in, and thus also in the cavities of the wells. The fluorescent signals of these beads could falsify the analysis of the depth explained in Section 4.3.1 and Figure 4.3. The measured depth for the four stiffnesses and the four diameters fabricated are shown in Figure 5.2 D and the corresponding diameters of the wells as determined with optical microscopy are shown in Figure 5.2 C and summarised in Table 5.1. Similar to the size reduction that occurred during the step of transferring the designed pattern into Si-moulds, it can be

seen that polyacrylamide gels have structures with smaller dimension than the silicon moulds. This is true for both diameter and depth. Similar to the construction of the Si-moulds, the shrinkage of the polyacrylamide gels is roughly constant, with around 10 μm below the target sized of the pattern designed, or around 5 μm below the measured Si-mould size. Which means that both processes, the transfer of patterns during the lithography step and the moulding during polyacrylamide polymerisation leads to the same shrinkage. Again, this suggests it is a systematic error which could either be improved with an optimised process or allowed for when designing the structures (design the patterns 10 μm wider than desired in L-edit).

The process of shrinking of pattern size could happen during the process of polymerisation as it has been observed with other polymers such as PDMS [186]. Another reason for the size difference could be the temperature used during polymerisation (room temperature) and storage (4°C overnight). Temperature not only has an influence on the stiffness of the polyacrylamide (as discussed above), but also on the swelling and shrinking behaviour [189]. Another reason for the reduction in size during the moulding process could be due to chemical properties of the silicon surface such as its hydrophobicity. Possibly, a combination of both temperature and surface properties of the silicon could be responsible for the smaller dimensions of the polyacrylamide. This would also explain why the storage of the gel at 4°C overnight, as well as the oxygen treatment of the Si-moulds prior to the polymerisation are critical steps to enable the easy removal of the Si-mould from the polymerised gel.

When replicating the experiments explained here, it should be kept in mind that the results of the characterisation are not completely independent of the chosen characterisation method. Macroscale, such as rheometers, and microscale methods, such as the AFM method used here, exist for characterising mechanical properties of polyacrylamide gels [120]. Especially for soft gels, the chosen method can lead to different results for the same polyacrylamide gel formulation [190]. As cell experiments take place on the microscale, it is best to use a characterisation method on the same scale.

Overall, the analysis of both diameter and depth show that the moulding process is working correctly. Structures on the Si-mould are transferred into the polyacrylamide gels, independently of the designed diameter of the pattern or stiffness of the used polymerisation composition of acrylamide and bis-acrylamide. The characterisation of the

Table 5.1: Volume available for cultured cells in wells of the microstructured polyacrylamide gels. Calculated using the measured diameters and depth of the structures.

Target diameter [μm]	Meas. diameter [μm]	Meas. depth [μm]	Volume [μm^3]
20	10.4	7.5	638
30	20.0	8.0	2,490
40	27.4	7.2	4,250
60	49.9	7.5	14,700

fabricated microstructured polyacrylamide gels allows the calculation of the volumes available to cells cultured on these gels, as listed in Table 5.1.

5.1.3 Protein transfer for cell experiments

To ensure that the protein transfer was successful, fluorescent gelatin was used instead of collagen for the μ -contact printing process explained in Section 4.1.3. Gelatin is hydrolysed collagen I and a fluorescently labelled form is commercially available. The PDMS stamping pad was covered with the fluorescent protein solution and an image was taken after the Si-mould was pressed onto the PDMS surface to pick up the protein. As can be seen in Figure 5.3 A, the fluorescent gelatin layer (bright in the image) was still present in the areas with no contact to the moulds. The protein was removed by the circular Si-pillars during the μ -contact printing process as explained in Section 4.1.2, leading to a dark pattern of circles. The protein was successfully transferred into the polyacrylamide gels, as shown in Figure 5.3 B. The bright appearance of the protein pattern in the image shows that a selective protein transfer combined with a 3D structuring of the polyacrylamide gels is possible by using Si-moulds.

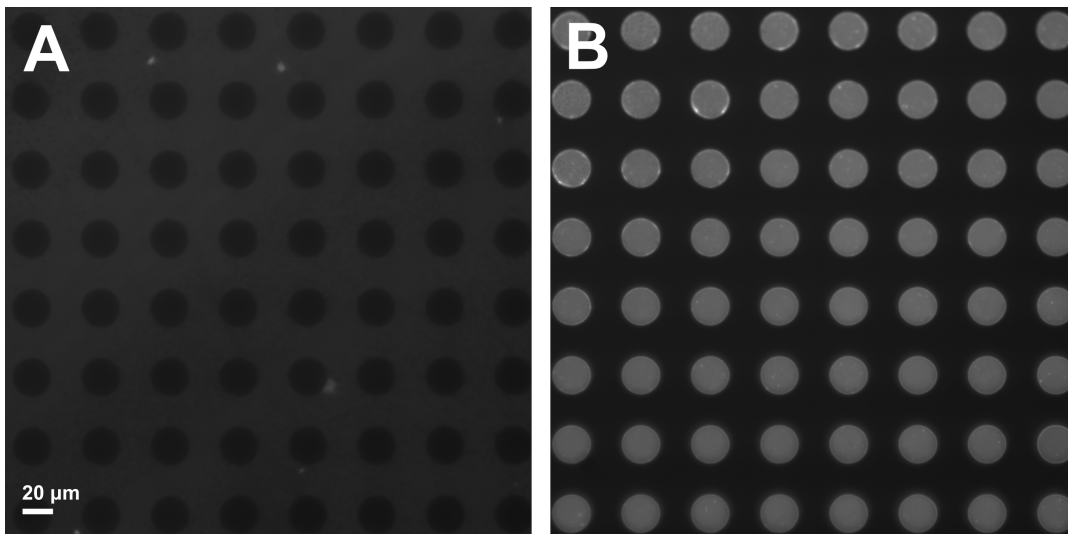


Figure 5.3: Protein transfer of fluorescent gelatin during μ -contact printing. After transfer, the PDMS substrate (A) has no gelatin left where the silicon pillars removed it during the μ -contact printing process. It has been transferred to the wells in the structured polyacrylamide gel (B).

5.2 Cell experiments

After it had been demonstrated, that the individual steps of the fabrication process for microstructured and protein patterned polyacrylamide gels are working correctly, it was possible to culture cells on these gels. The aim was first to fabricate a cell culture platform in which well known behaviour of cells, such as spreading out on stiff substrate with enough space available, could be replicated to ensure that the whole experimental set-up is working reliably for cell culture experiments. Without these reviews, the results of further experiments would have been questionable. In the next step, physical parameters of the experimental set-up were changed to investigate cellular responses to changes in their microenvironment.

5.2.1 Cells cultured on microstructured and protein patterned polyacrylamide gels

As explained in Section 4.1.3, several steps of the fabrication process of microstructured and protein patterned polyacrylamide gels are critical. Examples are the maintenance of the right pH level of 6 during protein incubation and that the PDMS stamp as well as the Si-mould have to be oxygen plasma treated for a successful outcome. Before these steps had been optimised, cells were able to attach to the bottom of the fabricated microstructured polyacrylamide gels but did not spread out over the whole surface at the bottom of the well. It was noted that the cell appearance of the ovarian cancers cells of the cell line SKOV3, seeded in the wells of the microstructured and protein patterned polyacrylamide gels, was different in comparison to healthy cells in culture. The cells in the wells looked more rounded than usual, as shown in the example in Figure 5.4 A. This appearance is normally typical for cells cultured on soft gels, as it is known that substrate stiffness influences cell spreading behaviour [70]. It was only when the protein transfer was further improved that the cells spread out and attached to the substrate, similar as they do on flat hard substrates (Figure 5.4 B). Therefore, it is assumed that the cells develop a round shape if the protein transfer is incomplete. If no protein had been transferred at all during the μ -contact printing, the cells could not adhere to the substrate. As long as the cells attached strongly enough to the polyacrylamide gel, they were able to stay attached even after several washing steps. This was also observed on rounded shape cells, which indicates that a small amount of protein was present that helped their adhesion. It could be that the low protein concentration allows the cells solely to attach to the gel but not to spread out. This rounding effect of cell shapes has been observed previously when cells were cultured on well-defined islands of proteins [191]. This is also supported by Chaudhuri et al., who found that the density of extracellular matrix protein ligands can overwrite the effect of stiffness on responses of endothelial cells, such as the spreading behaviour [192].

To confirm whether the low protein concentration was responsible for the rounding of cells, the optimised fabrication process of the microstructured and protein patterned

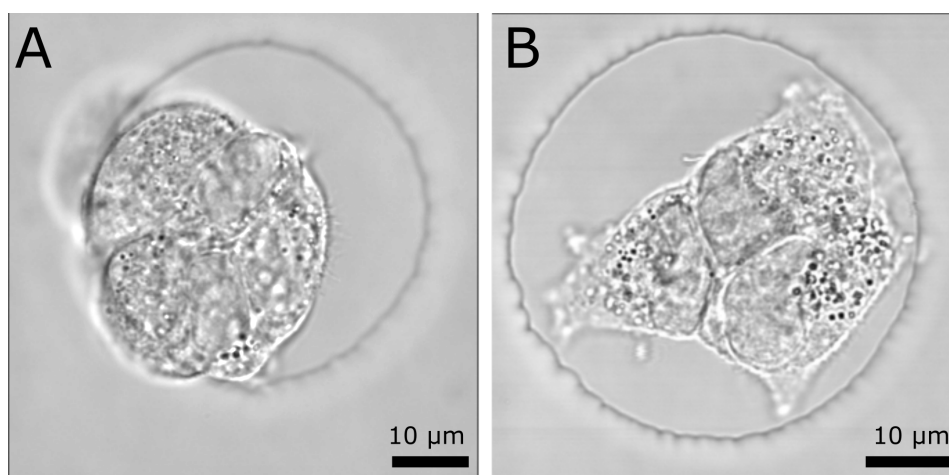


Figure 5.4: Cells of the ovarian cancer cell line SKOV3 on microstructured and protein patterned polyacrylamide gels (30 kPa) before A) and after B) optimisation of the fabrication protocol.

polyacrylamide gels could be used with varying protein concentrations in future experiments. This could be achieved by using a range of concentrations for the protein coating of the PDMS stamping pad during the μ -contact printing step. To determine the amount of protein transferred, fluorescently labelled gelatin can be used and the concentration analysed with fluorescence spectroscopy. It would also be possible to combine these two techniques and use a mixture of collagen and fluorescently labelled gelatine to gain a direct link between protein concentration on the gel and the morphology of the cells.

Fluorescent staining of cells

Fluorescence microscopy enables detailed cell structure investigations beyond the analysis of cell morphology obtained in brightfield images. Various proteins in cells can be fluorescently labelled as explained in Section 3.3.3 and Section 4.2. For this work, ovarian cancer cells of the cell line SKOV3 were stained to label DNA (blue), actin cytoskeleton (green) and vinculin, a protein of the focal adhesion complex (red). The cells were cultured on the microstructured and protein patterned polyacrylamide gels for 24 h, fixed with paraformaldehyde and then incubated with the fluorescent dyes. An example of a fluorescent image of cells trapped in a well with a diameter of 60 μm are shown in Figure 5.5. Staining of the DNA shows that there is more than one cell in all four wells after 24 h. This indicates that a cell division is highly likely to occur within the first 24 hours after seeding, as multiple cells per well were also found in other experiments. In general, the seeding density used ensured that only one cell is present in each well initially. As the seeding density was kept the same for all cell culture substrates, the probability that two cells present in one well increases with larger diameters.

By analysing the green and red channels in Figure 5.5, in which the signals of the actin

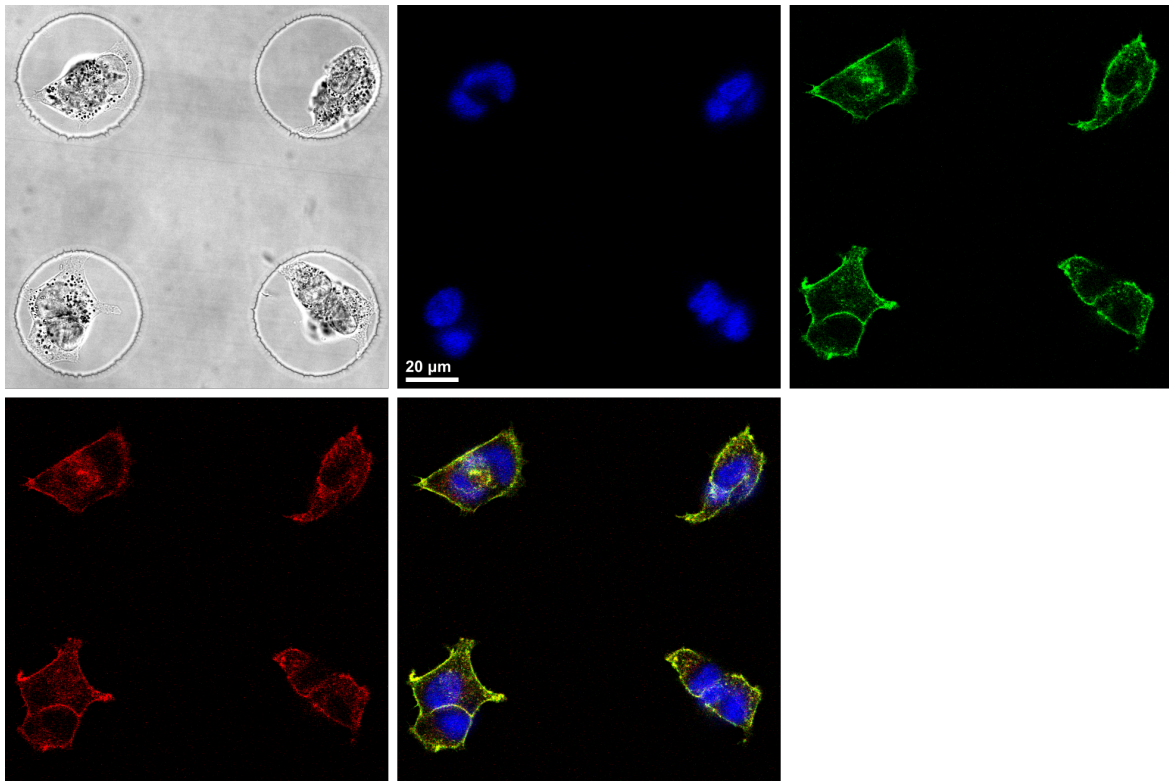


Figure 5.5: Fluorescent staining of ovarian cancer cells SKOV3 on microstructured and protein patterned polyacrylamide gels with a stiffness of 30 kPa and a diameter of 60 μm . DNA is shown in blue (Höchst 33342), actin in green (Phalloidin-iFluor 488) and vinculin in red (Vinculin Monoclonal Antibody 7F9, eFluor 570). In the second image in the second row, all three fluorescent channels are merged; yellow areas indicate where signals from actin and vinculin overlap.

and vinculin stains are shown, a high degree of similarity of the fluorescent images can be observed. Although focal adhesions and the actin cytoskeleton are expected to be located in the same areas and their signals are not exactly the same, as seen in the merged last frame of Figure 5.5, the reason for this high level of agreement between the two channels is probably an artefact of cross-correlation as explained in Section 3.3.3. The effect of signals from one fluorophore being present in an image where a targeted fluorophore is under investigation is called bleeding-through. This is a common challenge in multi stained fluorescent microscopy [193]. There are many parameters which influence the quality of a fluorescence image. These can be divided into three categories: sample preparation including staining, the employed microscope and its settings, and image post-processing. To improve the quality of the image in Figure 5.5, the visual image quality and intensity of the individual fluorescence markers used should be examined. Hence, in some samples only one stain should be used to ensure that there is

no cross-correlation while taking the image and finding the right parameter settings for the microscope. When taking an image with multiple organelles of a cell being stained, bleeding-through can be minimised by using narrow excitation wavelength bands and taking sequential images of the different stains instead of detecting all channels simultaneously [194]. Another approach to further reduce the effect of bleed-through in fluorescent images already recorded is to use an image processing software [195]. If these steps do not lead to the desired results, further optimisations of the image acquisition should be taken into account as described in the literature [195–198].

Although the set-up for taking fluorescent images as seen in Figure 5.5 needs further improvement, the images show that cells spread on the microstructured and protein patterned polyacrylamide gels and can be stained for further analysis. With the described optimisations of fluorescent images implemented, precise actin stress fibres and focal adhesions within the images of the cells could be detected. Actin densities and focal adhesion densities and areas could then be analysed by using ImageJ (Fiji) [199, 200]

5.2.2 Cellular traction forces

The results presented previously showed that the developed microstructured and protein patterned polyacrylamide gels can be used as a cell culture substrate. It was also verified that several properties of the cell substrate can be changed, such as the diameter and the stiffness of the gel. In this section, their suitability for performing traction force microscopy will be examined.

For measuring cellular traction forces, fluorescent beads embedded in the microstructured polyacrylamide gels were tracked as explained in Section 3.3.4 and Section 4.3.2. Two images were taken, one with the cells in place and one after detaching the cells by trypsinising them. The detected movement of the beads was converted into a displacement field, in which the displacements of a defined area were represented by a vector. By knowing the mechanical properties of the polyacrylamide gel, such as its Young's modulus, its Poisson's ratio and the assumption that the material is linear elastic and isotropic, the displacement field could be converted into a force field. The force field, which is again a vector field, indicates where the cell has pulled or pushed its microenvironment.

Three cells were studied in three differently sized patterns to show that traction forces can be measured in the microstructured polyacrylamide gels developed and fabricated in this work. The results give an idea on how forces applied by cells trapped in three dimensional wells differ depending on the volume available. Microstructured and protein patterned polyacrylamide gels with a stiffness of 30 kPa and diameters of 30 μm , 40 μm and 60 μm , leading to wells with a volume of 640 μm^3 , 2,490 μm^3 , 4,250 μm^3 and 14,700 μm^3 , were fabricated. On these substrates cells of the cell line SKOV3 were cultured for 24 h in an incubator. Traction forces of these cells were analysed at the bottom of the gel (Figure 5.6 and in the middle of the wells, 3 μm above the bottom (Figure 5.7). During the analysis process it was noted that in the second fluorescent

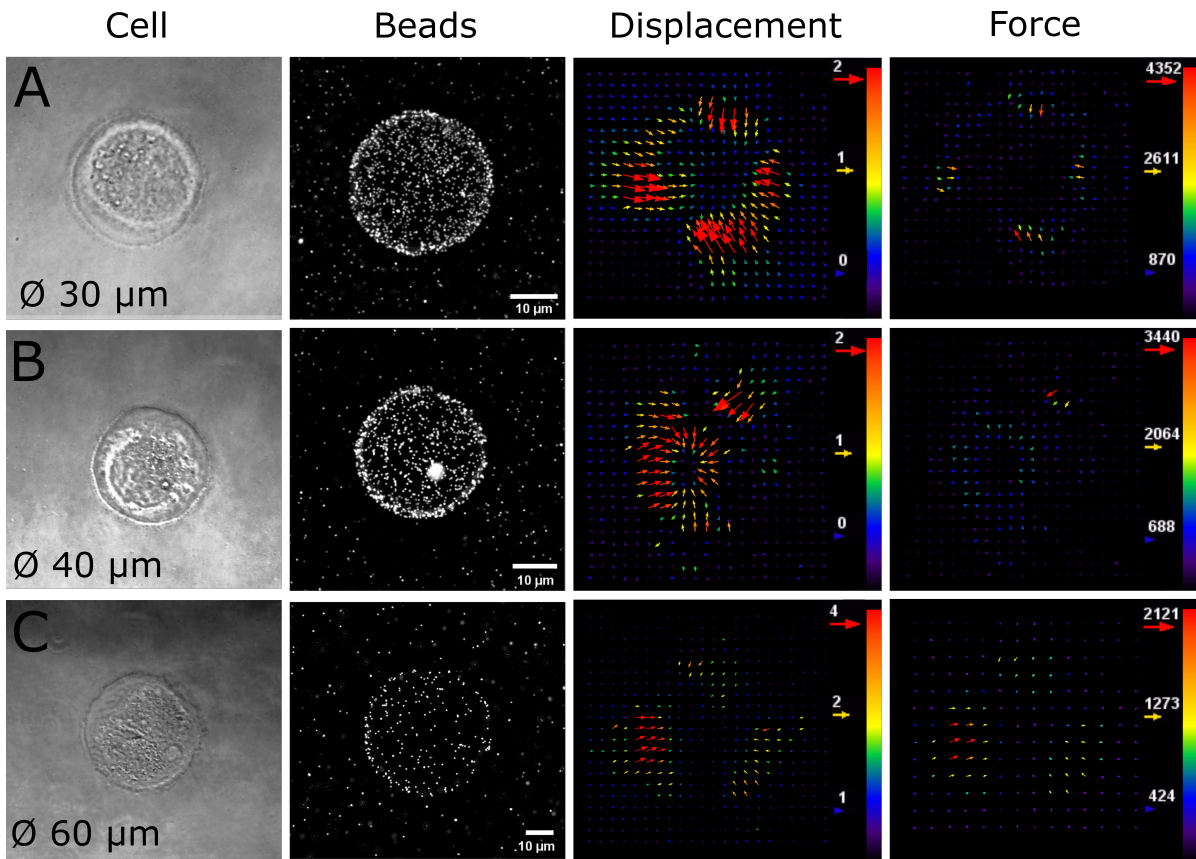


Figure 5.6: Analyses of cellular traction forces of ovarian cancer cells SKOV3 on the bottom of wells in microstructured and protein patterned polyacrylamide gels with a stiffness of 30 kPa and a well diameter of A) 30 μm , B) 40 μm and C) 60 μm . Brightfield image of the cell, distribution of fluorescent beads, displacement map of the beads (in pixels) and the force map (in Pa) estimated from the displacement map are shown.

image taken, after the cell was detached, almost all fluorescent beads which were displaced by the cells were moved away from the centre of the circular well. This leads to the conclusions that the cell pulls on the well boundaries it is surrounded by. This effect was seen for both analyses, the one at the bottom and the one in the middle of the wells. This first conclusion was confirmed by the analyses of displacement and traction force maps shown in Figure 5.6. The vectors of the displacement map of the fluorescent beads and the vectors of the estimated force maps of all three gels investigated point towards the middle of the well. The result suggests that the direction of the force cells apply is independent of the size of surface area the cell is attached to, or the volume available to the cell. The analyses of the results for traction forces applied by cells at the middle of the same structure, 3 μm above the bottom of the well, shown in Figure 5.7, do not yield clear trends in terms of the location where cells exert and apply force. Many vectors of

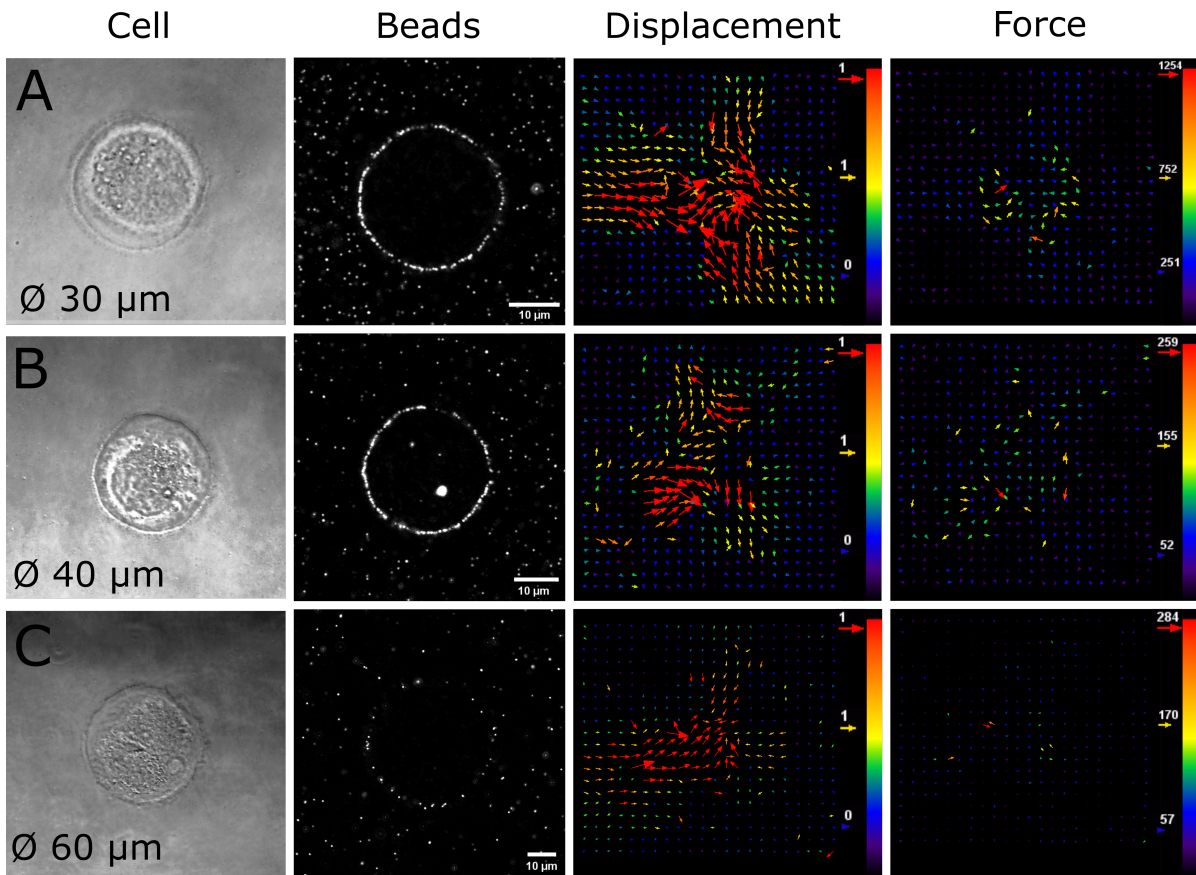


Figure 5.7: Analyses of cellular traction forces of ovarian cancer cells SKOV3 3 μm above the bottom of the wells in microstructured and protein patterned polyacrylamide gels with a stiffness of 30 kPa and a well diameter of A) 30 μm , B) 40 μm and C) 60 μm . Brightfield image of the cell, distribution of fluorescent beads, displacement map of the beads (in pixels) and the force map (in Pa) estimated from the displacement map are shown.

the displacement and force maps of all three well sizes investigated point towards the centre of the well. However, a number of vectors point in other directions, including away from the centre of the well. The characteristics of traction forces pointing towards the middle of the cell has been seen before in 2D [66] and 3D [81]. It has also been previously observed that traction forces are higher at the edges of the cell than in the middle [201, 202]. This can be explained by the molecular clutch model mechanism and the direction of the actin retrograded flow as described in Section 2.2.

In general, cellular traction forces detected with traction force microscopy range between a few Pa up to hundreds of kPa [82]. This is in agreement with the traction forces measured in this work on ovarian cancer cells and summarized in Table 5.2. The cellular traction forces measured at the bottom of the fabricated microstructured and protein

Table 5.2: Measured traction forces of SKOV3 cells on PAA gels (shown in Figures 5.6 and 5.7) with a stiffness of 30 kPa and different well diameters.

Diameter [μm]	Position in well	Average Force [kPa]	Maximum Force [kPa]
30	bottom	0.47	4.23
40	bottom	0.30	3.44
60	bottom	0.25	2.12
30	middle	0.19	1.25
40	middle	0.04	0.26
60	middle	0.03	0.28

patterned acrylamide gels had an average value of 0.47 kPa, 0.30 kPa and 0.25 kPa for cells grown in wells with a diameter of 30 μm , 40 μm and 60 μm , respectively. The associated maximum forces obtained were 4.23 kPa, 3.44 kPa and 2.12 kPa. This means the data obtained in this work show an inverse proportion between the diameter (and therefore the volume) of the well the cells are cultured in and the average and maximum traction forces of the cells. These results were unexpected as most experiments in the literature have seen an increase of traction forces with an increase in spreading area as discussed in Section 2.2.2. However, in this experimental set-up here the volume available for cell growth increases simultaneously to the spreading area, the data indicate that volume can overwrite the effect of 2D spreading area on traction forces of ovarian cancer cells. This thesis is supported by the work of Bao et al., who showed a decisive influence of cell volume on the formation of actin stress fibres and focal adhesion formation in human mesenchymal stem cells [64].

The traction forces of ovarian cancer cells measured here are in good agreement with the values found by McKenzie et al., who also used cells of the cell line SKOV3 [70]. They found mean traction forces of around 0.35 kPa and 0.51 kPa on 25 kPa and 125 kPa stiff gels, respectively, but did not observe a significant difference in the detected maximum traction forces on the same gels. It would be interesting to verify if this increase of applied traction force of ovarian cancer cells with increasing substrate stiffness is still valid in case of an increase or reduction of volume available for cell growth. The microstructured and protein patterned polyacrylamide gels developed in this work could be employed for such a study as stiffness and volume available for the cell can be tuned independently.

Interestingly, we were able to observe some displacement of fluorescent beads embedded within the wall surface of the fabricated wells 3 μm above the bottom of the wells. The calculated forces at the middle of the wells with diameters of 30 μm , 40 μm and 60 μm were 0.19 kPa, 0.04 kPa, 0.03 kPa on average and 1.25 kPa, 0.26 kPa and 0.28 kPa maximum, respectively. These forces show the same trends of increasing force with decreasing volume as the results on the bottom of the well. However, it is not clear yet how exactly

the displacements and forces measured in the middle of the gel are applied by the cell. As the fabrication process of the gel only leads to a protein layer on the bottom of the wells but not on their inside walls, there is nothing on the non-adhesive polyacrylamide gel in this area for cells to attach and pull on. It is likely that these forces are not lateral forces applied by the cell in the middle of the gel, but an effect of the cellular forces on the bottom of the gel. It could be that if the cell pulls the outer area of the bottom of the well, the sidewalls get pulled towards the middle simultaneously. Further investigations of different focus levels of the CLSM, and therefore different heights above the bottom of the gels, are necessary to prove this hypothesis.

However, it should be taken into consideration that the results presented here have only limited significance as only one cell was measured for each diameter. Furthermore, the average was calculated over the whole associated force map shown in Figure 5.6. To obtain a more meaningful measurement, data for evaluation should be limited to the area the cell actually grows on (thus the bottom of the well). Solely this data and the data of a thin defined area around the well should be taken into account to calculate the average traction force. Also, enough cells need to be investigated to be able to make a statement about whether and how the cellular forces are influenced by the area they can spread on or the volume they have available. This would be especially interesting because it is not clear yet which physical characteristic of the microenvironment actually influences the cellular traction forces the most.

5.2.3 Cell fluctuation analysis

Live cell videos were taken of ovarian cancer cells of the cell line SKOV3 on polyacrylamide gels with three different stiffnesses of 100 kPa, 30 kPa and 8 kPa and a diameter of 60 μm to investigate the influence of the substrate stiffness on the cell behaviour. These videos were formed from images taken every five minutes and brightness fluctuations of the wells cells adhered to were analysed as explained in Section 4.3.3.

The combined examination of cells in the videos and their corresponding fluctuation traces revealed some correlations between fluctuation peaks and cell behaviour. In the fluctuation traces, prominent peaks were detected for multiple stiffnesses of the substrate the cells were cultured on, as shown in Figure 5.8 A. These peaks can be linked to temporary rounding of the cells, which is in most cases caused by a cell division. This striking fluctuation in brightness is evident when observing the cell in the video as shown in the image sequence of Cell 1 in Figure 5.8 C. The bright edges of the dividing round cell at 29:30 h after seeding are in stark contrast to the dark, flat cell/cells at 28:25 h and 31:20 h. Although most of the peaks are caused by a temporary rounding of cells, not all of them automatically mean that there is also a cell division occurring. 46 prominent peaks were analysed, of which 34 were linked to cell division and the other 12 peaks were classified as “false peaks”. In three cases of cell division, no characteristic peak was detected. However, the general shape of a curve is already a good indicator for whether a prominent peak is linked to a cell division or not. If a low base line of

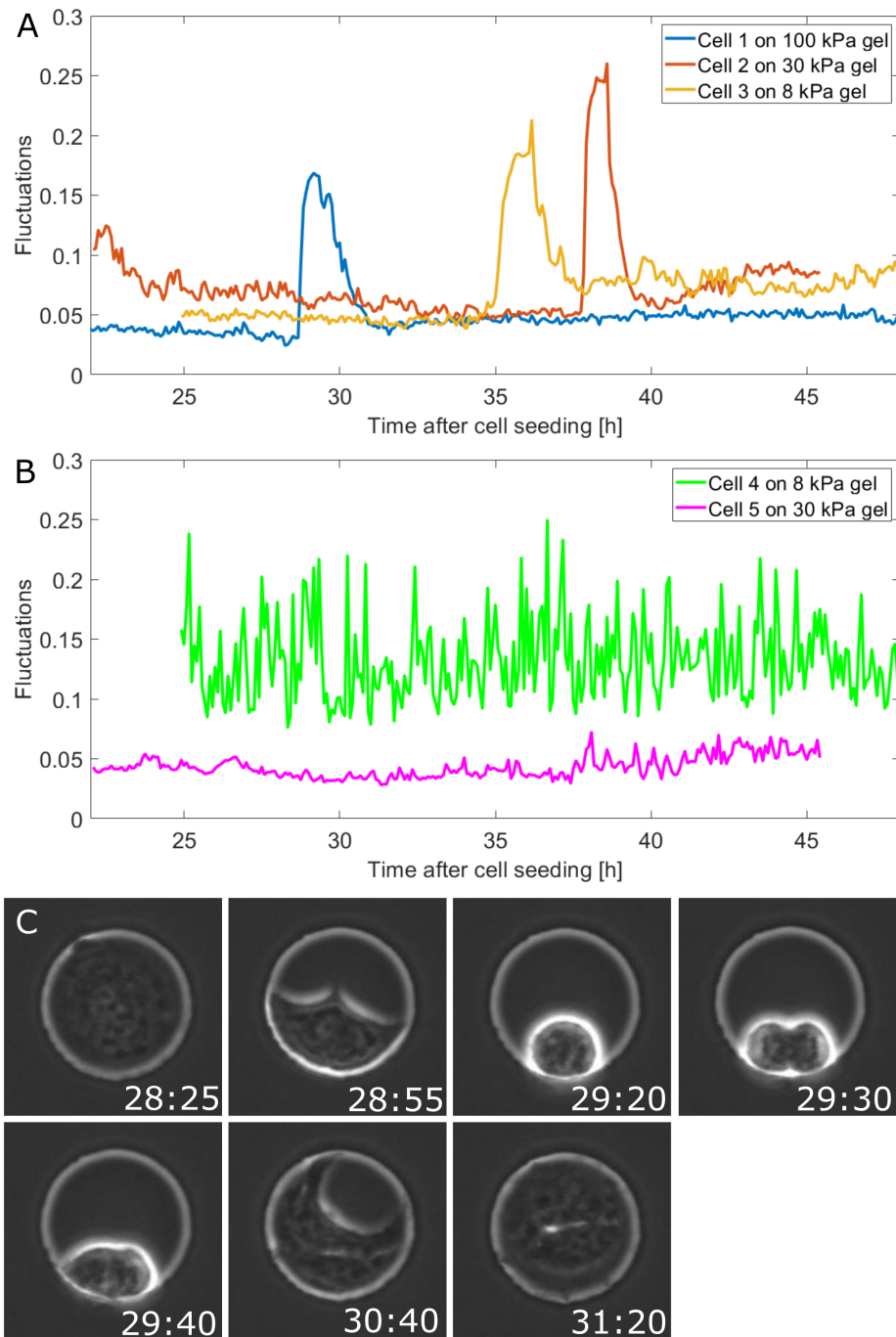


Figure 5.8: Analysis of cell fluctuation traces: A) Examples of cell division peaks of ovarian cancer cells in microstructured and protein patterned polyacrylamide gels with a radius of $60\ \mu\text{m}$ and various stiffnesses (Cell 1-3). B) Typical fluctuation trace of a rounded cell (Cell 4) and a completely spread and surface active cell (Cell 5). C) Brightfield images of cell division of Cell 1. Time in lower right corner is in hours after seeding.

fluctuation exists before and after the peak, it is very likely that the peak can be linked to a cell division. It was also noted that the general “noise” of the fluctuation curve of a well can give information about how much the cell has spread. A rounded cell which was only loosely attached to the bottom of the well has a typical fluctuation trace such as the example Cell 4 shown in Figure 5.8 B. The fluctuations were hectic and “noisy”. Another observation was that the fluctuation curves do not contain information about how active a cell surface is. Cell 5 shown in Figure 5.8 B for example had a very active cell surface, but was completely spread out and covered the whole well bottom surface. Therefore, the fluctuation trace has a low base line without much noise. Only movements of cell edges lead to a change in brightness noticeable in the fluctuation traces. Autocorrelation functions and the corresponding time constants of cells were analysed. By fitting an exponential function to the autocorrelation function of the fluctuation traces, time constants were calculated. In addition to the experiments used for analysing fluctuation traces of cells on 100 kPa, 30 kPa and 8 kPa structured polyacrylamide gels with a diameter of 60 μm , the effect of available volume on autocorrelation functions and time constants of cells was analysed by taking videos of cells in structures with diameters of 30 μm and 40 μm and keeping the stiffness constant at 100 kPa. The average time constant for the different sizes of pattern and stiffnesses of the gel, were calculated and are presented in Figure 5.9 A. Unfortunately, no clear trend was seen among the time constants of the cells in different volumes. However, a big jump was noted in the average time constant between the cells in structures with a diameter of 30 μm and the one in structures with a diameter of 40 μm . This could be due to the lack of space cells have in the smaller wells. Here, they only have enough space to “squeeze” in the well and often fill the whole volume, without much space available to move around or change their shape. It would be interesting to know how these ideas could be linked to the higher traction forces observed in smaller volumes for ovarian cancer cells. The results also show that there could be an increase of the average time constants of cells on stiffer substrates. Nevertheless, all these statements are a bit bold due to the large standard deviations of the results. If the time constant is understood as a decay time, a high value would indicate a stable cell without many changes of shape, and a low number a very active cell which changes its shape continuously. For the results in Figure 5.9 A, this would mean that cells are more active or change their shape more on soft gels than on stiff ones. On the other hand, this would also be plausible in the context of more rounded and less adhered cells on soft substrates and the observed fluctuation traces in Figure 5.8 B. For investigations of a possible correlation between substrate stiffness and cell activity, further experiments using both fluctuation analysis and traction force microscopy are needed. As the standard deviations of the averaged time constants are so large, the distribution of the time constants of the cells depending on structure size and stiffness of the polyacrylamide gel were analysed. Histograms were plotted as shown in Figure 5.9 B-F. The idea was to search for two populations of cells with a corresponding low and high time constant. If two such populations existed, the group size of each population could be

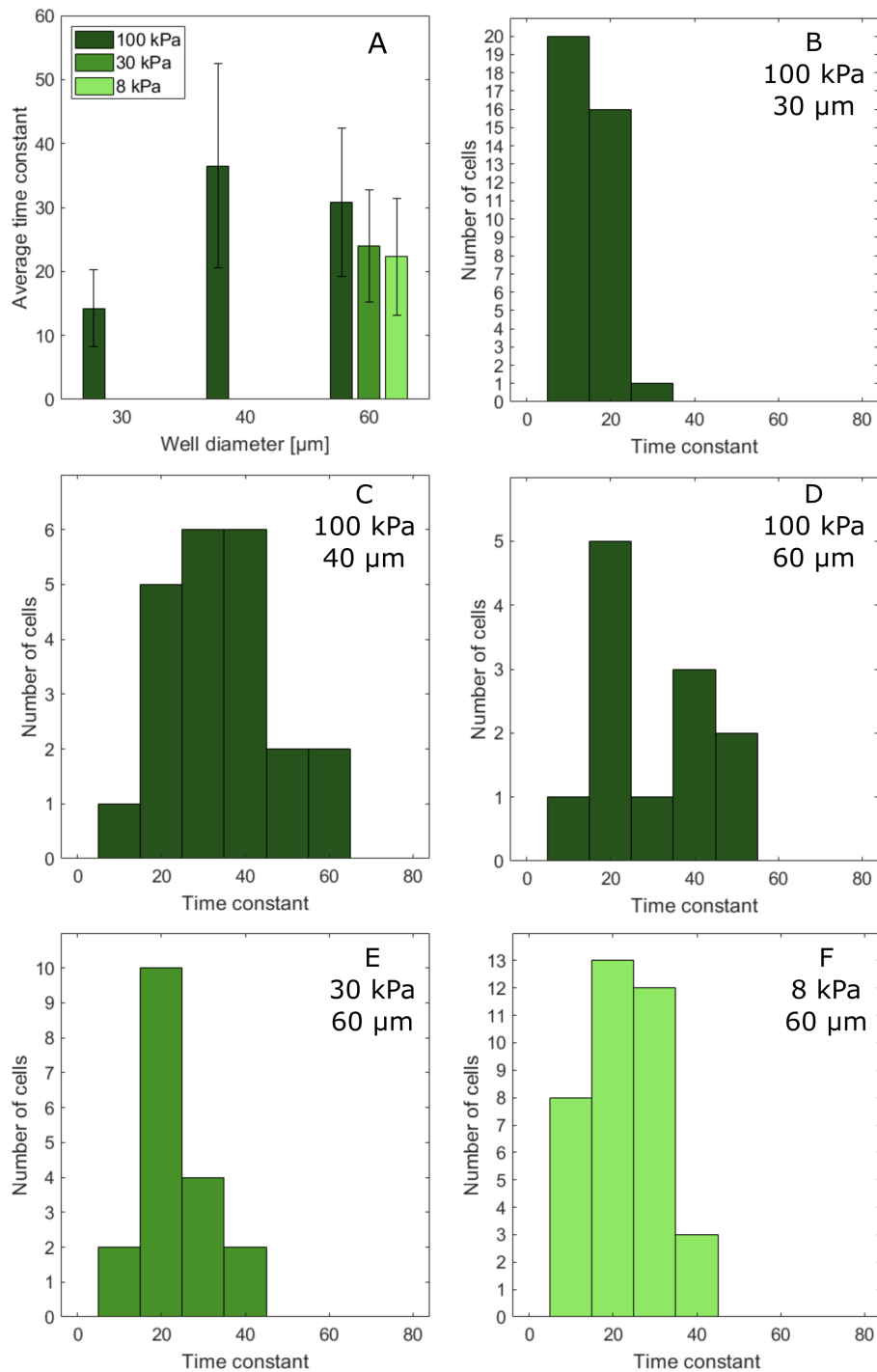


Figure 5.9: Analysis of time constants of autocorrelations functions of ovarian cancer cells: A) Average time constants of cells (standard deviation as error bars) depending on pattern size and substrate stiffness. B)-F) Distribution of time constants used for the average time constants in A).

effected by volume or stiffness of the wells. However, the distribution of the time constants do not allow any such conclusions to be drawn. While the data in C, E and F in Figure 5.9 could probably be fitted by a normal distribution, the distributions in B and D are not that obvious. As analysis of distributions of average time constants do not explain why the standard deviations are that high, it should be checked if a function other than the exponential one used for fitting the autocorrelation functions would lead to better results. This idea is supported by analysis of the shape of the autocorrelation functions of the cells 1-3 in Figure 5.8, which are presented in Figure 5.10. Here it can be seen that the correlations functions follow an exponential function around the first 30 images, but show significant oscillations afterwards. It may be possible to fit the exponential function to only the initial trajectory of the autocorrelation data and compare influence of changes in the microenvironment on the short-time correlations of cells.

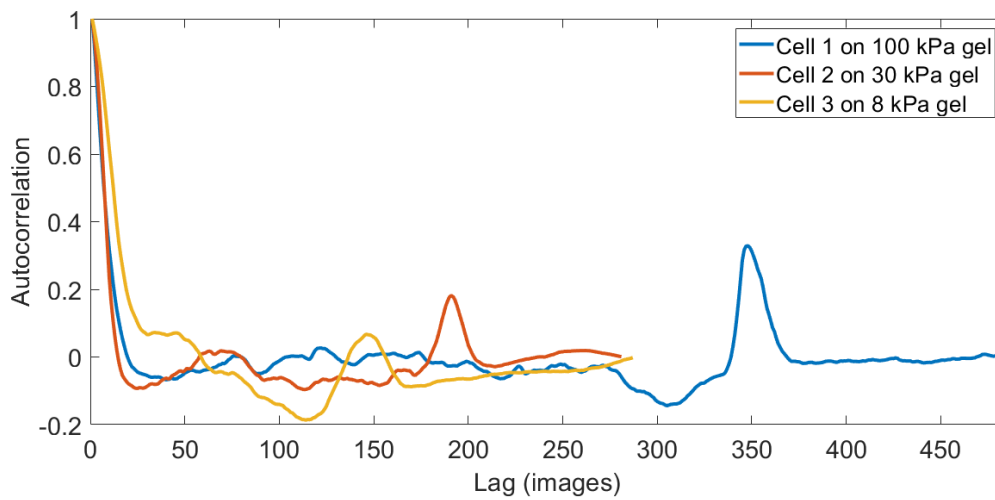


Figure 5.10: Autocorrelation functions of cells 1-3 of Figure 5.8. Note: The time difference between two images was 5 min.

5.3 Conclusion

The results presented in this chapter show that the development and establishment of a fabrication protocol for microstructured and protein patterned polyacrylamide gels for cell experiments was successful. Four diameters, 20 μm , 30 μm , 40 μm and 60 μm , were used to create circular patterns of different sizes, first on Si-substrates. Etching of these Si-substrates led to structures of pillars with a height of around 8 μm high which were used subsequently as moulds during polymerisation of polyacrylamide gels. Four different stiffnesses of polyacrylamide gels were successfully prepared and characterised. The characterisation was performed with an AFM and confirmed that the expected stiffnesses of 100 kPa, 30 kPa, 8 kPa and 1 kPa were satisfactorily achieved.

The moulding process from the Si-mould to the polyacrylamide gels worked independently of the diameter of the structures or the stiffness of the polyacrylamide gels used. This was examined by analysing brightfield and 3D images of fluorescent beads embedded in the polyacrylamide gels, taken with a CLSM. The protein transfer was implemented by using a μ -contact printing approach. In this work the structured Si-mould was employed to transfer protein from the PDMS surface to the polyacrylamide gel as well as for simultaneously forming the micro sized wells used for cell studies.

By culturing ovarian cancer cells of the cell line SKOV3 on these substrates, it was shown that the microstructured and protein patterned polyacrylamide gels fabricated can be used for cell experiments and analysis. The cells adhered and spread out on the bottom of the wells as expected. However, an incomplete protein transfer and a resulting low protein concentration in the structures can probably lead to a more rounded cell shape. Investigations of cellular structures such as the actin cytoskeleton and focal adhesions are possible by using fluorescent microscopy. Nevertheless, the microscope settings used in this work need further improvements to avoid artefacts such as cross-correlation of fluorescent dyes.

By tracking embedded fluorescence beads within the microstructured polyacrylamide gels, traction forces exerted by ovarian cancer cells were determined at the bottom and in the middle of the wells. Traction forces could be detected in structures of different sizes. For the results presented in this chapter, 30 kPa stiff gels were combined with pattern diameters of 30 μm , 40 μm and 60 μm for the microstructured and protein patterned polyacrylamide gels. The detected average forces were between 0.2-0.47 kPa and 0.03-0.19 kPa and maximum forces of 2.12-4.23 kPa and 0.28-1.25 kPa, at the bottom and in the middle of the gel, respectively. These results were in good agreement with values reported in the literature for cells of the same cell line [70]. It was seen that cellular forces increase with decreasing volume available for the cell, which applies for both the average and the maximum forces exerted by the cells in differently sized wells. As these findings are in contrast with results of 2D measurements in literature where traction forces in-

crease with spreading area, we state that volume available for cell growth overwrites the effect of 2D spreading on cellular traction forces. However, a statistical relevance was not given yet, as more than one cell measurement per well size is needed. The forces detected in the middle of the well are likely to be caused by a deformation of the wall structure, rooted in the cell applying forces to the bottom of the well.

Brightness fluctuations of cell videos, made out of brightfield images taken every five minutes, were analysed and showed that characteristic patterns in the fluctuation traces can often be linked to cellular events such as cell division or a rounded shape. However, analysis of the autocorrelation functions and the time constant of an exponential fit did not clearly show an effect of pattern size or substrate stiffness on the time constant. Therefore, standard deviations are too large, which could also not be explained by analysis of time constant distributions. More experiments are necessary to obtain more meaningful data. A different approach for the definition of the time constant by using a different fitting function for the autocorrelation data, other than the exponential function used, could help to understand the impact of available volume and substrate stiffness on the behaviour of cancer cells.

6 Summary and future outlook

Ovarian cancer is one of the most lethal gynaecological diseases due to its poor survival rates at late stage diagnosis. A better understanding of when, why and how ovarian cancer emerges and progresses is crucial for the development of better detection methods and treatment success. As it is known that the tumour microenvironment differs greatly from a healthy tissue and that it can even influence drug resistance during cancer therapy, changes of physical properties of the microenvironment on cellular responses need to be investigated. For this, a framework is needed which allows systematic studies of the influence of individual components of the microenvironment on cells.

In the work presented, an experimental set-up, in which physical properties of the cell's environment can be tuned independently of each other, has successfully been established for cell analysis. Optical lithography and inductively coupled plasma etching were used to fabricate Si-moulds, which served as a mould, as well as a stamp, during a μ -contact printing approach to simultaneously microstructure and protein pattern a polyacrylamide gel during polymerisation. The reliability of the process was verified by characterisation of Si-moulds and polyacrylamide gels while varying pattern sizes and Young's module of the polyacrylamide gels.

The produced polyacrylamide gels were used as cell culture substrates to obtain a better understanding of the impact of external stimuli on ovarian cancer cells. The analysis of cellular responses included protein expressions (using fluorescent staining and a CSLM), cellular forces (by traction force microscopy) and brightness fluctuations of the cell (with live cell measurements). The cellular forces detected are in an expected range and indicate that there could be a correlation between increasing forces applied by the cell and decreasing volume available. Furthermore, the 3D structures allow to draw conclusions about how far reaching these cellular forces are, especially in the vertical direction. The analyses of protein expressions and brightness fluctuations need more data and further improvements before the results can be analysed in a meaningful way.

Nevertheless, the results presented show that the experimental set-up developed, with the ability of controlling parameters of the cell substrate easily during fabrication, is suitable to investigate the influence of defined physical properties of the microenvironment on cellular behaviour. The microstructured and protein patterned polyacrylamide gels in this project can be varied in stiffness and volume available for cell culture. Additionally to the properties already mentioned, it is possible to change the shape of the

pattern of the structured gels, from a circular one to e.g. a square or triangle by changing the design in the lithography step. Furthermore, another ECM protein can be used for coating the wells, such as fibronectin or laminin. It could also be interesting to use a mixture of these proteins to mimic a microenvironment closer to the natural ECM of the cell.

One of the big advantages of the experimental set-up developed is that in the case that two parameters cause two opposite reactions of the cell, it is possible to combine the changes of both parameters simultaneously. This will lead to insights into whether the cellular response to a change of one parameter can be overwritten by another one. Another big advantage of the developed fabrication process of microstructured and protein patterned acrylamide gels is the robustness. While almost the whole processes of design, development and improvement of these gels were done in Christchurch, New Zealand, only some of the cell experiments were carried out there. Most of the cell experiments which led to the results presented in this work were completed in the last six months of the project in Göttingen, Germany. As polyacrylamide gels need to be freshly prepared for cell measurements, the process of μ -contact printing has been established at both locations without any problems.

Possibilities and ideas how to use this flexible and robust experimental set-up to obtain a better understanding on cells in general, and cancer cells in particular, are countless and only a few of them will be mentioned here.

Further investigations of traction forces, cell fluctuations and correlation functions

The experiments presented in this work could be further extended by changing volume, stiffness and protein coating of the microstructured and protein patterned polyacrylamide gels for further investigations of how these parameters influence cellular traction forces, the (re)organisation of the actin cytoskeleton, the number and area of focal adhesions and cellular fluctuation and correlation functions. More data obtained by the developed experimental set-up presented here will provide clarification if there is a significant correlation between cellular traction forces and volume available for the cell and how these results could be influenced by the stiffness of the cell culture substrate. Fluorescence staining of cells could help to relate these results to changes at the molecular level by indicating changes of numbers of focal adhesions and the appearance of the actin cytoskeleton. The findings could also be linked to cell fluctuation and autocorrelation behaviour of the cell, after further development of the analysis processes. The combination of all these experiments would already help to decipher the influence of the microenvironment on the behaviour of the cells, however, they could be complemented by analysing further cell reactions as explained in the next sections.

Cell cycle investigation for a better understanding of tumour growth

A useful further development of the work explained here would be the establishment of live cell traction force microscopy. Here, the same procedure for gel fabrication and cell culturing would be used as explained for the traction force microscopy experiments in Section 4.1.3. Instead of taking only one image, a time series could be taken. For each time point, a brightfield image of the cell, as well as an image of the fluorescence beads, could be captured. The reference image for the gel without a cellular force applied could be taken at the end of the experiment as the last image. Establishing such a set-up would allow many interesting experiments such as the investigation of the cell cycle, cellular forces applied during cell division and the influence of volume and stiffness of the microenvironment on these processes. For these experiments, fluorescent ubiquitin-based cell cycle indicator (FUCCI) reporter system for cells could be used. The FUCCI system enables the fluorescence staining of the cell depending on the cell cycle phase it is in [203]. Vianay et. al used human epithelial cells of the cell line RPE1-FUCCI and showed that traction forces depend on the cell cycle phase [204]. An investigation of the cell cycle and how it is influenced by physical properties of the microenvironment is especially of interest in the context of cancer and tumour growth.

Measuring the microrheology of cells

While the Young's modulus is a characteristic value which describes how axial strain and tensile or compressive stress are related to each other in linear elastic materials, rheology also takes into account the viscous properties, many substances have. To describe the viscoelastic behaviour of a material with its solid-like and fluid-like component, a complex shear modulus is used. The microrheology of cells is interesting, as it has been shown that cancer cells are significantly softer than healthy cells [100, 205–207]. Particularly in connection with ovarian cancer can that parameter help to investigate which external trigger could have the potential of increasing the metastatic potential of cancer cells [208]. Microstructured and protein patterned polyacrylamide gels lend themselves nicely to the study of cells' metastatic behaviour using microrheology in the context of a changing tumour microenvironment, due to the possibility of tuning various parameters such as stiffness, volume or protein coating.

Several methods exist to measure mechanical properties of cells, such as optical stretcher, the AFM or intracellular particle tracking microrheology [205, 207, 209]. Based on the experiments carried out in this work, intracellular particle tracking microrheology would be a good choice. Here, fluorescence beads are ballistically injected into the cell and the Brownian motion of these beads is captured with a high-speed camera and then used to measure mean square displacements (MSDs) [210]. MSDs can then be used to calculate the complex shear modulus.

Drugs and the chemoresistance of cancer cells

Drug resistance of cancer cells is a major problem in cancer treatment and investigation of that resistance is an important branch of cancer research. Several potential mechanisms were proposed to explain how drug resistance may arise. These mechanisms include intrinsic and extrinsic factors such as tumour heterogeneity and tumour microenvironment [6]. Even though it is known that the cell-microenvironment contact influences the drug response and resistance of cancer cells, this field of research receives surprisingly little attention. For ovarian cancer cells it is known that the chemoresistance against chemotherapeutic drugs increases under shear stress and is altered when cells are cultured on bioimprints of cells [211, 212]. On microstructured and protein patterned polyacrylamide gels, thousands of ovarian cancer cells can be cultured under exactly the same controlled conditions at a time, which allows to measure metabolic assays or use cell lysates for protein quantifications. A systematic research study how physical properties of the microenvironment alter the chemoresistance of cancer cells will not only increase the understanding of the disease cancer, but can also help to support the efforts of improving artificial cell culture conditions during drug discovery. If *in vitro* microenvironments for cells can be matched more closely to those of the natural environment, more meaningful data during the initial steps of drug development can be obtained.

Evidently, there are many interesting ideas how the experimental set-up of microstructured and protein patterned polyacrylamide gels could be used to investigate the influence of the physical properties of the microenvironment on the behaviour of cells. Not only the analysis of proteins within the cell or measurement of traction forces and cell fluctuations as implemented in this work, but also many other cellular studies are possible. Unfortunately, there was not enough time during the project presented to realise these ideas, but hopefully it could be shown how helpful the developed system can be for future cellular measurements. This becomes particularly important in the context of a better understanding of such an important disease as cancer.

7 Appendix

7.1 Protocols

All process steps are made at room temperature, if not other marked.

7.1.1 Optical lithography

Preparing a chrome mask

- Design pattern and create file for mask writer
- Write pattern into photoresist covered chrome mask, using a mask writer
- Develop resist on chrome mask (AZ326 for photoresist AZ1518)
- Etch chrome (10.9 % ceric ammonium nitrate, 4.25 % perchloric acid and 84.85 % water)
- Remove remaining photoresist on the chrome mask with acetone
- Clean chrome mask with methanol and isopropanol

Preparing Si-moulds

- Clean Si-wafer with acetone and isopropanol in an ultrasonic bath (5 min each)
- ICP etch of SiO₂ layer (1 min)
25 sccm SF₆, 25 sccm Ar, HF power 10 W, ICP power 1000 W, chamber pressure 5 mTorr
- Spincoat liquid photoresist AZ1518 (3000 rpm; 1 min)
- Softbake (1:30 min, 90°C)
- Transfer pattern from mask to photoresist covered Si-wafer
- Hardbake (6 min; 120°C)
- ICP etch of SiO₂ etch 30 sec

- ICP etch of Si 5:30 min
(40 sccm SF₆, 80 sccm CHF₃, Helium backing 10 torr, HF power 50 W, ICP power 1000 W, chamber pressure 15 mTorr)
- Remove photoresist with NMP
- Ultrasonic bath (10 min)
- Wash with DI water and dry
- Cut into right size

7.1.2 Polyacrylamide gels

Preparing glass substrates

- Oxygen plasma treatment (10 min)
- Ultrasonic bath in Ethanol (5 min)
- Dry the cover slips with a clean room wipe or carefully with nitrogen
- Cover with freshly prepared NaOH (250 µl/cover slip; 0.1 M; 5 min) Note: from this step on it should always be ensured to know which side had been treated
- Dry and cover with APTMS (100 µl/cover slip; 3 min)
- Wash with water (3 x 10 min)
- Dry and cover with GDA (200 µl/cover slip; 0.5 %; 30 min)
- Wash with water (3 x 10 min)

Prepare PDMS stamping pad

- Mix PDMS 1:10 w:w and degas until no bubbles are left
- Pour into petri-dish, cure at 80°C (1 h)
Note: Curing time may need to be adapted to thickness of PDMS layer

µ-contact printing

- Premix 300 µl collagen stock (3 mg/ml) and 900 µl AA-NHS-ester stock (1000 µg/ml) in 7.8 ml PBS (1 h)
- Cover plain PDMS substrate with premixed collagen-AA-NHS-ester solution (1 h)
- Clean Si-moulds with plasma O₂ asher (10 min)

- Clean Si-moulds in DI water (ultrasonic bath; 10 min)
- Dry Si-moulds and PDMS substrate
- Push Si-moulds on PDMS substrate (10 min, 5 g weight)
- Use Si-mould for PAA gel polymerisation

Polyacrylamide gels pre-solutions

Table 7.1: Composition and volumes used for the polyacrylamide solutions to prepare gels with defined stiffnesses (E-modulus).

E-modulus [kPa]	AA[%]	Bis-AA [%]	Overall vol.	AA vol. [g]	Bis-AA vol. [g]
1	3	0.14	4 ml	0.12	0.0056
8	4	0.25	4 ml	0.16	0.01
30	10	0.10	4 ml	0.4	0.004
100	10	0.50	4 ml	0.4	0.02

7.1.3 Polyacrylamide gel preparation with APS and TEMED

- 0.5 ml PAA stock solution + 5 μ l APS (1:100) + 0.5 μ l TEMED (1:1000) in eppi and vortex
- Place PAA pre-solution on Si -mould (150 μ l/mould)
- Put glass substrates on top
- Polymerisation (45 min)
- Incubate in PBS at 4°C overnight
- Remove Si-mould

7.2 Scanning Electron microscopy results

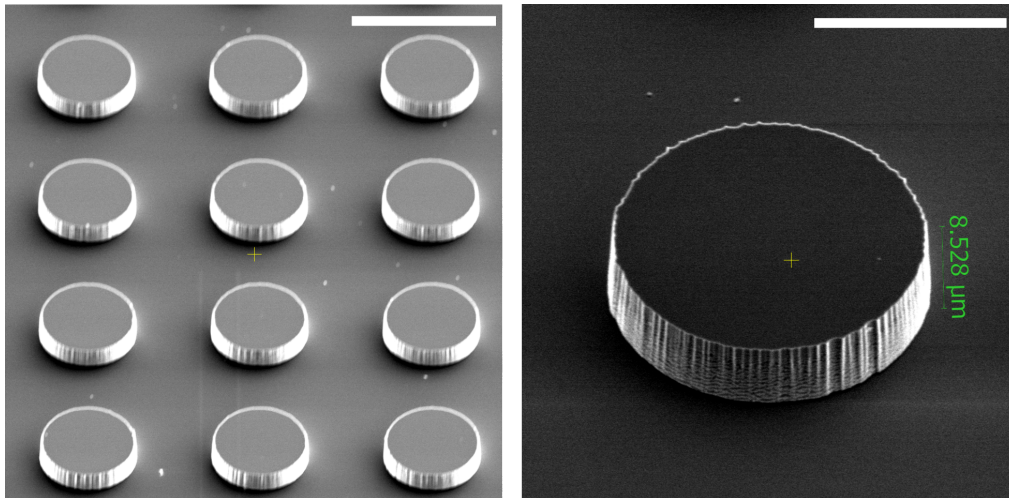


Figure 7.1: SEM images of Si-moulds. Scale bar left 50 µm, right 20 µm.

Bibliography

- [1] H. Ritchie, M. Roser, “Causes of Death”, *Our World in Data* **2018**.
- [2] D. Hanahan, R. A. Weinberg, “Hallmarks of Cancer: The Next Generation”, *Cell* **2011**, *144*, 646–674.
- [3] A. Chandra et al., “Ovarian cancer: Current status and strategies for improving therapeutic outcomes”, *Cancer Medicine* **2019**, *8*, 7018–7031.
- [4] P. Anand et al., “Cancer is a Preventable Disease that Requires Major Lifestyle Changes”, *Pharmaceutical Research* **2008**, *25*, 2097–2116.
- [5] E. K. Paluch et al., “Mechanotransduction: use the force(s)”, *BMC Biology* **2015**, *13*, 47.
- [6] B. Mansoori et al., “The Different Mechanisms of Cancer Drug Resistance: A Brief Review”, *Advanced Pharmaceutical Bulletin* **2017**, *7*, 339.
- [7] M. J. Bissell, W. C. Hines, “Why don’t we get more cancer? A proposed role of the microenvironment in restraining cancer progression”, *Nature Medicine* **2011**, *17*, 320–329.
- [8] W. J. Polacheck, C. S. Chen, “Measuring cell-generated forces: a guide to the available tools”, *Nature Methods* **2016**, *13*, 415–423.
- [9] C. Cadart et al., “Size control in mammalian cells involves modulation of both growth rate and cell cycle duration”, *Nature Communications* **2018**, *9*, 3275.
- [10] F.-M. Boisvert et al., “The multifunctional nucleolus”, *Nature Reviews Molecular Cell Biology* **2007**, *8*, 574–585.
- [11] T. E. Esterhouse, L. B. Petrinis, *Protein Biosynthesis*, Nova Science Publishers, Incorporated, New York, UNITED STATES, **2009**.
- [12] *The biogenesis of cellular organelles*, (Ed.: C. Mullins), Landes Bioscience/Eurekah.com ; Kluwer Academic/Plenum, Georgetown, Tex. : New York, N.Y, **2005**, 181 pp.
- [13] H. M. McBride, M. Neuspiel, S. Wasiak, “Mitochondria: More Than Just a Powerhouse”, *Current Biology* **2006**, *16*, R551–R560.
- [14] W. Stillwell, *An Introduction to Biological Membranes: Composition, Structure and Function*, Elsevier Science & Technology, Oxford, NETHERLANDS, THE, **2016**.
- [15] B. Alberts et al., *Molecular Biology of the Cell*, 4th, Garland Science, **2002**.

- [16] Y. A. Rovinsky in *Adhesive Interactions in Normal and Transformed Cells*, (Ed.: Y. A. Rovinsky), Humana Press, Totowa, NJ, **2011**, pp. 13–35.
- [17] A. Michelot, D. G. Drubin, “Building Distinct Actin Filament Networks in a Common Cytoplasm”, *Current Biology* **2011**, *21*, R560–R569.
- [18] K. Bhadriraju, L. K. Hansen, “Extracellular Matrix- and Cytoskeleton-Dependent Changes in Cell Shape and Stiffness”, *Experimental Cell Research* **2002**, *278*, 92–100.
- [19] J. E. Bear, J. M. Haugh, “Directed migration of mesenchymal cells: where signaling and the cytoskeleton meet”, *Current Opinion in Cell Biology*, Cell adhesion and migration **2014**, *30*, 74–82.
- [20] C. Jamora, E. Fuchs, “Intercellular adhesion, signalling and the cytoskeleton”, *Nature Cell Biology* **2002**, *4*, E101–E108.
- [21] F. Huber et al., “Emergent complexity of the cytoskeleton: from single filaments to tissue”, *Advances in Physics* **2013**, *62*, 1–112.
- [22] A. R. Harris, P. Jreij, D. A. Fletcher, “Mechanotransduction by the Actin Cytoskeleton: Converting Mechanical Stimuli into Biochemical Signals”, *Annual Review of Biophysics* **2018**, *47*, 617–631.
- [23] C. M. Kraning-Rush et al., “The role of the cytoskeleton in cellular force generation in 2D and 3D environments”, *Physical Biology* **2011**, *8*, 015009.
- [24] N. U. of Singapore, How are actin filaments distributed in cells and tissues?, MBInfo, <https://www.mechanobio.info/cytoskeleton-dynamics/what-is-the-cytoskeleton/what-are-actin-filaments/how-are-actin-filaments-distributed-in-cells-and-tissues/> (visited on 10/07/2021).
- [25] T. Fujii et al., “Direct visualization of secondary structures of F-actin by electron cryomicroscopy”, *Nature* **2010**, *467*, 724–728.
- [26] S. Shekhar, J. Pernier, M.-F. Carrier, “Regulators of actin filament barbed ends at a glance”, *Journal of Cell Science* **2016**, *129*, 1085–1091.
- [27] L. Blanchoin et al., “Actin Dynamics, Architecture, and Mechanics in Cell Motility”, *Physiological Reviews* **2014**, *94*, 235–263.
- [28] M. Krause, A. Gautreau, “Steering cell migration: lamellipodium dynamics and the regulation of directional persistence”, *Nature Reviews Molecular Cell Biology* **2014**, *15*, 577–590.
- [29] K. Adebawale et al., “Enhanced substrate stress relaxation promotes filopodia-mediated cell migration”, *Nature Materials* **2021**, *20*, 1290–1299.
- [30] P. Chugh, E. K. Paluch, “The actin cortex at a glance”, *Journal of Cell Science* **2018**, *131*.

- [31] A. Livne, B. Geiger, “The inner workings of stress fibers from contractile machinery to focal adhesions and back”, *Journal of Cell Science* **2016**, *129*, 1293–1304.
- [32] A. D. Theocharis et al., “Extracellular matrix structure”, *Advanced Drug Delivery Reviews*, Extracellular Matrix (ECM) and ECM-like materials: Therapeutic Tools and Targets in Cancer Treatment **2016**, *97*, 4–27.
- [33] Y. A. Rovinsky in *Adhesive Interactions in Normal and Transformed Cells*, (Ed.: Y. A. Rovinsky), Humana Press, Totowa, NJ, **2011**, pp. 7–12.
- [34] G. Karp, *Cell and Molecular Biology: Concepts and Experiments, 7th Edition*, Wiley Global Education, **2013**, 874 pp.
- [35] K. E. Kadler et al., “Collagens at a glance”, *Journal of Cell Science* **2007**, *120*, 1955–1958.
- [36] K. E. Kadler et al., “Collagen fibril formation”, *Biochemical Journal* **1996**, *316*, 1–11.
- [37] B. A. Roeder et al., “Tensile Mechanical Properties of Three-Dimensional Type I Collagen Extracellular Matrices With Varied Microstructure”, *Journal of Biomechanical Engineering* **2002**, *124*, 214–222.
- [38] C. Frantz, K. M. Stewart, V. M. Weaver, “The extracellular matrix at a glance”, *Journal of Cell Science* **2010**, *123*, 4195–4200.
- [39] M. L. Smith et al., “Force-Induced Unfolding of Fibronectin in the Extracellular Matrix of Living Cells”, *PLOS Biology* **2007**, *5*, e268.
- [40] N. Strohmeyer et al., “Fibronectin-bound $\alpha 5 \beta 1$ integrins sense load and signal to reinforce adhesion in less than a second”, *Nature Materials* **2017**, *16*, 1262–1270.
- [41] A. J. Engler et al., “Matrix Elasticity Directs Stem Cell Lineage Specification”, *Cell* **2006**, *126*, 677–689.
- [42] R. Sunyer et al., “Collective cell durotaxis emerges from long-range intercellular force transmission”, *Science* **2016**, *353*, 1157–1161.
- [43] C. De Pascalis, S. Etienne-Manneville, “Single and collective cell migration: the mechanics of adhesions”, *Molecular Biology of the Cell* **2017**, *28*, (Ed.: V. M. Weaver), 1833–1846.
- [44] A. Brugués et al., “Forces driving epithelial wound healing”, *Nature Physics* **2014**, *10*, 683–690.
- [45] T. M. Koch et al., “3D Traction Forces in Cancer Cell Invasion”, *PLOS ONE* **2012**, *7*, e33476.

- [46] N. U. of Singapore, How is integrin activated?, MBInfo, <https://www.mechanobio.info/what-is-mechanotransduction/what-is-the-extracellular-matrix-and-the-basal-lamina/what-is-integrin/how-is-integrin-activated/> (visited on 10/29/2021).
- [47] H. Harjunpää et al., “Cell Adhesion Molecules and Their Roles and Regulation in the Immune and Tumor Microenvironment”, *Frontiers in Immunology* **2019**, *10*, 1078.
- [48] S. J. Shattil, C. Kim, M. H. Ginsberg, “The final steps of integrin activation: the end game”, *Nature Reviews Molecular Cell Biology* **2010**, *11*, 288–300.
- [49] K. Chinthalapudi, E. S. Rangarajan, T. Izard, “The interaction of talin with the cell membrane is essential for integrin activation and focal adhesion formation”, *Proceedings of the National Academy of Sciences* **2018**, *115*, 10339–10344.
- [50] M. A. Wozniak et al., “Focal adhesion regulation of cell behavior”, *Biochimica et Biophysica Acta (BBA) - Molecular Cell Research*, Cell Adhesion and Signalling **2004**, *1692*, 103–119.
- [51] A. Elosegui-Artola, X. Trepate, P. Roca-Cusachs, “Control of Mechanotransduction by Molecular Clutch Dynamics”, *Trends in Cell Biology* **2018**, *28*, 356–367.
- [52] National University of Singapore, How do focal adhesions act as molecular clutches in lamellipodia?, MBInfo Defining Mechanobiology, <https://www.mechanobio.info/cytoskeleton-dynamics/what-are-lamellipodia-and-lamella/how-do-focal-adhesions-act-as-molecular-clutches-in-lamellipodia/> (visited on 10/03/2021).
- [53] V. Swaminathan et al., “Actin retrograde flow actively aligns and orients ligand-engaged integrins in focal adhesions”, *Proceedings of the National Academy of Sciences* **2017**, *114*, 10648–10653.
- [54] S. Mathieu, J.-B. Manneville, “Intracellular mechanics: connecting rheology and mechanotransduction”, *Current Opinion in Cell Biology* **2019**, *56*, 34–44.
- [55] B. Stutchbury et al., “Distinct focal adhesion protein modules control different aspects of mechanotransduction”, *Journal of Cell Science* **2017**, jcs.195362.
- [56] V. Rausch, C. G. Hansen, “The Hippo Pathway, YAP/TAZ, and the Plasma Membrane”, *Trends in Cell Biology* **2020**, *30*, 32–48.
- [57] F. Martino et al., “Cellular Mechanotransduction: From Tension to Function”, *Frontiers in Physiology* **2018**, *9*, 824.
- [58] D. Mitrossilis et al., “Real-time single-cell response to stiffness”, *Proceedings of the National Academy of Sciences* **2010**, *107*, 16518–16523.
- [59] K. Haase et al., “Extracellular Forces Cause the Nucleus to Deform in a Highly Controlled Anisotropic Manner”, *Scientific Reports* **2016**, *6*, 21300.

- [60] M. Maurer, J. Lammerding, “The Driving Force: Nuclear Mechanotransduction in Cellular Function, Fate, and Disease”, *Annual Review of Biomedical Engineering* **2019**, *21*, 443–468.
- [61] J. Swift et al., “Nuclear lamin-A scales with tissue stiffness and enhances matrix-directed differentiation”, *Science (New York N.Y.)* **2013**, *341*, 1240104.
- [62] A. Elosegui-Artola et al., “Force Triggers YAP Nuclear Entry by Regulating Transport across Nuclear Pores”, *Cell* **2017**, *171*, 1397–1410.e14.
- [63] S.-J. Heo et al., “Mechanically Induced Chromatin Condensation Requires Cellular Contractility in Mesenchymal Stem Cells”, *Biophysical Journal* **2016**, *111*, 864–874.
- [64] M. Bao et al., “3D microniches reveal the importance of cell size and shape”, *Nature Communications* **2017**, *8*, 1962.
- [65] M. Gupta et al., “Single cell rigidity sensing: A complex relationship between focal adhesion dynamics and large-scale actin cytoskeleton remodeling”, *Cell Adhesion & Migration* **2016**, *10*, 554–567.
- [66] J. P. Califano, C. A. Reinhart-King, “Substrate Stiffness and Cell Area Predict Cellular Traction Stresses in Single Cells and Cells in Contact”, *Cellular and Molecular Bioengineering* **2010**, *3*, 68–75.
- [67] L. A. Lautscham et al., “Migration in Confined 3D Environments Is Determined by a Combination of Adhesiveness, Nuclear Volume, Contractility, and Cell Stiffness”, *Biophysical Journal* **2015**, *109*, 900–913.
- [68] K. M. Yamada, M. Sixt, “Mechanisms of 3D cell migration”, *Nature Reviews Molecular Cell Biology* **2019**, *20*, 738–752.
- [69] L. Sigaut et al., “Correlation of cellular traction forces and dissociation kinetics of adhesive protein zyxin revealed by multi-parametric live cell microscopy”, *PLOS ONE* **2021**, *16*, e0251411.
- [70] A. J. McKenzie et al., “The mechanical microenvironment regulates ovarian cancer cell morphology, migration, and spheroid disaggregation”, *Scientific Reports* **2018**, *8*, 7228.
- [71] P. W. Oakes et al., “Geometry Regulates Traction Stresses in Adherent Cells”, *Biophysical Journal* **2014**, *107*, 825–833.
- [72] F. Basoli et al., “Biomechanical Characterization at the Cell Scale: Present and Prospects”, *Frontiers in Physiology* **2018**, *9*, 1449.
- [73] Y. F. Duf rene, A. E. Pelling, “Force nanoscopy of cell mechanics and cell adhesion”, *Nanoscale* **2013**, *5*, 4094–4104.
- [74] C. G. Galbraith, K. M. Yamada, M. P. Sheetz, “The relationship between force and focal complex development”, *Journal of Cell Biology* **2002**, *159*, 695–705.

- [75] C. Arbore et al., “Probing force in living cells with optical tweezers: from single-molecule mechanics to cell mechanotransduction”, *Biophysical Reviews* **2019**, *11*, 765–782.
- [76] S. C. Kuo, M. P. Sheetz, “Force of Single Kinesin Molecules Measured With Optical Tweezers”, *Science* **1993**, *260*, 232–234.
- [77] Y.-C. Poh et al., “Rapid Activation of Rac GTPase in Living Cells by Force Is Independent of Src”, *PLOS ONE* **2009**, *4*, e7886.
- [78] S. Hu et al., “Mechanical anisotropy of adherent cells probed by a three-dimensional magnetic twisting device”, *American Journal of Physiology. Cell Physiology* **2004**, *287*, C1184–1191.
- [79] J. L. Tan et al., “Cells lying on a bed of microneedles: An approach to isolate mechanical force”, *Proceedings of the National Academy of Sciences* **2003**, *100*, 1484–1489.
- [80] L. Feld et al., “Cellular contractile forces are nonmechanosensitive”, *Science Advances* **2020**.
- [81] J. Steinwachs et al., “Three-dimensional force microscopy of cells in biopolymer networks”, *Nature Methods* **2016**, *13*, 171–176.
- [82] M. Lekka et al., “Traction force microscopy – Measuring the forces exerted by cells”, *Micron* **2021**, *150*, 103138.
- [83] J. Liu et al., “Atomic Force Mechanobiology of Pluripotent Stem Cell-Derived Cardiomyocytes”, *PLOS ONE* **2012**, *7*, e37559.
- [84] A. G. Håti et al., “Energy Landscape of Alginate-Epimerase Interactions Assessed by Optical Tweezers and Atomic Force Microscopy”, *PLOS ONE* **2015**, *10*, e0141237.
- [85] H. Sung et al., “Global Cancer Statistics 2020: GLOBOCAN Estimates of Incidence and Mortality Worldwide for 36 Cancers in 185 Countries”, *CA: A Cancer Journal for Clinicians* **2021**, *71*, 209–249.
- [86] S. Sundar, R. D. Neal, S. Kehoe, “Diagnosis of ovarian cancer”, *BMJ* **2015**, *351*, h4443.
- [87] G. C. Jayson et al., “Ovarian cancer”, *The Lancet* **2014**, *384*, 1376–1388.
- [88] O. Miree et al. in *Ovarian Cancer: Molecular & Diagnostic Imaging and Treatment Strategies*, (Ed.: H. Schatten), Advances in Experimental Medicine and Biology, Springer International Publishing, Cham, **2021**, pp. 1–19.
- [89] A. Hallas-Potts, J. C. Dawson, C. S. Herrington, “Ovarian cancer cell lines derived from non-serous carcinomas migrate and invade more aggressively than those derived from high-grade serous carcinomas”, *Scientific Reports* **2019**, *9*, 5515.

- [90] J. J. Evans, M. M. Alkaisi, P. H. Sykes, “Tumour Initiation: a Discussion on Evidence for a “Load-Trigger” Mechanism”, *Cell Biochemistry and Biophysics* **2019**, *77*, 293–308.
- [91] F. R. Balkwill, M. Capasso, T. Hagemann, “The tumor microenvironment at a glance”, *Journal of Cell Science* **2012**, *125*, 5591–5596.
- [92] A. Nagelkerke et al., “The mechanical microenvironment in cancer: How physics affects tumours”, *Seminars in Cancer Biology* **2015**, *35*, 62–70.
- [93] V. Mieulet et al., “Stiffness increases with myofibroblast content and collagen density in mesenchymal high grade serous ovarian cancer”, *Scientific Reports* **2021**, *11*, 4219.
- [94] A. Cho, V. M. Howell, E. K. Colvin, “The Extracellular Matrix in Epithelial Ovarian Cancer – A Piece of a Puzzle”, *Frontiers in Oncology* **2015**, *5*.
- [95] Y. Shen et al., “Fibrillar type I collagen matrices enhance metastasis/invasion of ovarian epithelial cancer via $\beta 1$ integrin and PTEN signals”, *International Journal of Gynecological Cancer: Official Journal of the International Gynecological Cancer Society* **2012**, *22*, 1316–1324.
- [96] F. E. Franke et al., “Association between fibronectin expression and prognosis in ovarian carcinoma”, *Anticancer Research* **2003**, *23*, 4261–4267.
- [97] H. A. Kenny et al., “Mesothelial cells promote early ovarian cancer metastasis through fibronectin secretion”, *The Journal of Clinical Investigation* **2014**, *124*, 4614–4628.
- [98] M. A. Anttila et al., “High levels of stromal hyaluronan predict poor disease outcome in epithelial ovarian cancer”, *Cancer Research* **2000**, *60*, 150–155.
- [99] P. J. Coleman, “Evidence for a role of hyaluronan in the spacing of fibrils within collagen bundles in rabbit synovium”, *Biochimica et Biophysica Acta (BBA) - General Subjects* **2002**, *1571*, 173–182.
- [100] C. Alibert, B. Goud, J.-B. Manneville, “Are cancer cells really softer than normal cells?: Mechanics of cancer cells”, *Biology of the Cell* **2017**, *109*, 167–189.
- [101] T. Tzvetkova-Chevolleau et al., “The motility of normal and cancer cells in response to the combined influence of the substrate rigidity and anisotropic microstructure”, *Biomaterials* **2008**, *29*, 1541–1551.
- [102] K. Kushiro et al., “Differences in Three-Dimensional Geometric Recognition by Non-Cancerous and Cancerous Epithelial Cells on Microgroove-Based Topography”, *Scientific Reports* **2017**, *7*, 4244.
- [103] V. Peschetola et al., “Time-dependent traction force microscopy for cancer cells as a measure of invasiveness”, *Cytoskeleton (Hoboken N.J.)* **2013**, *70*, 201–214.

- [104] C. Mack, *Fundamental Principles of Optical Lithography: The Science of Microfabrication*, John Wiley & Sons, Incorporated, New York, United Kingdom, **2007**.
- [105] R. P. Seisyan, “Nanolithography in microelectronics: A review”, *Technical Physics* **2011**, *56*, 1061–1073.
- [106] P. W. Leech, N. Wu, Y. Zhu, “Application of dry film resist in the fabrication of microfluidic chips for droplet generation”, *Journal of Micromechanics and Microengineering* **2009**, *19*, 065019.
- [107] Microchemicals GmbH, Baking Steps in Photoresists Processing, https://www.microchemicals.com/downloads/application_notes.html (visited on 08/07/2021).
- [108] R. Langer et al., *Microfluidic Technologies For Human Health*, World Scientific Publishing Company, Singapore, **2012**.
- [109] Y. Sun et al., “Microfluidic platform for integrated compartmentalization of single zoospores, germination and measurement of protrusive force generated by germ tubes”, *Lab on a Chip* **2020**, *20*, 4141–4151.
- [110] Z. Huang et al., “Metal Assisted Chemical Etching of Silicon: A Review”, *Advanced Materials* **2011**, *23*, 285–308.
- [111] P. Verdonck, 1. Plasmas: useful but complex.
- [112] K. Nojiri in *Dry Etching Technology for Semiconductors*, (Ed.: K. Nojiri), Springer International Publishing, Cham, **2015**, pp. 11–30.
- [113] B. Wu, A. Kumar, S. Pamarthy, “High aspect ratio silicon etch: A review”, *Journal of Applied Physics* **2010**, *108*, 051101.
- [114] M. D. Henry, PhD thesis, California Institute of Technology, **2010**.
- [115] T. Bertrand et al., “Dynamics of Swelling and Drying in a Spherical Gel”, *Physical Review Applied* **2016**, *6*, 064010.
- [116] A. Chrambach, D. Rodbard, “Polyacrylamide Gel Electrophoresis”, *Science* **1971**, *172*, 440–451.
- [117] J. R. Tse, A. J. Engler, “Preparation of hydrogel substrates with tunable mechanical properties”, *Current Protocols in Cell Biology* **2010**, *Chapter 10*, Unit 10.16.
- [118] S. Sheth et al., “UV Dose Governs UV-Polymerized Polyacrylamide Hydrogel Modulus”, *International Journal of Polymer Science* **2017**, *2017*, 1–9.
- [119] S. J. Hepworth, M. O. Leach, S. J. Doran, “Dynamics of polymerization in polyacrylamide gel (PAG) dosimeters: (II) modelling oxygen diffusion”, *Physics in Medicine and Biology* **1999**, *44*, 1875–1884.
- [120] M. L. Oyen, “Mechanical characterisation of hydrogel materials”, *International Materials Reviews* **2014**, *59*, 44–59.

- [121] M. J. Poellmann, A. J. Wagoner Johnson, “Characterizing and Patterning Polyacrylamide Substrates Functionalized with N-Hydroxysuccinimide”, *Cellular and Molecular Bioengineering* **2013**, *6*, 299–309.
- [122] S. R. Polio et al., “A micropatterning and image processing approach to simplify measurement of cellular traction forces”, *Acta Biomaterialia* **2012**, *8*, 82–88.
- [123] M. Mrksich, G. M. Whitesides, “Patterning self-assembled monolayers using microcontact printing: A new technology for biosensors?”, *Trends in Biotechnology* **1995**, *13*, 228–235.
- [124] N. M. Oliveira et al., “Coculture of Spheroids/2D Cell Layers Using a Miniaturized Patterned Platform as a Versatile Method to Produce Scaffold-Free Tissue Engineering Building Blocks”, *Advanced Biosystems* **2018**, *2*, 1700069.
- [125] P. Tseng, D. Di Carlo, “Substrates with Patterned Extracellular Matrix and Subcellular Stiffness Gradients Reveal Local Biomechanical Responses”, *Advanced Materials* **2014**, *26*, 1242–1247.
- [126] D. Mohammed, “Substrate area confinement is a key determinant of cell velocity in collective migration”, *Nature Physics* **2019**, *15*, 13.
- [127] N. Wang et al., “Micropatterning tractional forces in living cells”, *Cell Motility and the Cytoskeleton* **2002**, *52*, 97–106.
- [128] E. Kassianidou et al., “Geometry and network connectivity govern the mechanics of stress fibers”, *Proceedings of the National Academy of Sciences* **2017**, *114*, 2622–2627.
- [129] B. Sarker, C. Walter, A. Pathak, “Direct Micropatterning of Extracellular Matrix Proteins on Functionalized Polyacrylamide Hydrogels Shows Geometric Regulation of Cell–Cell Junctions”, *ACS Biomaterials Science & Engineering* **2018**, *4*, 2340–2349.
- [130] J. Moeller et al., “Controlling cell shape on hydrogels using lift-off protein patterning”, *PLOS ONE* **2018**, *13*, (Ed.: N. D. Leipzig), e0189901.
- [131] T. Vignaud, H. Ennomani, M. Théry in *Methods in Cell Biology*, Vol. 120, Elsevier, **2014**, pp. 93–116.
- [132] M. Veiseh, M. H. Zareie, M. Zhang, “Highly Selective Protein Patterning on Gold Silicon Substrates for Biosensor Applications”, *Langmuir* **2002**, *18*, 6671–6678.
- [133] T. Le Sy et al., “An Introduction to Mammalian Cell Culture”, *Chemical Engineering Progress* **2016**, *112*, 34–40.
- [134] T.-L. Yeung et al., “Cellular and molecular processes in ovarian cancer metastasis. A Review in the Theme: Cell and Molecular Processes in Cancer Metastasis”, *American Journal of Physiology-Cell Physiology* **2015**, *309*, C444–C456.

- [135] C. M. Beaufort et al., “Ovarian Cancer Cell Line Panel (OCCP): Clinical Importance of In Vitro Morphological Subtypes”, *PLOS ONE* **2014**, *9*, e103988.
- [136] J. Fogh, J. M. Fogh, T. Orfeo, “One Hundred and Twenty-Seven Cultured Human Tumor Cell Lines Producing Tumors in Nude Mice²³”, *JNCI: Journal of the National Cancer Institute* **1977**, *59*, 221–226.
- [137] T. J. Shaw et al., “Characterization of intraperitoneal, orthotopic, and metastatic xenograft models of human ovarian cancer”, *Molecular Therapy* **2004**, *10*, 1032–1042.
- [138] N. instruments, Optical Profilometry, Nanoscience Instruments, <https://www.nanoscience.com/techniques/optical-profilometry/> (visited on 08/08/2021).
- [139] R. J. Whitefield, “Noncontact optical profilometer”, *Applied Optics* **1975**, *14*, 2480–2485.
- [140] K. D. Vernon-Parry, “Scanning electron microscopy: an introduction”, *III-Vs Review* **2000**, *13*, 40–44.
- [141] G. Binnig, C. F. Quate, C. Gerber, “Atomic Force Microscope”, *Physical Review Letters* **1986**, *56*, 930–933.
- [142] S. M. Cook et al., “Practical implementation of dynamic methods for measuring atomic force microscope cantilever spring constants”, *Nanotechnology* **2006**, *17*, 2135–2145.
- [143] H.-J. Butt, B. Cappella, M. Kappl, “Force measurements with the atomic force microscope: Technique, interpretation and applications”, *Surface Science Reports* **2005**, *59*, 1–152.
- [144] W. Commons, Atomic force microscope block diagram.svg, https://commons.wikimedia.org/wiki/File:Atomic_force_microscope_block_diagram.svg (visited on 10/12/2021).
- [145] H. Hertz, “Über die Berührung fester elastischer Körper”, *Journal für die reine und angewandte Mathematik* **1882**, *92*, 22.
- [146] G. G. Bilodeau, “Regular Pyramid Punch Problem”, *Journal of Applied Mechanics* **1992**, *59*, 519–523.
- [147] E. U. Condon, “The Franck-Condon Principle and Related Topics”, *American Journal of Physics* **1947**, *15*, 365–374.
- [148] U. Kubitschek, *Fluorescence Microscopy: From Principles to Biological Applications*, John Wiley & Sons, Incorporated, Weinheim, Germany, **2013**.
- [149] K. Im et al., “An introduction to Performing Immunofluorescence Staining”, *Methods in molecular biology (Clifton N.J.)* **2019**, *1897*, 299–311.
- [150] M. J. Sanderson et al., “Fluorescence Microscopy”, *Cold Spring Harbor protocols* **2014**, *2014*, pdb.top071795.

- [151] R. Style et al., “Traction force microscopy in physics and biology”, *Soft Matter* **2014**, *10*, 4047–4055.
- [152] B. Sabass et al., “High Resolution Traction Force Microscopy Based on Experimental and Computational Advances”, *Biophysical Journal* **2008**, *94*, 207–220.
- [153] N. A. Malik, T. Dracos, D. A. Papantoniou, “Particle tracking velocimetry in three-dimensional flows”, *Experiments in Fluids* **1993**, *15*, 279–294.
- [154] Q. Tseng et al., “Spatial organization of the extracellular matrix regulates cell–cell junction positioning”, *Proceedings of the National Academy of Sciences* **2012**.
- [155] J.-L. Martiel et al. in *Methods in Cell Biology*, Vol. 125, Elsevier, **2015**, pp. 269–287.
- [156] M. Raffel et al. in *Particle Image Velocimetry: A Practical Guide*, (Eds.: M. Raffel et al.), Springer International Publishing, Cham, **2018**, pp. 1–32.
- [157] M. Raffel et al. in *Particle Image Velocimetry: A Practical Guide*, (Eds.: M. Raffel et al.), Springer International Publishing, Cham, **2018**, pp. 145–202.
- [158] F. Scarano, “Iterative image deformation methods in PIV”, *Measurement Science and Technology* **2001**, *13*, R1.
- [159] L. D. Landau, E. M. Lifshits, *Theory of elasticity*, Vol. 7, 2d English, Pergamon Press, New York;Oxford; **1970**.
- [160] J. P. Butler et al., “Traction fields, moments, and strain energy that cells exert on their surroundings”, *American Journal of Physiology. Cell Physiology* **2002**, *282*, C595–605.
- [161] U. S. Schwarz et al., “Calculation of Forces at Focal Adhesions from Elastic Substrate Data: The Effect of Localized Force and the Need for Regularization”, *Biophysical Journal* **2002**, *83*, 1380–1394.
- [162] A. H. Kulkarni et al., “Traction cytometry: regularization in the Fourier approach and comparisons with finite element method”, *Soft Matter* **2018**, *14*, 4687–4695.
- [163] U. S. Schwarz, J. R. D. Soiné, “Traction force microscopy on soft elastic substrates: A guide to recent computational advances”, *Biochimica et Biophysica Acta (BBA) - Molecular Cell Research*, Mechanobiology **2015**, *1853*, 3095–3104.
- [164] F. Nazemroaya et al., “Induced Retro-Differentiation of Human Retinal Pigment Epithelial Cells on PolyHEMA”, *Journal of Cellular Biochemistry* **2017**, *118*, 3080–3089.
- [165] B. Holt, A. Tripathi, J. R. Morgan, “Designing polyHEMA substrates that mimic the viscoelastic response of soft tissue”, *Journal of Biomechanics* **2011**, *44*, 1491–1498.
- [166] F. Ye et al., “Improved single-cell culture achieved using micromolding in capillaries technology coupled with poly (HEMA)”, *Biomicrofluidics* **2015**, *9*, 044106.

- [167] F. Ye et al., “Fabrication of polyHEMA grids by micromolding in capillaries for cell patterning and single-cell arrays”, *Journal of Biomedical Materials Research Part B: Applied Biomaterials* **2015**, *103*, 1375–1380.
- [168] H. Shiku et al., “Oxygen Permeability of Surface-modified Poly(dimethylsiloxane) Characterized by Scanning Electrochemical Microscopy”, *Chemistry Letters* **2006**.
- [169] R. Simič et al., “Oxygen inhibition of free-radical polymerization is the dominant mechanism behind the “mold effect” on hydrogels”, *Soft Matter* **2021**, *17*, 6394–6403.
- [170] V. Rohnalter et al., “A multi-stage process including transient polyploidization and EMT precedes the emergence of chemoresistent ovarian carcinoma cells with a dedifferentiated and pro-inflammatory secretory phenotype”, *Oncotarget* **2015**, *6*, 40005–40025.
- [171] B. Toubhans et al., “Selenium nanoparticles trigger alterations in ovarian cancer cell biomechanics”, *Nanomedicine: Nanotechnology Biology and Medicine* **2020**, *29*, 102258.
- [172] Y. Hou et al., “Effect of docetaxel on mechanical properties of ovarian cancer cells”, *Experimental Cell Research* **2021**, *408*, 112853.
- [173] A. K. Denisin, B. L. Pruitt, “Tuning the Range of Polyacrylamide Gel Stiffness for Mechanobiology Applications”, *ACS Applied Materials & Interfaces* **2016**, *8*, 21893–21902.
- [174] A. Cretu, P. Castagnino, R. Assoian, “Studying the Effects of Matrix Stiffness on Cellular Function using Acrylamide-based Hydrogels”, *Journal of Visualized Experiments : JoVE* **2010**, 2089.
- [175] N. P. Mellott et al., “Evaluation of surface preparation methods for glass”, *Surface and Interface Analysis* **2001**, *31*, 362–368.
- [176] M. Zhu, M. Z. Lerum, W. Chen, “How to Prepare Reproducible, Homogeneous, and Hydrolytically Stable Aminosilane-derived Layers on Silica”, *Langmuir* **2012**, *28*, 416.
- [177] P. Rajagopalan et al., “Direct Comparison of the Spread Area, Contractility, and Migration of balb/c 3T3 Fibroblasts Adhered to Fibronectin- and RGD-Modified Substrata”, *Biophysical Journal* **2004**, *87*, 2818–2827.
- [178] D. Bodas, C. Khan-Malek, “Hydrophilization and hydrophobic recovery of PDMS by oxygen plasma and chemical treatment—An SEM investigation”, *Sensors and Actuators B: Chemical* **2007**, *123*, 368–373.
- [179] J. W. Lussi et al., “Pattern stability under cell culture conditions—A comparative study of patterning methods based on PLL-g-PEG background passivation”, *Biomaterials* **2006**, *27*, 2534–2541.

- [180] V. S. Raghuwanshi, G. Garnier, “Characterisation of hydrogels: Linking the nano to the microscale”, *Advances in Colloid and Interface Science* **2019**, *274*, 102044.
- [181] J. Schindelin et al., “Fiji: an open-source platform for biological-image analysis”, *Nature Methods* **2012**, *9*, 676–682.
- [182] S. Preibisch et al., “Software for bead-based registration of selective plane illumination microscopy data”, *Nature Methods* **2010**, *7*, 418–419.
- [183] M. Kass, A. Witkin, D. Terzopoulos, “Snakes: Active contour models”, *International Journal of Computer Vision* **1988**, *1*, 321–331.
- [184] S. Franssila, *Introduction to Microfabrication*, John Wiley & Sons, Incorporated, Hoboken, United Kingdom, **2010**.
- [185] M. J. Buie, J. T. P. P. Ventzek, “A Method for Identifying Sources of Reactive Ion Etch Lag and Loading in a Magnetically Enhanced Reactive Ion Etcher”, *Japanese Journal of Applied Physics* **1997**, *36*, 4838.
- [186] C. Moraes, Y. Sun, C. A. Simmons, “Solving the shrinkage-induced PDMS alignment registration issue in multilayer soft lithography”, *Journal of Micromechanics and Microengineering* **2009**, *19*, 065015.
- [187] J. Yeom et al., “Maximum achievable aspect ratio in deep reactive ion etching of silicon due to aspect ratio dependent transport and the microlading effect”, *Journal of Vacuum Science & Technology B: Microelectronics and Nanometer Structures Processing Measurement and Phenomena* **2005**, *23*, 2319–2329.
- [188] L. M. Lira, K. A. Martins, S. I. C. d. Torresi, “Structural parameters of polyacrylamide hydrogels obtained by the Equilibrium Swelling Theory”, *European Polymer Journal* **2009**, *45*, 1232–1238.
- [189] T. R. C. Boyde, “Swelling and contraction of polyacrylamide gel slabs in aqueous solutions”, *Journal of Chromatography A* **1976**, *124*, 219–230.
- [190] W. Megone, N. Roohpour, J. E. Gautrot, “Impact of surface adhesion and sample heterogeneity on the multiscale mechanical characterisation of soft biomaterials”, *Scientific Reports* **2018**, *8*, 6780.
- [191] K. Ye et al., “Matrix Stiffness and Nanoscale Spatial Organization of Cell-Adhesive Ligands Direct Stem Cell Fate”, *Nano Letters* **2015**, *15*, 4720–4729.
- [192] O. Chaudhuri et al., “Extracellular matrix stiffness and composition jointly regulate the induction of malignant phenotypes in mammary epithelium”, *Nature Materials* **2014**, *13*, 970–978.
- [193] I. D. Johnson in *Handbook Of Biological Confocal Microscopy*, (Ed.: J. B. Pawley), Springer US, Boston, MA, **2006**, pp. 353–367.
- [194] P. Montero Llopis et al., “Best practices and tools for reporting reproducible fluorescence microscopy methods”, *Nature Methods* **2021**, 1–14.

- [195] M. Roederer, “Spectral compensation for flow cytometry: visualization artifacts, limitations, and caveats”, *Cytometry* **2001**, *45*, 194–205.
- [196] J. Jonkman et al., “Tutorial: guidance for quantitative confocal microscopy”, *Nature Protocols* **2020**, *15*, 1585–1611.
- [197] J. C. Waters, “Accuracy and precision in quantitative fluorescence microscopy”, *Journal of Cell Biology* **2009**, *185*, 1135–1148.
- [198] J. Rietdorf, E. H. K. Stelzer in *Handbook Of Biological Confocal Microscopy*, (Ed.: J. B. Pawley), Springer US, Boston, MA, **2006**, pp. 43–58.
- [199] J. Zonderland, P. Wieringa, L. Moroni, “A quantitative method to analyse F-actin distribution in cells”, *MethodsX* **2019**, *6*, 2562–2569.
- [200] U. Horzum, B. Ozdil, D. Pesen-Okvur, “Step-by-step quantitative analysis of focal adhesions”, *MethodsX* **2014**, *1*, 56–59.
- [201] Z. Messi et al., “Traction Forces Control Cell-Edge Dynamics and Mediate Distance Sensitivity during Cell Polarization”, *Current Biology* **2020**, *30*, 1762–1769.e5.
- [202] A. D. Rape, W.-h. Guo, Y.-l. Wang, “The regulation of traction force in relation to cell shape and focal adhesions”, *Biomaterials* **2011**, *32*, 2043–2051.
- [203] A. Sakaue-Sawano et al., “Visualizing Spatiotemporal Dynamics of Multicellular Cell-Cycle Progression”, *Cell* **2008**, *132*, 487–498.
- [204] B. Vianay et al., “Variation in traction forces during cell cycle progression: Traction forces during cycle progression”, *Biology of the Cell* **2018**, *110*, 91–96.
- [205] J. Rother et al., “Atomic force microscopy-based microrheology reveals significant differences in the viscoelastic response between malignant and benign cell lines”, *Open Biology* **2014**, *4*, 140046.
- [206] J. Rheinlaender, T. E. Schäffer, “Mapping the mechanical stiffness of live cells with the scanning ion conductance microscope”, *Soft Matter* **2013**, *9*, 3230–3236.
- [207] Y. Li, J. Schnekenburger, M. H. G. Duits, “Intracellular particle tracking as a tool for tumor cell characterization”, *Journal of Biomedical Optics* **2009**, *14*, 064005.
- [208] W. Xu et al., “Cell Stiffness Is a Biomarker of the Metastatic Potential of Ovarian Cancer Cells”, *PLoS ONE* **2012**, *7*, (Ed.: S. K. Batra), e46609.
- [209] J. Guck et al., “Optical Deformability as an Inherent Cell Marker for Testing Malignant Transformation and Metastatic Competence”, *Biophysical Journal* **2005**, *88*, 3689–3698.
- [210] T. G. Mason et al., “Particle Tracking Microrheology of Complex Fluids”, *Physical Review Letters* **1997**, *79*, 3282–3285.
- [211] C. K. M. Ip et al., “Stemness and chemoresistance in epithelial ovarian carcinoma cells under shear stress”, *Scientific Reports* **2016**, *6*, 26788.

- [212] M. Sarwar et al., “Extracellular biophysical environment: Guilty of being a modulator of drug sensitivity in ovarian cancer cells”, *Biochemical and Biophysical Research Communications* **2020**, *527*, 180–186.

Acknowledgments

Many people have helped me on my PhD journey, who I would like to thank. Thank you Maan, for the supervision of my work and allowing me to work in such an interesting field of research. Thank you for your patience, for encouraging me to develop my own ideas and for always supporting me in implementing them. Thank you Volker, for being my co-supervisor, for taking care of challenges in the BAT-lab and for encouraging me to enjoy the beauty of New Zealand's nature. Thank you both for proofreading my thesis as well.

I would like to thank my examiners, Timo Betz and David Williams for taking the time to read and evaluate my thesis. Your comments, ideas and feedback were really helpful.

I would also like to thank the MacDiarmid institute and all the people involved there, for the scholarships, the financial support and the many exciting activities and workshops. I have met great people along the way. I would especially thank Jenny Malmström and her group for allowing me to join them for a week up in Auckland and allowing me to use their lab and AFM. Thank you for all the helpful discussions and tips!

Thank you Gary and Helen for your technical support in the nanolab and always having an open ear for me. Thank you Julian for listening and helping to develop new ideas when I was despairing. Thanks Azy, Sevgi and Nicola for your friendship. And of course a big thanks to the rest of the NEST-group, Louise, Caixia, Claude, Yiling, Miguel, Linda, Peter for always being friendly and helpful. Thank you Sierra for the many great lunches and fun times we had together. I would also like to mention how much I enjoyed to be part of the Electrical and Computer Engineering department and how much I enjoyed joining the Clearance rafting trips. I am amazed how many inspiring people I have met. And I would like to thank Deborah for always being compassionate and positive.

I would like to thank the DAAD for funding my travel to Germany and the short term research scholarship. And of course a big thank you to Andreas Janshoff and his group in Göttingen. I was welcomed with open arms, treated as I would have always been part of the group and got always a friendly and helpful answer from everyone when asking for help or advice. Thank you Burkhard for putting so much energy into the analysis of my brightfield videos. Thank you Angela and Tabea for your help with the cells, that made my life a lot easier.

I very much appreciate all of that and look forward to work with you all in the future.

I also would like to thank Blair, Peter and Tom for proof reading my thesis and the constructive comments.

Bibliography

Thanks to my family who always believed in me and encouraged me to follow my ideas and dreams. No matter if that meant to do a PhD at the other end of the world, crossing New Zealand within two days by cycling, running and kayaking or leaving the only COVID free place, when the rest of the world was coping with the pandemic.

And of course, thank you, Tom, for showing me what heaven on earth feels like.